NASA TECHNICAL NOTE

NASA TN D-7227

NASA TN D-7227

FLIGHT INVESTIGATION OF XB-70 STRUCTURAL RESPONSE TO OSCILLATORY AERODYNAMIC SHAKER EXCITATION AND CORRELATION WITH ANALYTICAL RESULTS

James M. McKay and Eldon E. Kordes

Flight Research Center
Edwards, Calif. 93523

and

John H. Wykes

North American Rockwell Corporation
Los Angeles, Calif. 90009

NATIONAL AERONAUTICS AND SPACE ADMINISTRATION • WASHINGTON, D. C. • APRIL 1973

1. Report No. NASA TN D-7227	2. Government Accession No.	3. Recipient's Catalog No.
4. Title and Subtitle FLIGHT INVESTIGATION OF XB-70 STRUCTURAL RESPONSE TO OSCILLATORY AERODYNAMIC SHAKER EXCITATION AND CORRELATION WITH ANALYTICAL RESULTS		5. Report Date April 1973 6. Performing Organization Code
7. Author(s) James M. McKay, Eldon E. Kordes (Flight Research Center), and John H. Wykes (North American Rockwell Corporation)		8. Performing Organization Report No. H-713
9. Performing Organization Name and Address NASA Flight Research Center P. O. Box 273 Edwards, California 93523		10. Work Unit No. 761-74-02-00-24 11. Contract or Grant No.
12. Sponsoring Agency Name and Address National Aeronautics and Space Administration Washington, D. C. 20546		13. Type of Report and Period Covered Technical Note 14. Sponsoring Agency Code
15. Supplementary Notes		

16. Abstract

The low frequency symmetric structural response and damping characteristics of the XB-70 airplane were measured at four flight conditions: heavyweight at a Mach number of 0.87 at an altitude of 7620 meters (25,000 feet); lightweight at a Mach number of 0.86 at an altitude of 7620 meters (25,000 feet); a Mach number of 1.59 at an altitude of 11,918 meters (39,100 feet); and a Mach number of 2.38 and an altitude of 18,898 meters (62,000 feet). The flight data are compared with the response calculated by using early XB-70 design data and with the response calculated with mass, structural, and aerodynamic data updated to reflect as closely as possible the airplane characteristics at three of the flight conditions actually flown.

The updated analysis made selective use of quasi-steady wing aerodynamic theory. These theoretical data are compared with results calculated for one high subsonic flight condition by using unsteady wing aerodynamic theory.

17. Key Words (Suggested by Author(s))	18. Distribution Statement
Structural response Aerodynamic shaker excitation Structural damping	Unclassified - Unlimited

19. Security Classif. (of this report)	20. Security Classif. (of this page)	21. No. of Pages	22. Price*
Unclassified	Unclassified	122	$3.00

* For sale by the National Technical Information Service, Springfield, Virginia 22151

FLIGHT INVESTIGATION OF XB-70 STRUCTURAL RESPONSE TO OSCILLATORY AERODYNAMIC SHAKER EXCITATION AND CORRELATION WITH ANALYTICAL RESULTS

James M. McKay and Eldon E. Kordes
Flight Research Center

and John H. Wykes
North American Rockwell Corporation

INTRODUCTION

As a result of recent aircraft mission and design requirements, new, more flexible airframe configurations are being developed. Among the factors contributing to the increased flexibility are thin lifting surfaces, long slender fuselages, low mass fraction structures, high design stress levels, and low design load factors. These factors, coupled with supersonic speeds, have made the prediction of aeroelastic response more complex. The structural deformations brought about by the increased flexibility result in significant changes in an airplane's aerodynamics and resultant stability. In addition, the problems associated with estimating the mass, structural, and aerodynamic characteristics that combine to form an analytical model of a large, flexible aircraft become more complex and difficult to resolve.

The XB-70 airplane is typical of the new generation of large, highly flexible aircraft. Early analysis of XB-70 flight data obtained in moderate-to-rough turbulence (ref. 1) at supersonic speeds indicated marked structural motion at the pilot's station in the first four symmetric structural modes. Although previous analytical studies (refs. 2 and 3) based on early XB-70 design characteristics had, in general, predicted this motion, the agreement between the calculated aircraft response and that obtained from flight data was, on the whole, not good (ref. 4). Thus it became important to examine and attempt to reconcile some of the differences between the flight-measured response of the airplane and the response predicted analytically.

A flight investigation was made with the XB-70-1 airplane to measure the low frequency symmetric structural response and damping characteristics throughout the operating envelope. A system was installed on the airplane that excited the low frequency symmetric modes by controlled inputs. This paper presents the vertical response measured at various locations on the airplane during subsonic and supersonic flight. The flight data are compared with calculated results from reference 3 and with an updated analysis.

SYMBOLS

Physical quantities in this report are given in the International System of Units (SI) and parenthetically in U.S. Customary Units. The measurements were taken in Customary Units. Factors relating the two systems are presented in reference 5.

f	forcing frequency
g	acceleration of gravity
g_i	structural mode damping (structural plus aerodynamic)
g_{s_i}	structural damping constant, mode i
h_p	pressure altitude
$i = \sqrt{-1}$	
$K_{(\ )}$	control system gain associated with subscripted parameter
l	distance from flight augmentation control system accelerometer to vehicle center of gravity
M	Mach number
n_z	normal load factor
Δn_z	incremental normal load factor
q	pitching rate about Y-axis
s	Laplace operator
V_o	resultant velocity at center of gravity
α	angle of attack
δ	control surface deflection
δ_s	servo output displacement
δ_{sc}	servo command input
δ_{sv}	shaker vane deflection; positive deflection produces positive lift force
δ_t	wingtip deflection
$\eta_{(\ )}$	generalized coordinate; subscript indicates mode
ρ	density of air
φ	phase angle
φ_i	i^{th} normalized mode shape

φ_i'	slope of i^{th} normalized mode
$\sigma_i = 57.3 \frac{d\omega}{d\varphi}$,	real part of the root of the characteristic equation as in $(s + \sigma_i \pm \omega_i)$
ω	forcing frequency
ω_i	natural frequency of i^{th} mode

Subscripts:

e	all elevons except inboard
FACS	flight augmentation control system
i	generalized structural mode identification
P	pilot
1	inboard elevon
2, 3, 4, 5, 6	identification of individual elevon panels exclusive of inboard panel

ABBREVIATIONS

BP	butt plane
FS	fuselage station
HS	canard horizontal station
VS	vertical stabilizer station
WP	waterplane

TEST APPARATUS

Airplane

The XB-70 (fig. 1) is a large, delta-winged, multiengined jet airplane designed by North American Rockwell Corporation for supersonic cruise at a Mach number of 3.0 at altitudes above 21,336 meters (70,000 feet). Two airplanes, designated the XB-70-1 and XB-70-2, were built. This investigation was conducted with the XB-70-1. The general configuration and overall dimensions of the XB-70-1 are shown in figure 2. The basic design incorporates a thin, low-aspect-ratio wing with the leading edge swept back 65.57°, folding tips, twin vertical stabilizers, and a movable canard with a trailing-edge flap. The dihedral of the wings of the XB-70-1 is 0°.

Stability Augmentation System

The structural response data presented in this report were obtained with the XB-70-1 stability augmentation system engaged.

The flight augmentation control system (FACS) is a conventional command augmentation system designed to improve handling qualities by operating simultaneously with the hydromechanical column-to-surface control system. A block diagram of the pitch augmentation system is shown in figure 3. Signals from a transducer actuated by pilot inputs are combined with signals from aircraft response sensors (gyro and accelerometer) in the electronics of the FACS to produce mechanical servo displacements. These displacements add to, or subtract from, the pilot' s mechanical inputs at the master cylinder to provide the desired control surface motion without force feedback to the controls. After the pilot' s input and the aircraft' s response signals are modified by the appropriate gains, they are filtered to reduce the transmission of high frequency motions. Then the gain levels are varied according to altitude by the central air data system (CADS) to compensate for changes in control surface effectiveness. Finally, the signals are transmitted to the control surface through the FACS servo. This signal commands the motion of the inboard elevon panel; the motion of this panel, in turn, commands the motion of all the remaining outboard panels (fig. 2). With the wingtips in the 0° position, all five outboard panels are slaved to the inboard panel. In the 25° and 65° wingtip positions, the two outer panels are disengaged and centered, and the three remaining outboard panels are slaved to the inboard panels.

The FACS and its frequency response characteristics are described in detail in reference 3.

Vibration Excitation System

As shown in figure 4, movable aerodynamic vanes, trapezoidal in planform and 0.185 square meter (2 square feet) per panel in area, were mounted on each side of the forward fuselage in front of the pilot' s station. The excitation system was designed to produce a controlled, oscillatory motion of the airplane in flight. The shaker vane system, operational procedures, and safety features are described in detail in appendix A.

INSTRUMENTATION AND RECORDING

The structural response of the airplane to shaker vane excitation was sensed by instrumentation installed for an earlier experiment (ref. 6). Table 1 lists the characteristics of the instrumentation and the parameters recorded. The locations of the accelerometers, which measured the airplane' s response, are shown in figure 5. The parameters used for monitoring the performance of the shaker vane system and the structural integrity of the airplane are listed in table 2.

Onboard flight data were recorded on magnetic tape using either analog or digital techniques, depending on the parameters and their frequency response requirements. The magnetic tape generated by the airborne system was processed by a ground station

computer to convert the data to engineering units. The analog and digital data acquisition systems are described in references 7 and 8.

Strain gages were installed at two locations on the shaker vane system, which is described in appendix A. A bending bridge was installed just inboard of the left vane to measure the vane' s vertical bending moment. An axial strain-gage bridge was installed on the link between the actuator and the center section bellcrank. Both the vane bending bridge and the link axial bridge were part of the automatic safety shutoff system, which protected the shaker vane system from excessive loads. A strain-gage control-position transmitter was installed between the actuating cylinder and the center section bellcrank, and was calibrated to record the rotary displacement of the vanes in degrees.

FLIGHT CONDITIONS

The flight conditions selected for the structural response tests were generally representative of the XB-70 flight envelope (fig. 6). The airplane weights, the location of the center of gravity, and other flight-test conditions are given in table 3.

TEST PROCEDURES

The first tests with the shaker vane were made at low Mach numbers. Because of flight safety restrictions, the tests were performed during wings-level, 1g, trimmed flight in smooth air. The system was not operated during maneuvers or when the airplane was in turbulence.

A flight-test buildup technique was used. A test was started at low vane amplitudes and the vane forcing frequency was gradually increased until the mode being investigated was excited. Each frequency sweep was made at a constant vane amplitude. This technique was used for each Mach number and altitude condition investigated. All the tests were made for a vane amplitude of $\pm 4^\circ$ after it was determined that this angle provided the required response without exceeding safety limits.

During shaker vane operation, the modal frequencies and amplitudes were monitored primarily by the accelerometer at the nose ramp (fig. 5), which was just in front of the cockpit near the shaker vane. The response at this location was also representative of the response at the pilot' s station; thus the telemetered data were indicative of the response experienced by the operator. The acceleration at the nose ramp, along with the other parameters telemetered for ground monitoring of the shaker vane system and the aircraft' s structural integrity, was monitored on strip charts.

Once a mode was defined, structural damping information was obtained. Because of fuel consumption and the associated change in airplane mass, it was necessary to reestablish the mode being investigated. Once excited, the modal frequency was allowed to stabilize. The shaker vane system was then shut down abruptly, and data were recorded until the telemetry indicated that the responses were completely damped out.

ANALYSIS

Although detailed calculations of the response of the XB-70 airplane were made in references 2 to 4, the conditions analyzed were not readily obtained in flight. To compare flight-test results and analytical results, response calculations were made as part of this investigation for the weights, altitudes, and Mach numbers actually tested. These conditions are shown in table 3 for Mach numbers of 0.87, 0.86, and 1.59. The method of analysis, which is based on the methods of reference 2, is described in appendix B. The approach taken to update the early design values of airplane mass and stiffness to the flight-test conditions is explained, and the calculations made to examine the effects of using quasi-steady and unsteady aerodynamics for the wing at subsonic speeds are described. The analytical description of the flight control system used in the analysis is presented in appendix C.

RESULTS AND DISCUSSION

Structural Response

Measured airplane response. – The measured vertical acceleration response due to sinusoidal shaker vane excitation for the flight conditions listed in table 3 is shown in figures 7 to 10 for locations on the fuselage, canard, and wing. The response is presented in terms of g per degree of shaker vane displacement at varying excitation frequencies. Incremental values of acceleration were used for the response. For a given shaker vane displacement, the vane force was constant throughout the frequency range of the tests.

For the heavyweight, Mach 0.87 flight condition, there was considerable scatter in the data for the canard and wing accelerations outboard of BP 7.11 meters (280 inches). Consequently, these data are not shown. Accelerometer output signals indicated that at this flight condition the surfaces were excited by a random force (noise) as well as by the shaker vane force. An investigation (ref. 9) revealed that leading-edge flow separation which had occurred at the canard upper surface was still present at Mach 0.9 and an angle of attack of 4°. Although this unsteady flow was more pronounced at lower Mach numbers, the heavyweight, Mach 0.87 condition was flown at an angle of attack of 5.5° in these tests, and it is believed that separated flow also existed for this flight condition. The flow separation subsided as speed increased or angle of attack decreased. Canard response for the Mach 1.59 flight condition (fig. 9) is not shown because of an instrumentation malfunction.

Calculated airplane response. – In figure 11 the measured vertical accelerometer response at the pilot's station is compared with the response calculated by using the modal solution discussed in reference 3. The calculations were based on early design information on structural stiffness and mass distribution. It was known that these data did not accurately describe the actual airplane. Inaccuracies were particularly pronounced in the airplane mass data, as is evident by comparing the flight weights in table 3 with those used in the analysis (table 4). Further, the measured ground vibration frequencies of the airplane indicated that the actual vehicle was stiffer than calculated by the analyses in reference 3. Because of these marked discrepancies, the calculated responses in figure 11 should more appropriately be considered as early design calculations.

As a consequence of these results, a study was initiated to determine how to reconcile the flight-measured characteristics of a flexible vehicle with the characteristics of an analytical model and to indicate whether it would be possible to predict a flexible flight vehicle's characteristics using state-of-the-art techniques to estimate the mass, structural, and aerodynamic characteristics. The first step was to determine how well the response characteristics of a flexible airplane could be predicted analytically if the best known information were utilized. An analysis of the response characteristics of the XB-70-1 airplane was made which incorporated the increased stiffness shown by the natural frequencies measured in ground vibration tests. The analysis was made first for the lightweight, Mach 0.86 condition, and the results were compared with the flight-measured response reported in reference 4. The better agreement between the measured and calculated response pointed out the improvement possible if more representative airplane characteristics were used. This, in turn, led to a more rigorous vehicle description.

The weight accounting on the airplane was reviewed to determine the total weight and mass distribution for the flight conditions flown. These data, together with the structural mode data measured in ground vibration tests, were used to calculate new structural mode characteristics. The aerodynamics were also updated to reflect all the new information available, including wind-tunnel-test data. The methods used in updating the aerodynamics are described in appendix B.

The revised data were used to analyze the airplane's frequency response at three of the flight conditions listed in table 3: Mach 0.87, 0.86, and 1.59. In figure 12 some of the results of the updated analysis for the pilot's station are compared with the flight-measured response. In both amplitude and frequency, better agreement between the measured and calculated response is apparent than shown in figure 11, which compares flight values with values calculated in the earlier analyses. The best agreement was for the first mode, particularly for the lightweight, Mach 0.86 condition, with the damping of the second-third mode somewhat underestimated for all three flight conditions. In figures 13 to 15 the measured response for fuselage locations other than the pilot's station for the three flight conditions is compared with results from the refined analysis using the quasi-steady aerodynamic theory. In general, the agreement of the calculated response with the flight-measured results was good enough to give confidence that the refined analysis could accurately predict the elastic nature of large, flexible aircraft.

All the flight-measured data presented were obtained with the FACS operating, inasmuch as the airplane was normally operated in this manner. However, it was considered to be of interest to present some of the calculations of the acceleration response of the vehicle without the FACS engaged. These data, which were calculated by using refined data and quasi-steady wing aerodynamic theory, are presented in figures 16 to 18 for the three flight conditions. The difference between modal response with and without the FACS can be seen by comparing these data with data for the same locations in figures 12 to 15. The comparison shows that the FACS reduced the magnitude of the first structural mode to some extent, and occasionally reduced the peak of the second-third mode slightly. For all the conditions analyzed, the FACS appeared to have little or no effect on the damping of the fourth mode. The data also show that the modal frequencies were the same with and without the FACS.

One of the most significant factors studied was the effect of using unsteady wing

aerodynamic theory in the response calculations (appendix B). Only the lightweight, Mach 0.86 condition was analyzed, because unsteady aerodynamics are likely to be more pronounced at this Mach number than at any of the supersonic speed conditions for which flight-test data were available. The results, presented in figure 19 for the pilot's station, show that although the calculated response overestimates the damping of the fourth mode, the amplitude and frequencies of the first and second-third modes were more precisely predicted than with quasi-steady wing aerodynamic theory (fig. 12(b)), particularly for the second-third mode. The effects of using unsteady wing aerodynamics to calculate the response characteristics at other locations on the airplane are presented in figure 20 for the basic vehicle without the FACS and in figure 21 with the FACS. As expected, the use of unsteady wing aerodynamic theory in the analysis resulted in generally lower response levels along the fuselage because the same description of the XB-70 structure (that is, the normal mode form) was used in both the quasi-steady and unsteady aerodynamic analyses. The effect of including unsteady aerodynamics in the calculated response was basically the same with and without the FACS.

It is believed that the lack of significant difference between the results found with quasi-steady and unsteady wing aerodynamic theory makes the use of unsteady aerodynamic theory, with its additional computations, unwarranted for this configuration and frequency range. However, this conclusion may not be valid for other configurations or other types of response analyses.

Damping

The damping of the total airplane in flight is shown in table 5 for each structural mode investigated. Damping data were obtained for heavyweight, Mach 0.87 and lightweight, Mach 0.86 conditions, and for the mediumweight, Mach 1.59 condition. Damping data were not obtained for the Mach 2.38 flight condition because the exact frequencies for the associated modes could not be determined from the telemetered readout in time to set up the proper test condition.

In general, the calculations predicted the damping of the higher structural modes adequately but overpredicted the damping of the lower structural modes at subsonic speeds. Damping was calculated analytically using methods described in appendix B.

CONCLUDING REMARKS

A flight investigation was conducted with the XB-70-1 airplane to measure the low frequency symmetric structural response and damping characteristics of the airplane that resulted from shaker vane excitation at subsonic and supersonic flight conditions. The flight-measured response was compared with the response calculated by using early XB-70 design data and the response calculated by using updated mass, structural, and aerodynamic information.

Although the early design analyses did not accurately predict the values of modal response or frequencies, they did estimate the general response of the airplane. Comparison of the calculated values of modal response with ground vibration test data showed that the analyses significantly underestimated the airplane's stiffness. Adjustment of the data used in the analyses to represent the airplane's actual stiffness

resulted in better predictions of the flight characteristics. Further improvement in the calculated response was realized when an analysis was made using the flight-test mass and structural characteristics of the airplane together with quasi-steady wing aerodynamic theory. For high subsonic speeds, lower response levels were generally realized by using unsteady wing aerodynamic theory in the analysis instead of quasi-steady wing aerodynamic theory; however, for the XB-70-1 configuration, this slight improvement was not believed to justify the increased computational complexity.

Although the flight tests were made with the stability augmentation system engaged, an analysis showed that the system had little effect on the airplane's modal response.

In general, the calculations predicted the damping of the higher structural modes adequately, but overpredicted the damping of the lower structural modes at subsonic speeds.

Flight Research Center,
National Aeronautics and Space Administration,
Edwards, Calif., August 15, 1972.

APPENDIX A

XB-70 VIBRATION EXCITATION SYSTEM

Description

The excitation system used in this study consisted primarily of a vane and torque tube assembly, an exciter drive assembly, and a control panel and amplifier (fig. 22). The vanes were composed of riveted skin and grid assemblies of 3340 stainless steel. Each vane had a span of 0.609 meter (24 inches) with root and tip chords of 0.406 meter (16 inches) and 0.203 meter (8 inches), respectively. The airfoil was symmetrical with 7.5 percent thickness at the root and 10 percent thickness at the tip. The maximum thickness was at 33 percent of the vane mean aerodynamic chord. The vane taper ratio was 2:1. The torque tube, or cross shaft, drove and interconnected the two vanes. The shaft was 0.102 meter (4 inches) in diameter and was fabricated from 4335 steel.

The outboard shaft bearings were supported by beam fittings running between two frames at fuselage stations 8.57 meters (337.50 inches) and 8.24 meters (324.27 inches), respectively. The inboard shaft bearings were supported by fittings adjacent to an existing vertical web. Local reinforcement was provided around the points of attachment of the support fittings and around the shaft cutouts in the fuselage skin.

The exciter vane drive assembly consisted of a hydraulic drive cylinder connected to the vanes through the torque tube. It was powered by one of the aircraft' s hydraulic systems and controlled by an amplifier-valve drive assembly. The drive unit provided a controlled steady-state vane neutral angle, along with a separately controlled sinusoidal input about the vane pitch axis of variable frequency and amplitude (fig. 23). Each of these parameters was varied by the use of calibrated cockpit controls.

If the system' s hydraulic pressure dropped as a result of hydraulic system failure, a check valve in the line to the main actuator held the fluid in the actuator cylinder and prevented loss of the fluid column stiffness. If hydraulic pressure were lost because of check valve failure or if the shaker system shut down, a mechanical lock returned the vanes to a preset trim position and locked them in place (fig. 24). More specifically, a spring-loaded mechanism forced a roller assembly into a V-shaped cam. This provided greater vane pitching restraint than provided by the operating hydraulic system, since it locked the vane shaft into position against rotation. A spring preload was chosen that exceeded the airload-induced torque predicted for any point in the flight envelope. An auxiliary hydraulic actuator acted against the spring force to hold the system in the unlocked position to allow normal operation of the vane.

Performance

The vane excitation system was capable of continuous operation in the frequency range from 0 cps to 8.0 cps. However, to prevent interference with airplane handling qualities, the frequency range was limited to 1.4 cps to 8.0 cps. Vane amplitude was variable from 0° to ±12° on either side of a preselected (no load) vane trim position.

The system was capable of operation up to a Mach number of 2.7, as shown in figure 25, except in the Mach number range from 1.0 to 1.59, where single-degree-of-freedom flutter was predicted.

When not in operation, the vanes were held in a locked position by a mechanical spring force, with the leading edge of each vane at -6° relative to the fuselage reference line. At the start of a test, the vanes were rotated for trim to zero load to a maximum of 5° on either side of the locked position.

Automatic Safety Shutoff

To protect the airplane and shaker system from unexpected vibration amplitudes, a safety system automatically shut off the vane drive system. The system returned the vanes to the preset trim position if preselected levels of forward fuselage vertical acceleration, nose-boom root vertical bending, vane actuator link load, or vane shaft vertical bending were exceeded.

Pilot Controls and Displays

A control and display panel (fig. 26) in the cockpit console area between the two pilots contained the following controls:

Vane frequency control - A rotary knob geared to a linear transformer controlled the rate of vane oscillation. The numerical value of frequency selection was shown in the window of the control to the nearest hundredth. For ease of control, one full rotation of the knob represented a change in frequency selection of 1 cps.

Vane amplitude control - A rotary knob was used to select a percentage of the available rotary movement of the shaker vanes. Maximum (100 percent) knob rotation represented a shaker vane rotation of 12° to either side of the preselected trim position.

Vane incidence angle control - A rotary trim control was used to trim the shaker vanes to a zero load condition at the start of a test. When not in operation, the control was positioned at L, which was the locked vane position with the leading edge of each vane at -6° relative to the fuselage reference line. At the start of a test, the control was rotated to either U or D to move the vane leading edge either up or down to obtain a zero load condition on the vane. Stops limited the knob movement to a maximum of 5° on either side of the locked position, which was adequate to trim the vanes for any flight condition encountered.

Master power switch - All power to the system was off when the master power switch was in the off position, and the vanes were held in the locked position by a mechanical spring force. When the switch was in the L (locked) position, hydraulic power was supplied to the locking cylinder and the vane was held in the locked position by both mechanical and hydraulic force. When the switch was in the on position, hydraulic power was supplied to the auxiliary hydraulic actuator, which moved the system to the unlocked position against the mechanical spring force and allowed normal vane operation. Hydraulic power was also supplied to the main actuating cylinder, and electrical power was supplied to the trim control. The actuating cylinder moved and held the vane at the position indicated by the rotary trim control.

Input switch - When the input switch was in the off position, power was cut off from the frequency and amplitude controls so that they could be preset for a test without causing vane movement. When the switch was in the on position, power was supplied to the amplitude and frequency controls, which, in turn, caused hydraulic power to flow to the actuating cylinder, which moved the vanes.

Emergency shutoff-reset - The reset push button, when depressed, released the latching relay which held the automatic system in the shutoff mode following an automatic shutdown. Pressing the button armed the automatic system for future operation.

The following displays were included on the panel:

Vane trim indicator - The vane trim indicator was activated when the master power switch was in the on position. When zero vane bending load was obtained, the pointer was at 0 and the vanes were trimmed at zero load, which was the trim desired at the beginning of a test. Positions between 0 and U or 0 and D indicated that the vane leading edge was up or down, respectively, relative to the airstream.

Safety shutoff warning load light - The shutoff warning load light indicated that one or more of the four automatic shutdown sensing units had sensed 80 percent of the load or accelerations required to shut the shaker system down. To extinguish the light, the amplitude or frequency settings had to be decreased.

Safety automatic off light - The automatic off light indicated that one or more of the four automatic sensing units had sensed the limiting load or acceleration and that the shaker system was shut down. The vanes were then driven to the preselected trim position. The light stayed on until the reset button was depressed and the vane amplitude or frequency controls were set at values that did not trigger automatic system shutdown.

Laboratory Tests

The shaker vane system was tested in the laboratory mounted on a steel framework to insure structural and system integrity. A vibration test was conducted to determine the natural frequencies, mode shapes, and generalized masses of the system. These results were then used in a theoretical analysis to determine flutter limits.

The system was loaded at a reference point just inboard of the left vane. Loadings were selected that induced shear, bending, and torque loads simultaneously. The loadings simulated critical load conditions, which were predicted for a Mach number of 0.95 and maximum vane angle. During these tests, calibrations and functional checkouts of the shaker system controls and displays were made.

APPENDIX B

ANALYTICAL MODEL OF XB-70 STRUCTURAL RESPONSE

Early Analysis

Predictions of the structural response of the XB-70 airplane were based upon a dynamic model of the airplane which was defined by the selective use of quasi-steady and unsteady aerodynamics. The dynamic model included four primary symmetrical structural modes. The theoretical foundation of the analysis is included in reference 2; however, a brief description of the structural and aerodynamic factors used in the analyses is given in this appendix.

Structures. – The structure of the XB-70 airplane is described in the analytical model of reference 2 in the normal mode form. It was believed that the equations describing the system could be handled more conveniently in this form. Before, the generalized mass and mode shapes of the airplane had been calculated for as many as 14 normal modes over a wide range of weight conditions. Figure 27 shows the grid system for the normal mode sets that were used in the response analyses. Although in theory an infinite number of modes are needed before exact deflections can be obtained if a modal description of an elastic airplane is used, in practice something less is sufficient. Experience showed that four symmetric structural modes provided enough accuracy, so only four modes were used in reference 2.

One flight condition was analyzed for structural mode activity at mode frequencies higher than the four structural modes used in the study of reference 3. To simplify the approach, it was assumed that five additional modes could be represented by equations in which aerodynamic coupling and the effects of aerodynamics on mode frequencies could be ignored. To check these assumptions, calculations were made for a lightweight, Mach 1.40 condition at an altitude of 12,192 meters (40,000 feet).

Vehicle aerodynamics. – The predominant problem in vehicle aerodynamics involves describing the excitation of the total vehicle and its structure in response to atmospheric turbulence or pilot inputs. Of particular importance are the frequency dependence (or unsteadiness) characteristics of the aerodynamics. The flight conditions for which aerodynamic studies were made included the flight conditions listed in table 4. The studies investigated the effects of atmospheric turbulence at high subsonic and supersonic speeds. The generation of aerodynamic data at supersonic speeds was relatively straightforward, because aerodynamic lags were minimal and quasi-steady aerodynamic techniques were believed to be adequate. Furthermore, it was easy to compute the generalized aerodynamic force for the elevon surfaces at supersonic speeds; all the forces generated by elevon deflection were assumed to act on the elevon surface. At subsonic speeds, unsteady aerodynamics were used for the elevons, even though quasi-steady aerodynamics were used for the wing. The aerodynamic approach is described in detail in reference 2.

Analytical model versus air vehicle. – As the design of an aircraft proceeds, the dynamic analysis must be updated to reflect the changes dictated by design compromises. However, the updating is usually incomplete because of its high cost, so that the final

analysis does not represent the airplane that is actually built. For this reason, the data used in the initial analyses of the flexibility of the XB-70 airplane did not accurately represent the flight-test vehicle. For example, the XB-70-1 airplane weighed approximately 24,948 kilograms (55,000 pounds) more than in the original specifications. This additional weight was structural rather than useful load, which resulted in a more rigid vehicle with higher frequencies than predicted. The mass characteristics, however, were monitored and recorded during the flight-test period. The combined effects of mass and structure were checked in ground vibration tests. Additional wind-tunnel data for the rigid airplane integrated aerodynamic characteristics were available over those used in the analysis of reference 3. It remained, however, to reconcile these data with past test data and then put these data in distributed loading form. The distributed form was required in order to obtain the generalized aerodynamic data in the modes because of these rigid body loadings.

In an attempt to generate a more realistic analytical model of the XB-70-1 airplane, a survey was made to determine what data were available and to select appropriate procedures and techniques.

Advanced Analytical Airplane Model

This section describes the characteristics of the XB-70-1 airplane used in the updated analytical studies.

Flight conditions. – Three flight conditions were selected for the refined analysis as being representative of the flights during which vehicle response data were recorded. These conditions are shown in table 3 for Mach numbers of 0.87, 0.86, and 1.59.

Weight distribution. – To obtain mass distribution data that were in agreement with the XB-70 flight conditions, the weight changes made in the vehicle structure were updated. Changes of 22.68 kilograms (50 pounds) or greater for items such as fuel, water, equipment, and ballast were taken into account in the data used in the design analyses. The disposition of these items was determined at the exact time in flight that the other parameters were recorded. These data were determined from flight records of the total airplane weight, the location of the center of gravity, the moments of inertia, and the fuel remaining in each tank. The fuel weight was distributed in a grid system that was compatible with that used in processing the ground vibration test data. Weight was also distributed to specific control points as required by the structural mode calculations. These new mass characteristics were used to obtain a set of mode shapes, frequencies, and generalized masses for the vibration modes of the entire vehicle.

Structures. – New structural mode data were determined which reflected the vehicle weight for the three flight conditions selected for analysis. The original symmetric, orthogonalized, measured ground vibration test modal data were used as the basis for the new technique of modal vibration analysis which became necessary. The original ground vibration tests were conducted for a condition of zero fuel and wingtip positions of 25° and 65°. The tests were performed with the vehicle mounted on soft spring air pillows through the landing gear. A digital computer program was used to remove the influence of the mounting constraints and to determine modal characteristics for a number of fuel loads, specifically, 5 percent, 52 percent, and 100 percent of fuel loading capability. These shake-test-based modes gave indications of providing a much better

description of the vehicle than the analytical description in reference 3. The ground-measured natural frequencies and generalized masses defined the structural stiffness of the basic vehicle.

New equations of motion were written to determine the modal characteristics that existed with the three actual fuel loadings. These equations included a mass matrix which had off diagonal, or mass coupling, terms reflecting the fuel loading. An eigenvalue solution of the new equations of motion resulted in the definition of new free-free mode shapes, natural frequencies, and generalized masses. The new shapes were defined in a 97-point grid system which corresponded to the ground vibration test control points. Data were calculated for nine wing-fuselage modes, four canard modes, and three vertical stabilizer modes. These data were, in turn, interpolated and re-normalized for a grid system with 118 control points. Only the wing-fuselage modes were converted to the 118 control point system. All response calculations were based on data derived from the 118 control point set of modal data.

The 97 and 118 control point grid systems are described in detail in reference 10. Corresponding structural frequencies, generalized masses, and tabulated data descriptions of the mode shapes are also presented.

Aerodynamics. – The change with angle of attack of data for the aerodynamic force, moment, and distributed load of the rigid vehicle was reevaluated with respect to all available wind-tunnel data. The reevaluation showed that no change in the data used in the analyses of reference 3 was required. Although there were no changes in distributed loads with angle of attack, aerodynamic derivative data from reference 3 are different from those shown herein because of differences in the location of the center of gravity and the characteristics of the mode shapes. Aside from these differences, the 25° wingtip configuration data used in reference 3 had been assumed to be equivalent to the zero tip deflection data of reference 2. Actual 25° wingtip configuration data were used in the present analysis.

The main change in aerodynamic force, moment, and distributed load data for the rigid vehicle was associated with the elevons. The data used in the reference 3 analyses assumed that elevon gaps had no effect on the aerodynamics. More complete elevon test data revealed that these gaps significantly affected control effectiveness. The analysis of the present study included these new data.

Because of the structural mode shapes, the high subsonic quasi-steady aerodynamics of the wing were determined by using a lifting surface theory (vortex lattice, based on ref. 11). The corresponding data in reference 3 were determined by using a modified strip theory. Similar wing data at a Mach number of 1.59 were also determined by using lifting surface theory (Etkin Mach box, refs. 12 and 13). This approach does not take into account the wingtip deflection when determining mutual interference effects between Mach boxes. In effect, the structural deformations are referenced to a flat plane. Once the aerodynamic loading due to mode shape was determined for the wing with the flat plane as a reference, the loading on the deflectable tip was isolated. Because the tip was deflected 65° at a Mach number of 1.59, the component of the tip load due to structural deformation in the vertical plane was determined through the cosine relationship with the vertical axis. In this way it was possible to compute the tip contributions to the total normal force and the moment due to the mode shape.

To determine the effect of calculating the response characteristics of the wing by using unsteady aerodynamic theory, data were obtained for the lightweight, M = 0.86 flight condition. Unsteady aerodynamics are likely to be more pronounced at this Mach number than at any of the supersonic speed conditions for which flight-test data were available. For this reason, the Mach 0.86 condition was studied. A digital program based on the theory of reference 14 was used.

The aerodynamics of the elevons at the high subsonic conditions were unsteady for both the heavyweight and lightweight cases. Modified subsonic strip theory was used in accordance with the method explained in reference 2. The zero frequency (quasi-steady) elevon force, moment, and generalized modal force coefficients were ratioed to the force, moments, and generalized modal force coefficients obtained by using the previously mentioned rigid air vehicle data and load distributions. The elevon data at Mach 1.59 were quasi-steady. The structural generalized force coefficients for these data were computed by using pressure distributions based on static wind-tunnel data.

All aerodynamic data used in the present analysis are included in reference 10.

Elevon response analyses. – The analytical model of the FACS is described in appendix C, in which the numerical details of the system used in this study for the high subsonic and Mach 1.59 conditions are explained.

In the digital program that was used to obtain frequency responses with the FACS operating, there was no automatic way to coordinate the magnitude of elevon response with the amplitude characteristics of the nonlinear system dynamics. Consequently, an iterative scheme was used. If the assumed elevon amplitudes did not agree with assumed system dynamics, a new estimate was made and the elevon response was recalculated. This technique was used to obtain the results presented in this report. However, completely converged solutions were not always obtained because of the computer time required.

The frequency response of the outboard elevons due to inboard elevon deflection is shown in figure 28. The solid curves are constructed from data presented in reference 3. They do not connect points of equal inboard elevon deflection as in reference 3, but, rather, pass through points of various inboard elevon deflections at the indicated frequencies. The inboard elevon deflections used to construct these curves were obtained from flight-test results. The curves were used to start the iterative process discussed previously.

The dashed curves are estimates that best represent flight-measured quantities obtained by using the above described iterative technique. Only amplitude data could be obtained accurately from flight records. The phase characteristics were estimated by using the described iterative procedure that produced the best agreement between measured and computed amplitude characteristics.

Table 6 compares flight-test data and analytical data obtained from the study at several points in the control system as well as at the pilot's station. These data justify the dashed-line data in figure 28, since they provide the best analytical agreement with flight data. Because the solid-line data are based on ground vibration test measurements, it can be inferred that flight aerodynamic loads or some unidentified influences

changed the frequency response characteristics of the system.

Control-surface responses. – The calculated frequency response of elevon action due to the operation of the flight augmentation control system per unit shaker vane input is shown in figures 29 to 31 for Mach numbers of 0.87, 0.86, and 1.59. As indicated in the description of the FACS operation, the FACS servo drives the inboard elevon and the motion of the inboard elevon activates the remaining elevon panels. For the flight conditions analyzed, panels 2 to 4 were activated, since the wingtips were deflected and the two outer panels were disengaged and centered. Because of the inboard and outboard panel arrangement, it was most convenient to monitor the inboard and outboard elevon motion separately in the analyses.

Structural mode damping. – When a dynamic system is lightly damped, the technique of reference 15, as expanded in reference 16, provides a useful analytical means of obtaining the damping (structural plus aerodynamic) in each structural mode. The technique makes it necessary to evaluate the dynamic system characteristic determinant in the form of phase angle as a function of the forcing frequency. By plotting the data as shown in the adjacent sketch (only one structural mode is shown), it is possible to obtain enough information graphically to determine the total damping. The natural mode frequency, ω_i, and the phase angle slope with frequency, $\frac{d\varphi}{d\omega}$, at the natural frequency are required. From the characteristic equation,

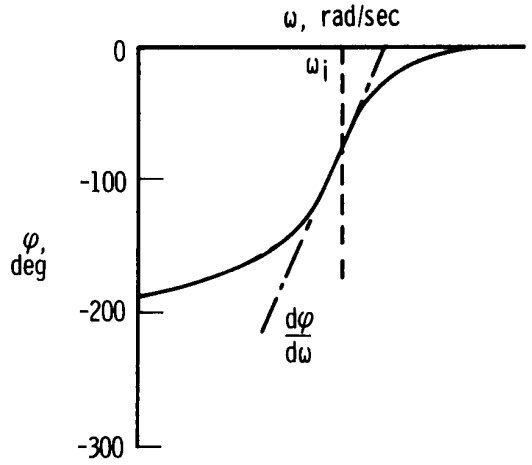

$$\sigma_i = 57.3 \frac{d\omega}{d\varphi}$$

where σ_i is the real part of the root of the characteristic equation as in $(s + \sigma_i \pm i\omega_i)$ and

$$g_i = \frac{2\sigma_i}{\omega_i}$$

which has the same form as structural damping, g_{s_i}.

The structural mode damping data determined from these studies are presented in table 7.

Symmetric structural mode characteristics. – The control point geometry for the 97 point ground vibration test (GVT) modal data is shown in figure 32. The similar control point geometry for the 118 point modal data is given in figure 27. Point 93 in the 97 point GVT grid set is the normalizing point; point 118 is the normalizing point for the 118 point grid set.

The modal data for the 118 point grid were obtained by interpolating from the 97 point GVT grid and renormalizing to point 118 from point 93. Linear interpolation between points was used; however, the interpolation scheme separated the wing surface from the elevon surfaces. Consequently, lines were not faired across the elevon hinge line. The change to the 118 point grid system was made because most existing XB-70 aerodynamic digital programs utilized this larger grid system, and it was judged to be more efficient to use the existing programs than to reprogram to a 97 point grid system. The existing digital programs use only deflection data; mode slope data are determined from internal curve fit routines. Because the linear interpolation scheme can sometimes distort slopes, slope data required for other than aerodynamic purposes were obtained manually. The 118 point data presented contain only those modes that are primarily wing-body modes in the 97 point grid system. These modes are identified in table 8 for the heavyweight, lightweight, and mediumweight mode sets. Modal frequencies and generalized masses are also presented.

APPENDIX C

ANALYTICAL DESCRIPTION OF FLIGHT AUGMENTATION CONTROL SYSTEM

Two sets of transfer functions were used in describing the analytical model for the FACS. The first set described the motion of the inboard elevon, and the second set described the motion of the remaining three elevon segments. In the following analysis these transfer functions are developed in the format presented in tables 9 to 11, which present the actual numerical values used for the flight conditions analyzed. The development is general, but the specific numerical data used as an example are for the mediumweight, Mach 1.59 condition.

The inboard elevon deflection is

$$\delta_1 = \left[\left(\frac{10}{s+10}\right)\left(\frac{2500}{s^2 + 2(0.6)50\,s + 2500}\right)\left(\frac{10}{s+10}\right)\right] K_{h_p}\left(K_{n_z} n_{z_{FACS}} + K_q q_{gyro}\right)$$

$$\delta_1 = K_{h_p}\left[\frac{2.5\times10^5}{(s+10)^2(s+30\pm i40)}\right]\left(K_{n_z} n_{z_{FACS}} + K_q q_{gyro}\right)$$

Substituting for n_z and gyro in terms of modal characteristics,

$$\delta_1 = K_{h_p}\left[\frac{2.5\times10^5}{(s+10)^2(s+30\pm i40)}\right]\left[-K_{n_z}\frac{V_o}{g}(s)\alpha + \left(K_{n_z}\frac{l}{g}s + K_{n_z}\frac{V_o}{g} + K_q\right)q - \sum\left(K_{n_z}\frac{\varphi_i}{g}s^2 + K_q\varphi_i' s\right)\eta_i\right]$$

where

$K_{h_p} = 0.62$

$K_{n_z} = 0.104$ rad/g units

$K_q = 2.4$ rad/rad/sec

$V_o = 470.91$ m/sec (1545 ft/sec)

$l = 7.92$ m (26 ft)

φ_i, φ_i' from table 12 (FS 32.61 m (1284 in.))

Thus

$$\delta_1 = 0.62\left[\frac{2.5\times10^5}{(s+10)^2(s+30\pm i40)}\right]\left\{-0.104\left(\frac{470.91}{9.81}\right)(s)\alpha+\left[0.104\left(\frac{7.92}{9.81}\right)s+0.104\left(\frac{470.91}{9.81}\right)+2.4\right]q\right.$$

$$-\left[0.104\left(\frac{-0.420}{9.81}\right)s^2+2.4(0)\,s\right]\eta_1$$

$$-\left[0.104\left(\frac{0.025}{9.81}\right)s^2+2.4(0.00252)s\right]\eta_2$$

$$-\left[0.104\left(\frac{-0.190}{9.81}\right)s^2+2.4(-0.0961)s\right]\eta_3$$

$$-\left[0.104\left(\frac{-0.0045}{9.81}\right)s^2+2.4(-0.00236)s\right]\eta_4$$

$$\left.-\left[0.104\left(\frac{-0.110}{9.81}\right)s^2+2.4(0.0236)s\right]\eta_5\right\}$$

Therefore

$$\delta_1 = 0.62\left[\frac{\textcircled{1}\quad 2.5\times10^5}{(s+10)^{\textcircled{2}2}(s+30\pm i40)^{\textcircled{3}}}\right]\left[\textcircled{4}\textcircled{5}-4.79(s)\alpha+\textcircled{6}0.081(s+\textcircled{7}87.9)q\right.$$

$$+\,\textcircled{8}\textcircled{9}\textcircled{10}0.00453(s)(s+0)\eta_1$$

$$-\,\textcircled{11}\textcircled{12}\textcircled{13}0.000264(s)(s+22.8)\eta_2$$

$$+\,\textcircled{14}\textcircled{15}\textcircled{16}0.00205(s)(s+112)\eta_3$$

$$+\,\textcircled{17}\textcircled{18}\textcircled{19}0.0000492(s)(s+113)\eta_4$$

$$\left.+\,\textcircled{20}\textcircled{21}\textcircled{22}0.00118(s)(s-46.4)\eta_5\right]$$

In U.S. Customary Units these expressions are as follows:

$$\delta_1 = 0.62\left[\frac{2.5\times10^5}{(s+10)^2(s+30\pm i40)}\right]\left\{-0.104\left(\frac{1545}{32.2}\right)(s)\alpha+\left[0.104\left(\frac{26}{32.2}\right)s+0.104\left(\frac{1545}{32.2}\right)+2.4\right]q\right.$$

$$-\left[0.104\left(\frac{-0.420}{32.2}\right)s^2+2.4(0)s\right]\eta_1$$

$$-\left[0.104\left(\frac{0.025}{32.2}\right)s^2+2.4(0.00077)s\right]\eta_2$$

$$-\left[0.104\left(\frac{-0.190}{32.2}\right)s^2+2.4(-0.0293)s\right]\eta_3$$

$$-\left[0.104\left(\frac{-0.0045}{32.2}\right)s^2+2.4(-0.00072)s\right]\eta_4$$

$$\left.-\left[0.104\left(\frac{-0.110}{32.2}\right)s^2+2.4(0.0072)s\right]\eta_5\right\}$$

Therefore

$$\delta_1 = 0.62\left[\frac{\textcircled{1}\ 2.5\times10^5}{\textcircled{2}\ (s+10)^2\ \textcircled{3}\ (s+30\pm i40)}\right]\left[\textcircled{4}\textcircled{5}-4.79(s)\alpha+\textcircled{6}\ 0.081(s+\textcircled{7}\ 87.9)q\right.$$

$$+\ \textcircled{8}\textcircled{9}\ 0.00138(s)(s+\textcircled{10}\ 0)\eta_1$$

$$-\ \textcircled{11}\ \textcircled{12}\ 0.000082(s)(s+\textcircled{13}\ 22.8)\eta_2$$

$$+\ \textcircled{14}\ \textcircled{15}\ 0.000626(s)(s+\textcircled{16}\ 112)\eta_3$$

$$+\ \textcircled{17}\ \textcircled{18}\ 0.000015(s)(s+\textcircled{19}\ 113)\eta_4$$

$$\left.+\ \textcircled{20}\ \textcircled{21}\ 0.000361(s)(s-\textcircled{22}\ 46.4)\eta_5\right]$$

The circled numbers are keyed to the data in table 10(a), which presents the computer printout of this data used in the analyses.

The outboard elevon deflection transfer function is the same as the transfer function for the inboard elevon except for an additional lag function, $\frac{20}{s + 20}$:

$$\delta_{2-4} = 0.62\left[\frac{5 \times 10^6}{(s + 10)^2(s + 20)(s + 30 \pm i40)}\right]\left[-4.79(s)\alpha + 0.081(s + 87.9)q\right.$$

$$+ 0.00453(s)(s + 0)\eta_1$$

$$- 0.000264(s)(s + 22.8)\eta_2$$

$$+ 0.00205(s)(s + 112)\eta_3$$

$$+ 0.0000492(s)(s + 113)\eta_4$$

$$\left. + 0.00118(s)(s - 46.4)\eta_5\right]$$

In U.S. Customary Units this expression is as follows:

$$\delta_{2-4} = 0.62\left[\frac{5 \times 10^6}{(s + 10)^2(s + 20)(s + 30 \pm i40)}\right]\left[-4.79(s)\alpha + 0.081(s + 87.9)q\right.$$

$$+ 0.00138(s)(s + 0)\eta_1$$

$$- 0.000082(s)(s + 22.8)\eta_2$$

$$+ 0.000626(s)(s + 112)\eta_3$$

$$+ 0.000015(s)(s + 113)\eta_4$$

$$\left. + 0.000361(s)(s - 46.4)\eta_5\right]$$

Table 10 presents the numerical data that describe the FACS for the mediumweight, Mach 1.59 condition. Tables 11 and 12 present similar data for the heavyweight, Mach 0.87 and lightweight, Mach 0.86 conditions, respectively.

It should be noted that the value of l used in this analysis (7.92 meters (26 feet)), is from the early XB-70 design analysis, when the FACS accelerometer was at FS 29.82 meters (1174 inches). During this investigation the FACS accelerometer was moved to FS 32.61 meters (1284 inches), so the actual value of l was 10.72 meters (35.18 feet). Thus the calculated elevon deflections should be considered to be nominal, although the effect of the discrepancy on the calculated results is small.

REFERENCES

1. Kordes, Eldon E.; and Love, Betty J.: Preliminary Evaluation of XB-70 Airplane Encounters With High-Altitude Turbulence. NASA TN D-4209, 1967.

2. Wykes, John H.; and Mori, Alva S.: An Analysis of Flexible Aircraft Structural Mode Control. Tech. Rep. AFFDL-TR-65-190, Part I, Wright-Patterson AFB, U. S. Air Force, June 1966.

3. Wykes, John H.; Nardi, Louis U.; and Mori, Alva S.: XB-70 Structural Mode Control System Design and Performance Analyses. North American Rockwell Corp. (NASA CR-1557), 1970.

4. Wykes, John H.; and Kordes, Eldon E.: Analytical Design and Flight Tests of a Modal Suppression System on the XB-70 Airplane. Part 1: Design Analysis. Part 2: Flight Tests. Aeroelastic Effects From a Flight Mechanics Standpoint, AGARD Conf. Proc. No. 46, Mar. 1970, pp. 23-1 - 23-18.

5. Mechtly, E. A.: The International System of Units - Physical Constants and Conversion Factors. NASA SP-7012, 1969.

6. Wilson, Ronald J.; Love, Betty J.; and Larson, Richard R.: Evaluation of Effects of High-Altitude Turbulence Encounters on the XB-70 Airplane. NASA TN D-6457, 1971.

7. Edwards, E. L.: A Data Processing Facility for the XB-70 Flight Test Program. Flight Test Instrumentation, AGARD Conf. Proc. No. 32, 1967, pp. 243-258.

8. Ince, D. B.: Application Experience With the B-70 Flight Test Data System. Aerospace Instrumentation. Vol. 4 - Proceedings of the Fourth International Aerospace Symposium, College of Aeronautics, Cranfield, Eng., March 21-24, 1966, M. A. Perry, ed., Pergamon Press, Ltd., 1967, pp. 195-208.

9. Jenkins, Jerald M.; DeAngelis, V. Michael; Friend, Edward L.; and Monaghan, Richard C.: Flight Measurements of Canard Loads, Canard Buffeting, and Elevon and Wing-Tip Hinge Moments on the XB-70 Aircraft Including Comparisons With Predictions. NASA TN D-5359, 1969.

10. Wykes, John H.; and Mori, Alva S.: XB-70 Aerodynamic, Geometric, Mass, and Symmetric Structural Mode Data. North American Aviation, Inc. (NASA CR-116773), 1970.

11. Falkner, V. M.: The Calculation of Aerodynamic Loading on Surfaces of Any Shape. R & M No. 1910, British A. R. C., 1943.

12. Etkin, Bernard; and Woodward, Frank A.: Lift Distribution on Supersonic Wings With Subsonic Leading Edges and Arbitrary Angle of Attack Distribution. J. Aeron. Sci., vol. 21, no. 11, Nov. 1954, pp. 783-785.

13. Etkin, Bernard: Lift Distribution on Warped Supersonic Wings. Can. Aeron. J., vol. 1, no. 1, Apr. 1955, pp. 16-20.

14. Watkins, C. E.; Woolston, D. S.; and Cunningham, H. J.: A Systematic Kernel Function Procedure for Determining Aerodynamic Forces on Oscillating or Steady Finite Wings at Subsonic Speeds. NASA TR R-48, 1959.

15. Landahl, Marten T.: Graphical Technique for Analyzing Marginally Stable Dynamic Systems. J. Aircraft, vol. 1, no. 5, Sept.-Oct. 1964, pp. 293-299.

16. Siegel, Sidney; and Andrew, Lowell V.: Evaluations of Methods To Predict Flutter of Wings With External Stores. Tech. Rep. AFFDL-TR-69-101, Wright-Patterson AFB, U.S. Air Force, May 1970.

TABLE 1 - CHARACTERISTICS OF THE XB-70 INSTRUMENTATION

Parameter	Transducer		System resolution	Accuracy, percent full range	Sample rate, sample/sec	Location					
	Type	Range				Fuselage station, m (in.)		Butt plane, m (in.)		Waterplane, m (in.)	
Airplane basic data -											
Nose-boom angle of attack:	Angle of attack and sideslip sensor										
High response		0° to 8.0°	0.0087°	0.8	40	2.308	(91.875)	0.152	(6.0)	0.508	(20.0)
Low response		-10° to 30.0°	.0435°	.8	40	2.308	(91.875)	.152	(6.0)	.508	(20.0)
True velocity	Airplane electrical system	66 knots to 1632 knots	+1.702 knots	[1].1	40	------	---------	-----	-----	------	-----
Angle of pitch at center of gravity	Attitude gyro	-10.45° to 35.3°	±.0497°	2.0	40	41.58	(1637.0)	-----	-----	------	-----
Rate of pitch at center of gravity	Rate gyro	±5.33 deg/sec	±.0116 deg/sec	2.0	40	35.54	(1399.0)	-----	-----	------	-----
Rate of yaw at center of gravity	Rate gyro	±5.7 deg/sec	±.0124 deg/sec	2.0	20	35.66	(1404.0)	.406	(16.0)	-1.626	(-64.0)
Rate of roll at center of gravity	Rate gyro	±21.66 deg/sec	±.047 deg/sec	2.0	20	35.66	(1404.0)	.406	(16.0)	-1.626	(-64.0)
Left elevon position at inboard actuator	Position transmitter	±30.0°	±.0652	1.2	20	------	---------	-----	-----	------	-----
Right elevon position at inboard actuator	Position transmitter	±30.0°	±.0652	1.2	20	------	---------	-----	-----	------	-----
Outside air temperature, total:	Temperature sensing probe										
Low range		218° K to 433° K (-67° F to 320° F)	±.234° K (±.042° F)	1.2	4	------	---------	-----	-----	------	-----
High range		422° K to 650° K (300° F to 711° F)	±.248° K (±.45° F)	1.2	4	------	---------	-----	-----	------	-----
Nose-boom pressure:	Absolute pressure transducer										
Total		0 N/m^2 to 206.843 N/m^2 (0 psia to 30 psia)	224.8 N/m^2 (.0326 psia)	.05	20	------	---------	-----	-----	------	-----
Static		0 N/m^2 to 110.316 N/m^2 (0 psia to 16 psia)	119.9 N/m^2 (.0174 psia)	.05	20	------	---------	-----	-----	------	-----
Altitude:	Airplane subsystem										
Coarse		-304.8 m to 30.480 m (-1000 ft to 100,000 ft)	33.5 m (109.8 ft)	2.0	40	------	---------	-----	-----	------	-----
Fine		1524 m/revolution (5000 ft/revolution)	1.66 m/revolution (5.43 ft/revolution)	2.0	40	------	---------	-----	-----	------	-----
Airspeed:	Airplane subsystem										
Coarse		50 knots to 800 knots	.815 knot	2.0	40	------	---------	-----	-----	------	-----
Fine		70 knots/revolution	.076 knot/revolution	2.0	40	------	---------	-----	-----	------	-----
Mach number:	Airplane subsystem										
Coarse		Mach 5 to 3.2	Mach 0.0029	2.0	40	------	---------	-----	-----	------	-----
Fine		Mach 0.3/revolution	Mach 0.00033/revolution	2.0	40	------	---------	-----	-----	------	-----
Vertical airplane response -											
Normal acceleration:											
At nose	Accelerometer	±2.84g	±0.0062g	2.0	40	4.95	(194.75)	-----	-----	------	-----
At pilot station	Accelerometer	±3.0g	±.0065g	2.0	40	11.12	(438.00)	0.305	(12.0)	0.914	(36.0)
Near center of gravity	Accelerometer	±1.37g	±.00298g	2.0	40	37.72	(1485.0)	.279	(11.0)	-1.803	(-71.0)
At center of gravity	Accelerometer	-1.0g to 3.0g	±.00435g	2.5	40	41.99	(1653)	-----	-----	------	-----
At left wing	Accelerometer	±5.88g	±.01275g	2.0	40	46.23	(1820.0)	9.53	(375.0)	------	-----
At right wing	Accelerometer	±6.40g	±.014g	2.0	40	46.23	(1820.0)	9.53	(375.0)	------	-----
At left wing	Accelerometer	±6.44g	±.014g	2.0	40	55.17	(2172.0)	9.53	(375.0)	------	-----
At right wing	Accelerometer	±6.81g	±.0148g	2.0	40	55.17	(2172.0)	9.53	(375.0)	------	-----
At left wing	Accelerometer	-1.0g to 3.0g	±.00435g	2.5	40	56.18	(2212)	7.11	(280)	------	-----
At right wing	Accelerometer	-1.0g to 3.0g	±.00435g	2.5	40	56.18	(2212)	7.11	(280)	------	-----
At left wingtip	Accelerometer	±9.24g	±.021g	2.0	40	55.88	(2200.0)	13.21	(520.0)	------	-----
At mixer bay	Accelerometer	-1.2g to 3.2g	±.0048g	2.0	40	51.70	(2035.5)	-----	-----	------	-----
Left canard	Flutter vibrometer	±5.0g	--------	2.5	--	15.19	(598)	[2]4.32	(170)	------	-----
Right canard	Flutter vibrometer	±5.0g	--------	2.5	--	15.70	(618)	[2]4.32	(170)	------	-----

[1] Mach 0.1.

[2] Canard horizontal station.

TABLE 2 - CHARACTERISTICS OF THE SHAKER VANE INSTRUMENTATION AND PERFORMANCE AND MONITORING PARAMETERS

Parameter	Transducer			Location	
	Type	Range	Accuracy, percent of full range	Fuselage station, m (in.)	Butt plane, m (in.)
Normal flutter -					
Left wing	Flutter vibrometer	±0.3810 m/sec (±15 in/sec)	2.5	46.23 (1820)	9.53 (375)
Left wing	Flutter vibrometer	±.3810 m/sec (±15 in/sec)	2.5	55.17 (2172)	9.53 (375)
Right wing	Flutter vibrometer	±.3810 m/sec (±15 in/sec)	2.5	55.17 (2172)	9.53 (375)
Left wing[1]	Flutter vibrometer	±1.537 m/sec (±60.5 in/sec)	2.5	55.88 (2200)	12.06 (475)
Left canard[1]	Flutter vibrometer	±5.0g	2.5	15.70 (618)	[3]4.32 (170)
Lateral flutter -					
Left vertical	Flutter vibrometer	±.5080 m/sec (±20 in/sec)	2.5	58.09 (2287)	[4]4.17 (164)
Right vertical	Flutter vibrometer	±.5080 m/sec (±20 in/sec)	2.5	58.09 (2287)	[4]4.17 (164)
Left vertical[1]	Flutter vibrometer	±.5080 m/sec (±20 in/sec)	2.5	58.88 (2318)	[4]4.17 (164)
Right vertical	Flutter vibrometer	±.5080 m/sec (±20 in/sec)	2.5	58.88 (2318)	[4]4.17 (164)
Vertical acceleration - nose ramp strut[1,2]	Piezeolectric vibration accelerometer	±3.0g	2.5	7.43 (292.5)	---- ----
Exciter vane -					
Position	Position transmitter	±12.0°	2.0	----- -----	---- ----
Shaft vertical bending[2]	Bonded strain gage	±5085 mN (±45,000 in-lb)	2.5	----- -----	---- ----
Actuator link load[2]	Bonded strain gage	±1723.7 kg (±3,800 lb)	2.5	----- -----	---- ----
Nose-boom vertical bending[1,2]	Bonded strain gage	±153,752,925 N/m^2 (±22,300 psi)	2.5	3.25 (128.0)	---- ----

[1]Telemetered data.

[2]Shaker vane automatic shutdown parameter.

[3]Canard horizontal station.

[4]Vertical fin station.

TABLE 3 - FLIGHT-TEST CONDITIONS

Mach number	Altitude, m (ft)	Weight, kg (lb)	True velocity, knots	Dynamic pressure, N/m^2 (lb/ft^2)	Wingtip position, deg	Center-of-gravity location, m (in.)
0.87	7620 (25,000)	Heavy, 195,680 (431,400)	521	19,727 (412)	25	FS 40.3 (1585.4)
0.86	7620 (25,000)	Light, 147,417 (325,000)	515	19,248 (402)	25	FS 40.6 (1598.1)
1.59	11,918 (39,100)	Medium, 172,184 (379,600)	909	34,522 (721)	65	FS 40.3 (1586.8)
2.38	18,898 (62,000)	Medium, 163,974 (361,500)	1365	25,999 (543)	65	FS 40.5 (1594.8)

TABLE 4 - CONDITIONS OF REFERENCE 3 ANALYSIS

Mach number	Altitude, m (ft)	Weight, kg (lb)	Wingtip position, deg	Center-of-gravity location, m (in.)
0.90	7620 (25,000)	Heavy (100 percent fuel), 245,847 (542,000)	25	40.6 (1598.3)
0.90	7620 (25,000)	Light (5 percent fuel), 104,780 (231,000)	25	41.05 (1616.5)
1.60	12,192 (40,000)	Medium (55 percent fuel), 178,715 (394,000)	65	40.55 (1596.4)
2.40	19,507 (64,000)	Medium (47 percent fuel), 166,922 (368,000)	65	39.91 (1571.1)
3.00	21,336 (70,000)	Medium (55 percent fuel), 178,715 (394,000)	65	40.55 (1596.4)

TABLE 5 - TOTAL DAMPING OF THE XB-70 AIRPLANE

Condition	Mode	Damping, percent critical	
		Calculated	Measured
Heavyweight, M = 0.9 [0.87],[1] h_p = 7620 m (25,000 ft)	1	8.0	4.4
	2	11.5	4.2
	3	2.4	2.7
	4	2.4	2.5
Lightweight, M = 0.9 [0.86], h_p = 7620 m (25,000 ft)	1	13.9	2.9
	2	14.1	---
	3	2.4	2.9
	4	2.8	6.4
Mediumweight, M = 1.6 [1.59], h_p = 12,192 m (40,000 ft) [11,918 m (39,100 ft)]	1	----	3.3
	2	----	---
	3	----	3.0
	4	----	---
Mediumweight, M = 3.0 h_p = 21,336 m (70,000 ft)	1	5.0	---
	2	1.1	---
	3	2.0	---
	4	2.0	---

[1] Actual flight conditions in brackets.

TABLE 6 - COMPARISON OF FLIGHT-MEASURED AND CALCULATED CONTROL SYSTEM PERFORMANCE WITH FACS INPUT FOR $\delta_{sv} = \pm 4°$

Parameter	Heavyweight, M = 0.80 to 0.90, h_p = 7620 m (25,000 ft), δ_t = 25°		Lightweight, M = 0.80 to 0.90, h_p = 7620 m (25,000 ft), δ_t = 25°				Mediumweight, M = 1.59, h_p = 11,918 m (39,100 ft), δ_t = 65°			
	Mode 1, f = 2.2 cps		Mode 1, f = 2.4 cps		Modes 2, 3, f = 5.6 cps		Mode 1, f = 2.4 cps		Modes 2, 3, f = 5.0 cps	
	Flight	Calculated	Flight	Calculated	Flight	Calculated	Flight	Calculated	Flight	Calculated
$(\Delta n_z)_P$, g	±0.15	±0.13	±0.14	±0.116 [1][±0.095]	±0.18	±0.204 [1][±0.156]	±0.30	±0.251	±0.22	±0.316
$(\Delta n_z)_{FACS}$, g	-----	-----	±.05	±.038	±.10	±.076	±.10	±.085	±.07	±.052
δ_1, deg	0+	±.053	0+	±.045	0+	±.032	±.22	±.122	±.05	±.076
δ_2, deg	0+	±.043	0+	±.035	0+	±.015	±.12	±.097	0+	±.039

[1]Calculated by using unsteady wing aerodynamic theory.

TABLE 7 - STRUCTURAL MODE DAMPING OF THE XB-70

$$\left[g_i = \frac{2\sigma_i}{\omega_i}\right]$$

Mode	Heavyweight, M = 0.87, h_p = 7620 m (25,000 ft), δ_t = 25°		Lightweight, M = 0.86, h_p = 7620 m (25,000 ft), δ_t = 25°				Mediumweight, M = 1.59, h_p = 11,918 m (39,100 ft), δ_t = 65°	
	g_i	σ_i	g_i	σ_i	Unsteady aerodynamics g_i	Unsteady aerodynamics σ_i	g_i	σ_i
Without FACS								
1	0.161	1.150	0.184	1.430	0.192	1.510	0.122	0.890
2	.159	1.910	.185	2.290	.187	2.290	.082	1.040
3	.046	.716	.044	.795	.057	1.042	.041	.682
4	.072	1.510	.083	1.910	.097	2.280	-----	-----
With FACS								
1	0.193	1.365	0.174	1.365	0.203	1.640	0.103	0.763
2	.159	1.910	.178	2.210	.193	2.390	.090	1.145
3	.052	.810	.049	.885	.062	1.125	.049	.820
4	.068	1.435	.083	1.910	.106	2.490	-----	-----

TABLE 8 - XB-70 SYMMETRIC FREE-FREE VACUUM VIBRATION MODE CHARACTERISTICS

Mode number		Mode description	Frequency, cps		
118 point grid	97 point grid		Heavyweight, M = 0.87	Lightweight, M = 0.86	Mediumweight, M = 1.59
1	1	Wing-fuselage 1	2.3270	2.4868	2.3704
2	2	Wing-fuselage 2	3.6003	3.7357	3.7799
3	3	Wing-fuselage 3	5.1360	5.7760	5.2933
-	4	Vertical stabilizer 1	6.0086	6.1068	5.8821
4	5	Wing-fuselage 4	6.6645	7.3332	6.9633
5	6	Wing-fuselage 5	7.9809	8.5870	7.5398
-	7	Canard 1	9.4910	9.6967	8.9335
6	8	Wing-fuselage 6	10.2304	10.8087	11.0415
7	9	Wing-fuselage 7	14.8350	15.3600	16.2104
8	10	Wing-fuselage 8	19.6666	20.3424	19.1179
-	11	Vertical stabilizer 2	22.1393	22.6182	23.0056
9	12	Wing-fuselage 9	24.6532	24.9361	25.2822
-	13	Canard 2	26.3977	26.6771	26.1689
-	14	Vertical stabilizer 3	26.7159	27.0232	26.6156
-	15	Canard 3	40.3124	40.3783	40.8039
-	16	Canard 4	52.0627	52.0642	52.8775

TABLE 9 - COMPUTER PRINTOUT OF TRANSFER FUNCTION DATA FOR THE FACS[1]

[Mediumweight, $\delta_t = 65°$, M = 1.59, h_p = 11,918 m (39,100 ft), $K_{h_p} = 0.62$, $K_{n_z} = 0.104$ rad/g, $K_q = 2.4$ rad/rad/sec]

(a) Inboard elevon

COMMCN COMPENSATION

(1) GAIN(GN)= 0.25000E 06

NUMERATOR

DENOMINATOR
(2) NUMBER OF REAL ROOTS= 2
-0.10000E 02 -C.1CCCCE C2
(3) NUMBER CF COMPLEX PAIR ROOTS= 1
-0.30000E 02-0.40000E 02

COMPLEX COEFFICIENT OF FEEDBACK VARIABLE

MODE	GAIN(GNK)	ROOTS	
1	(4) -0.47900E 01	(5) C.C	
2	(6) 0.81000E-01	(7) -C.879C0E 02	
3	(8) 0.13800E-02	(9) C.C	(10) C.C
4	(11) -0.82000E-04	(12) C.0	(13) -C.228CCE C2
5	(14) 0.62600E-03	(15) C.C	(16) -C.112CCE C3
6	(17) 0.15000E-04	(18) C.C	(19) -C.113CCE 03
7	(20) 0.3610CE-03	(21) C.0	(22) C.4640CE C2

(b) Outboard elevons

COMMCN COMPENSATION

GAIN(GN)= 0.5000CE 07

NUMERATOR

DENOMINATOR
NUMBER OF REAL ROOTS= 3
-0.10000E 02 -C.10CCCE C2 -C.2CCCCE C2
NUMBER OF COMPLEX PAIR ROOTS= 1
-0.30000E 02-0.40000E 02

COMPLEX COEFFICIENT OF FEEDBACK VARIABLE

MODE	GAIN(GNK)	ROOTS	
1	-0.47900E 01	C.C	
2	0.81000E-01	-C.879C0E C2	
3	0.1380CE-02	C.0	C.C
4	-0.82000E-04	C.C	-C.228CCE C2
5	0.62600E-03	C.0	-C.112CCE 03
6	0.15000E-04	C.0	-0.113CCE C3
7	0.3610CE-03	C.C	C.4640CE C2

[1]For expediency, this table is given only in U.S. Customary Units.

TABLE 10 - COMPUTER PRINTOUT OF TRANSFER FUNCTION DATA FOR THE FACS[1]

[Heavyweight, $\delta_t = 25°$, M = 0.87, h_p = 7620 m (25,000 ft), $K_{h_p} = 0.50$, $K_{n_z} = 0.104$ rad/g, $K_q = 2.4$ rad/rad/sec]

(a) Inboard elevon

```
 COMMON COMPENSATION

    GAIN(GN)= 0.25000E 06

      NUMERATOR

      DENOMINATOR
      NUMBER OF REAL ROOTS= 2
 -0.10000E 02    -0.10000E 02
      NUMBER OF COMPLEX PAIR ROOTS= 1
-0.30000E 02-0.40000E 02

  COMPLEX COEFFICIENT OF FEEDBACK VARIABLE

 MODE     GAIN(GNK)          ROOTS
    1   -0.28000E 01
                          -0.0
    2    0.80100E-01
                          -0.66900E 02
    3    0.81000E-03
                          -0.0              0.36000E 01
    4   -0.97000E-04
                          -0.0             -0.31500E 02
    5   -0.17800E-02
                          -0.0             -0.12400E 03
    6   -0.97000E-04
                          -0.0              0.73100E 02
    7    0.91000E-04
                          -0.0              0.25600E 02
```

(b) Outboard elevons

```
 COMMON COMPENSATION

    GAIN(GN)= 0.50000E 07

      NUMERATOR

      DENOMINATOR
      NUMBER OF REAL ROOTS= 3
 -0.10000E 02    -0.10000E 02    -0.20000E 02
      NUMBER OF COMPLEX PAIR ROOTS= 1
-0.30000E 02-0.40000E 02

  COMPLEX COEFFICIENT OF FEEDBACK VARIABLE

 MODE     GAIN(GNK)          ROOTS
    1   -0.28000E 01
                          -0.0
    2    0.80100E-01
                          -0.66900E 02
    3    0.81000E-03
                          -0.0              0.36000E 01
    4   -0.97000E-04
                          -0.0             -0.31500E 02
    5   -0.17800E-02
                          -0.0             -0.12400E 03
    6   -0.97000E-04
                          -0.0              0.73100E 02
    7    0.91000E-04
                          -0.0              0.25600E 02
```

[1]For expediency, this table is given only in U.S. Customary Units.

TABLE 11 - COMPUTER PRINTOUT OF TRANSFER FUNCTION DATA FOR THE FACS[1]

[Lightweight, $\delta_t = 25°$, M = 0.86, h_p = 7620 m (25,000 ft), $K_{h_p} = 0.50$, $K_{n_z} = 0.104$ rad/g, $K_q = 2.4$ rad/rad/sec]

(a) Inboard elevon

COMMON COMPENSATION

GAIN(GN)= C.5000CE C7

NUMERATOR

DENOMINATOR
NUMBER OF REAL ROOTS= 3
-0.10000E C2 -C.1CCC0E 02 -0.2000CE 02
NUMBER OF COMPLEX PAIR ROOTS= 1
-0.30000E 02-C.40CCCE C2

COMPLEX COEFFICIENT OF FEEDBACK VARIABLE

MODE	GAIN(GNK)	ROOTS	
1	-0.294C0E 01		
		C.C	
2	0.863C0E-01		
		-C.619C0E 02	
3	0.848C0E-03		
		C.C	C.13700E 01
4	-0.129C0E-C3		
		C.0	-0.18600E 02
5	-0.780C0E-C3		
		C.C	-C.68CC0E 02
6	-0.71000E-C4		
		C.C	C.72800E 02
7	0.126CCE-C3		
		C.C	0.18200E 02

(b) Outboard elevons

COMMON COMPENSATION

GAIN(GN)= C.25000E 06

NUMERATOR

DENOMINATOR
NUMBER OF REAL ROOTS= 2
-0.10000E 02 -0.1000CE 02
NUMBER OF COMPLEX PAIR ROOTS= 1
-0.30000E 02-0.40000E C2

COMPLEX COEFFICIENT OF FEEDBACK VARIABLE

MODE	GAIN(GNK)	ROOTS	
1	-0.294C0E 01		
		C.C	
2	0.863CCE-01		
		-C.619C0E 02	
3	0.84800E-03		
		C.C	C.1370CE 01
4	-0.129C0E-03		
		C.C	-C.18600E 02
5	-0.78CC0E-C3		
		C.C	-0.68000E 02
6	-0.71000E-C4		
		C.C	0.72800E 02
7	0.126C0F-C3		
		C.C	0.18200E 02

[1]For expediency, this table is given only in U.S. Customary Units.

TABLE 12 - MODE SHAPE CHARACTERISTICS AT SELECTED LOCATIONS

[Mediumweight, $\delta_t = 65°$, M = 1.59]

Location	Mode number	φ_i	φ_i', rad/m (rad/ft)
Fuselage nose, FS 4.95 m (194.75 in.)	1	2.1200	
	2	-.1500	
	3	3.7300	----------
	4	.0680	
	5	-.8600	
Pilot's station, FS 11.12 m (438 in.)	1	1.2500	
	2	-.0650	
	3	1.1000	----------
	4	.2100	
	5	-.1500	
Nosewheel well, FS 32.61 m (1284 in.)	1	-0.4200	0 (0)
	2	.0250	.00252 (.00077)
	3	-.1900	-.0961 (-.02930)
	4	-.0045	-.00236 (-.00072)
	5	-.1100	.0236 (.00720)
Near center of gravity, FS 37.72 m (1485 in.)	1	-0.3817	
	2	.0037	
	3	.2125	----------
	4	.0068	
	5	-.1529	
Wing accelerometer, FS 56.18 m (2212 in.)	1	0.6000	
	2	-.0600	
	3	-.9000	----------
	4	-.0550	
	5	-.4300	
Center of gravity, FS 41.99 m (1653 in.)	1	-0.2992	
	2	-.0162	
	3	.4240	----------
	4	.0112	
	5	-.1190	

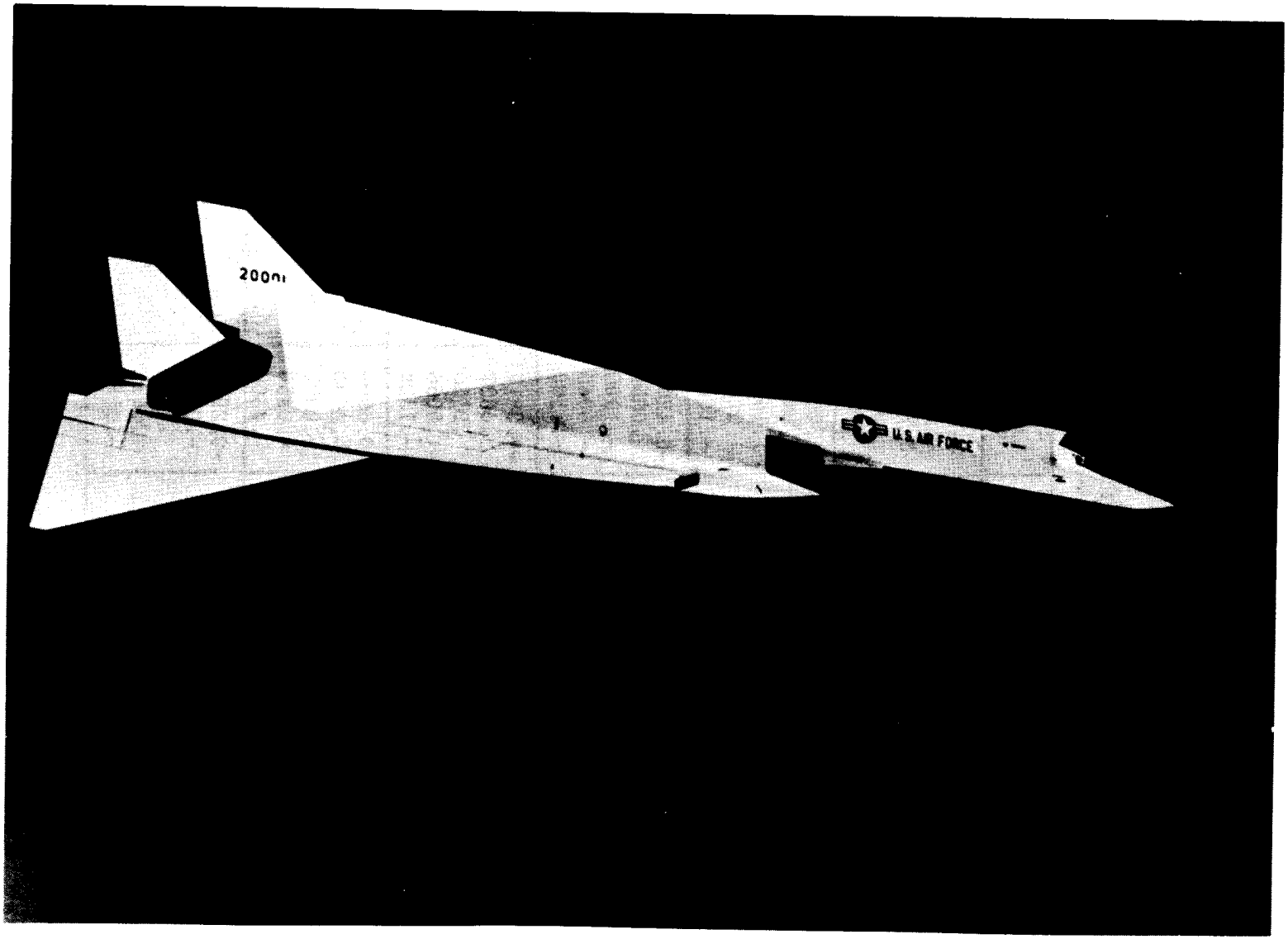

Figure 1. XB-70-1 airplane. Supersonic configuration, $\delta_t = 65°$.

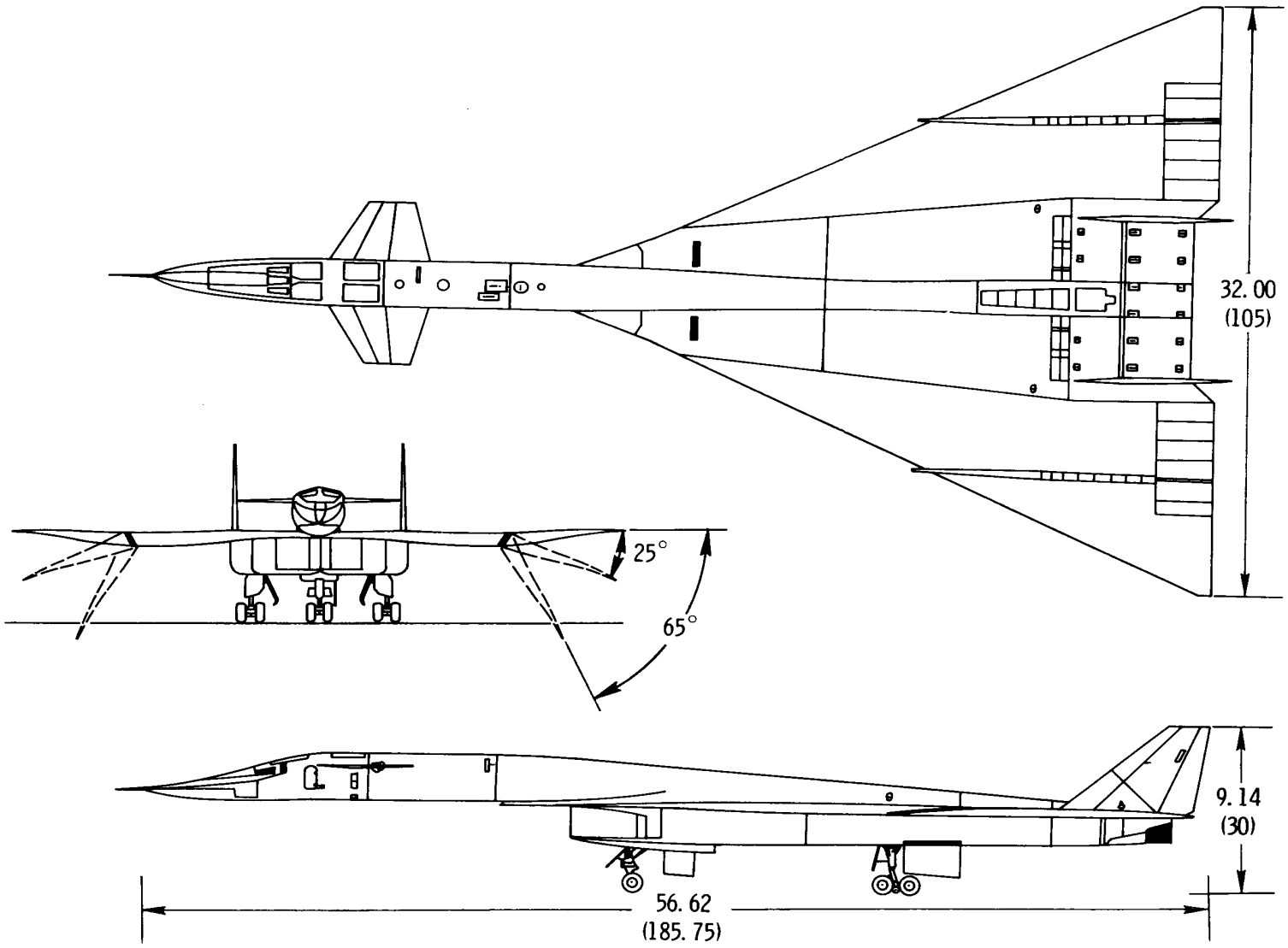

Figure 2. Three-view drawing of the XB-70-1 airplane. Dimensions in meters (feet) except as otherwise noted.

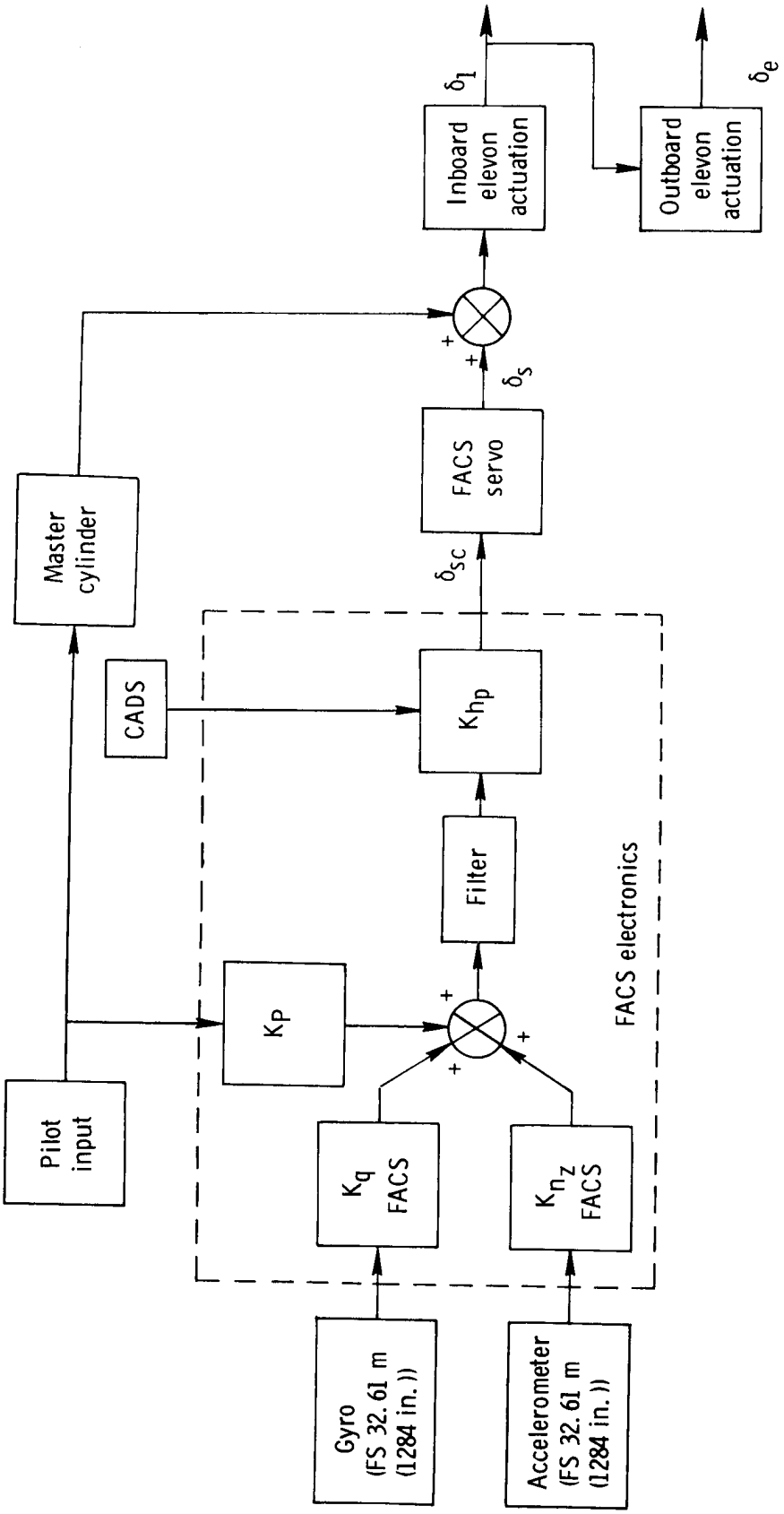

Figure 3. Block diagram of the XB-70 pitch flight augmentation control system.

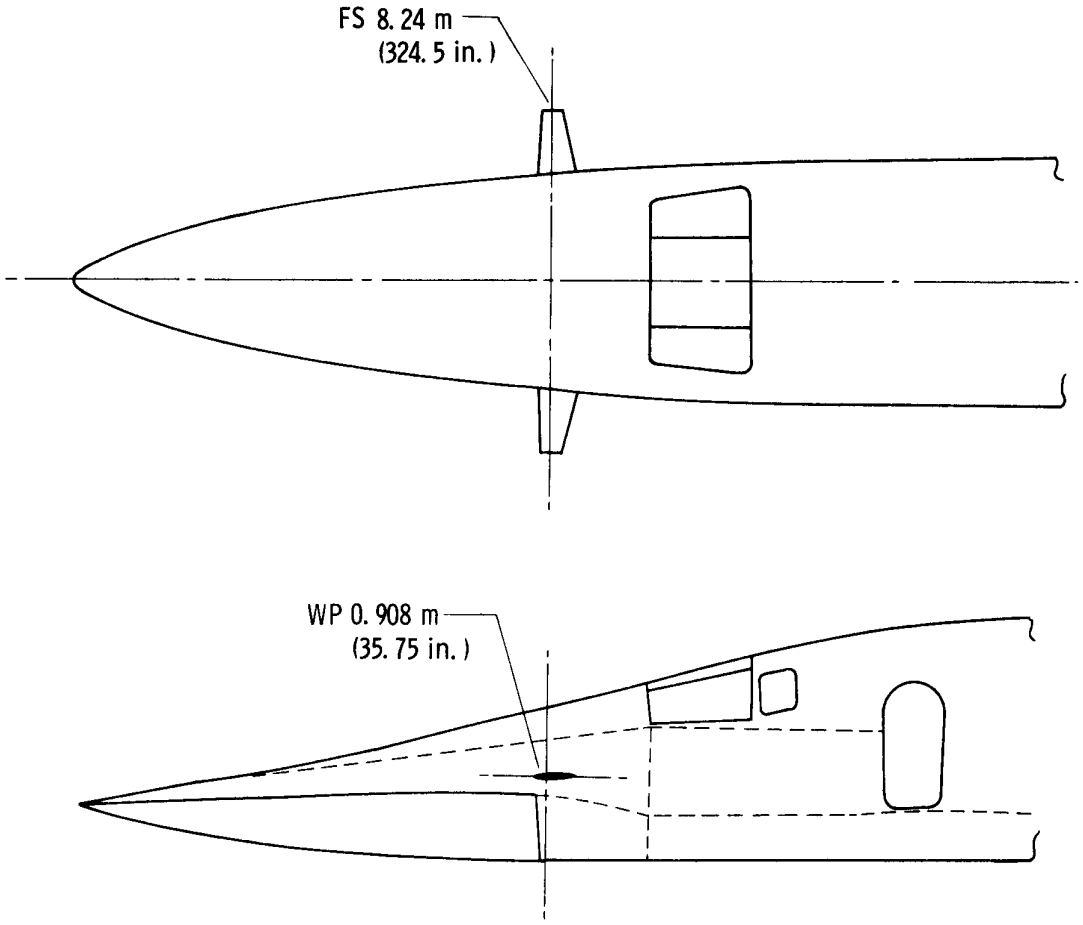

(a) Location.

Figure 4. XB-70 shaker vanes.

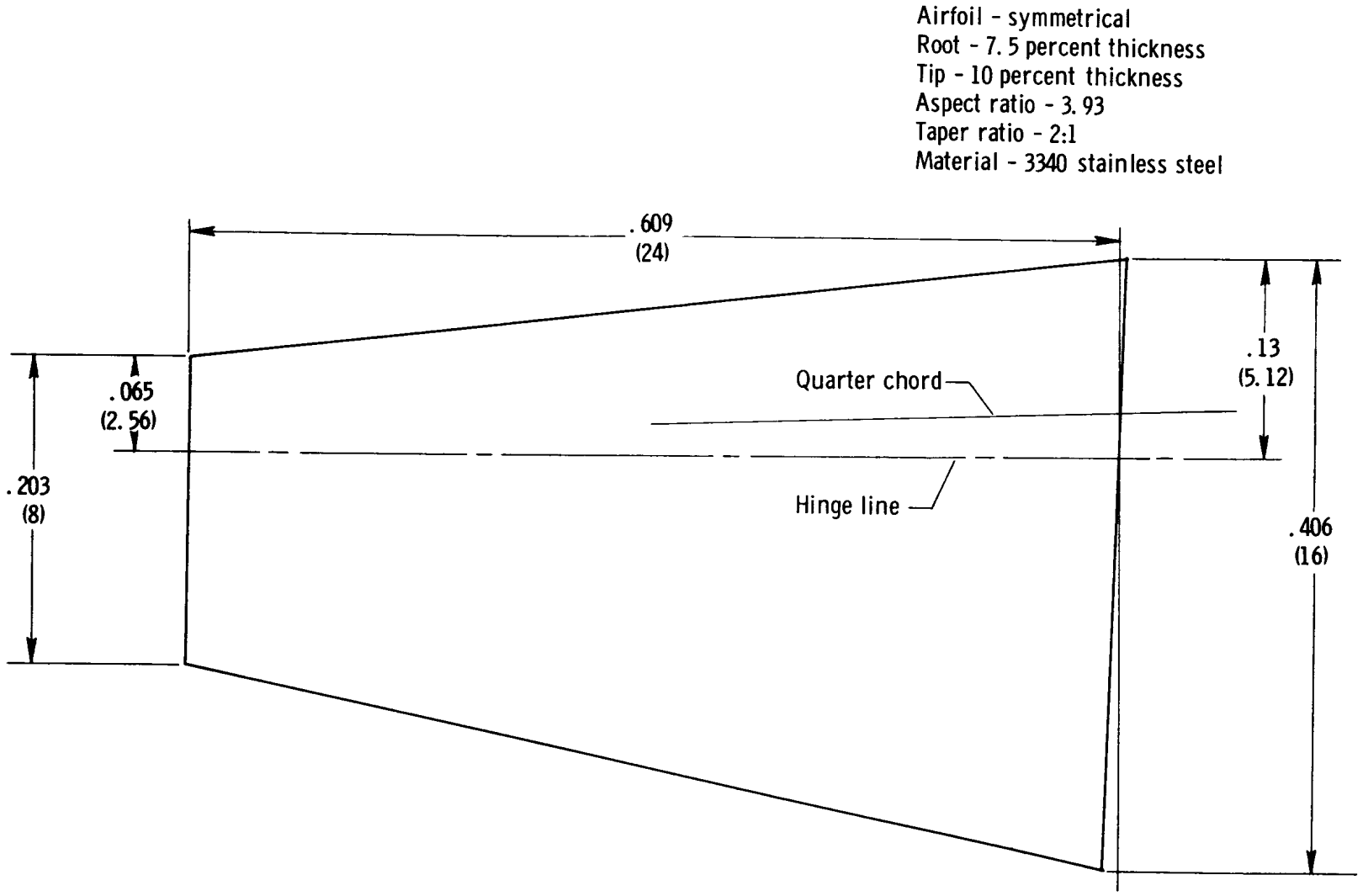

(b) Physical dimensions, meters (inches).

Figure 4. Concluded.

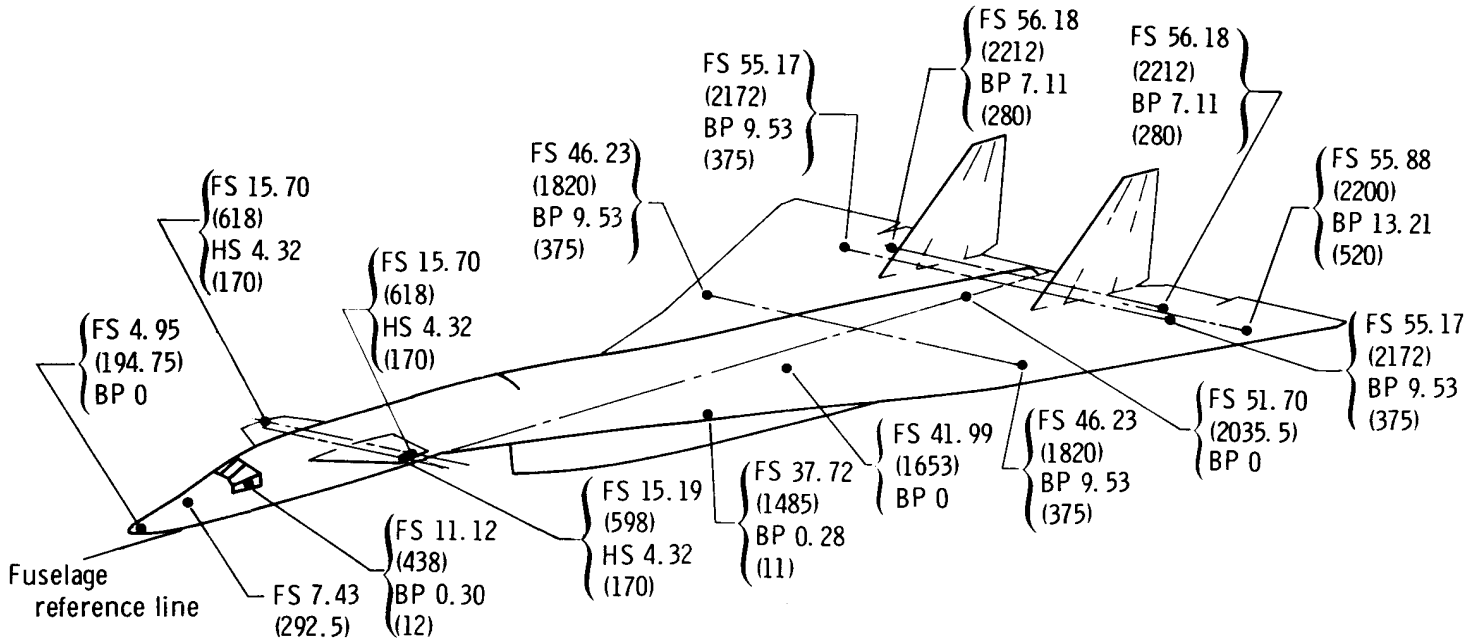

Figure 5. Location of accelerometers for measuring XB-70 airplane response to shaker vane excitation. Dimensions in meters (inches).

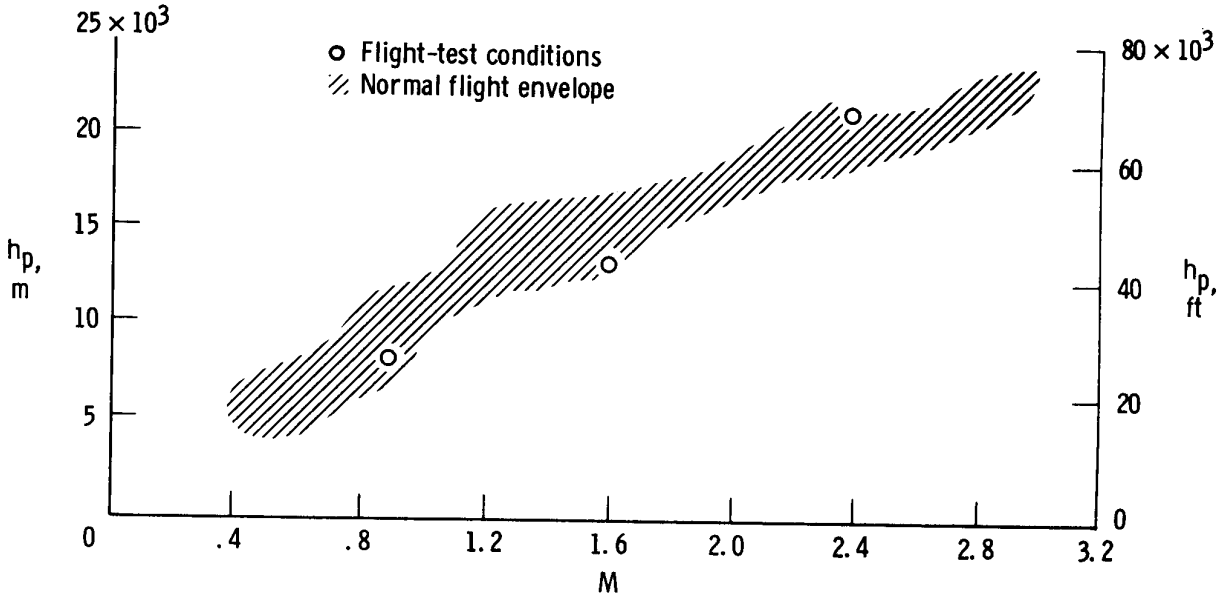

Figure 6. Flight-test conditions for structural response tests on the XB-70 airplane.

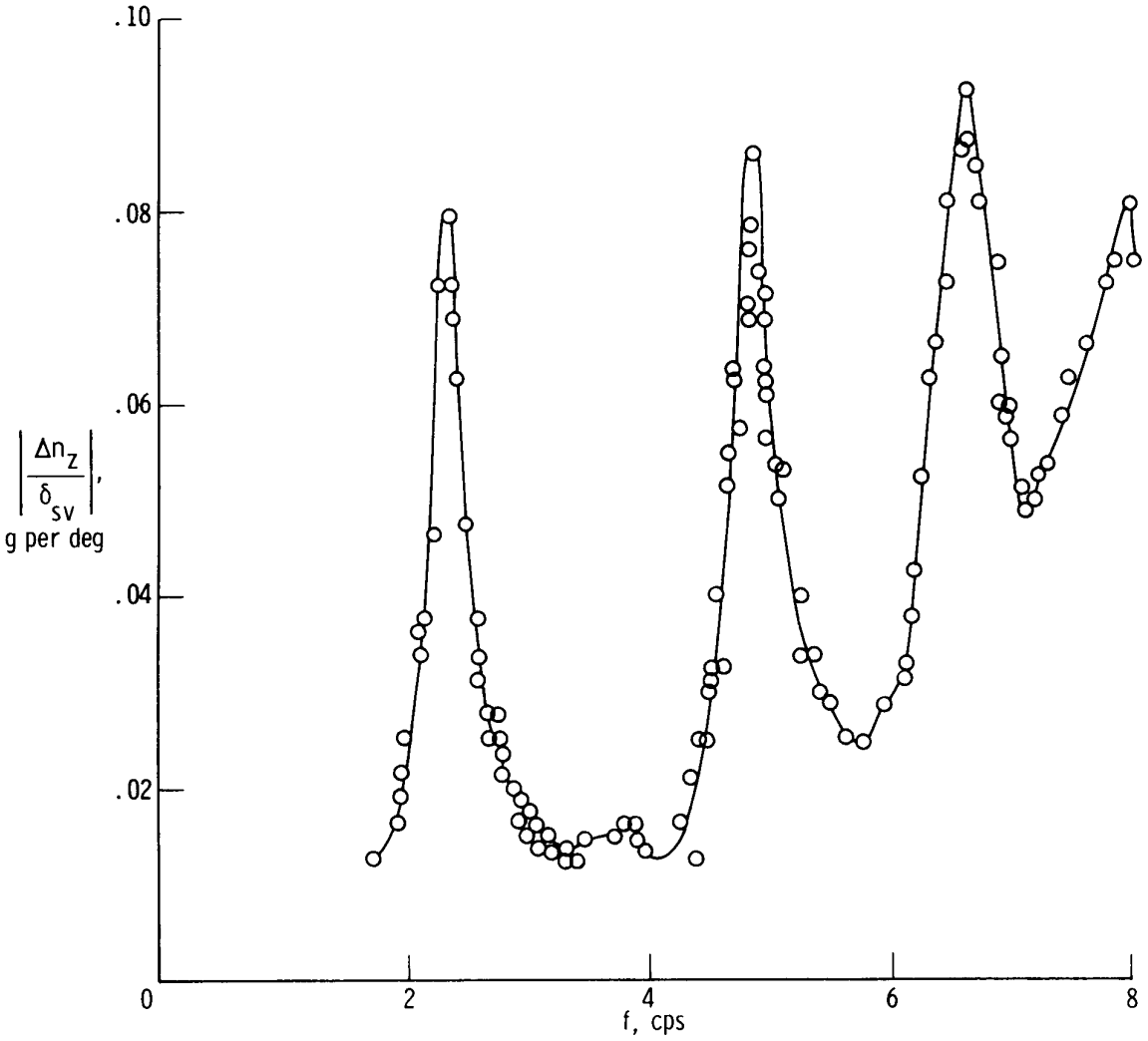

(a) Fuselage nose; FS 4.95 m (194.75 in.).

Figure 7. Flight-measured vertical acceleration response to shaker vane excitation. Heavyweight; M = 0.87; h_p = 7620 m (25,000 ft); $\delta_t = 25°$.

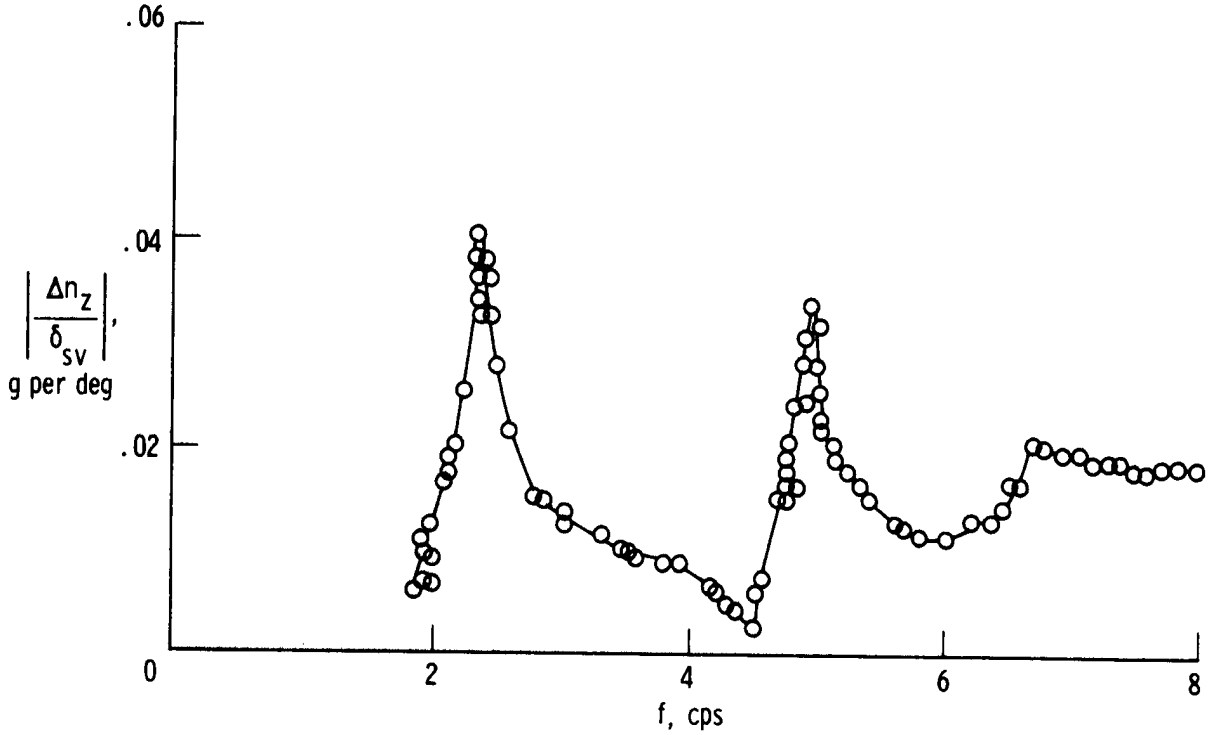

(b) Pilot's station; FS 11.12 m (438 in.).

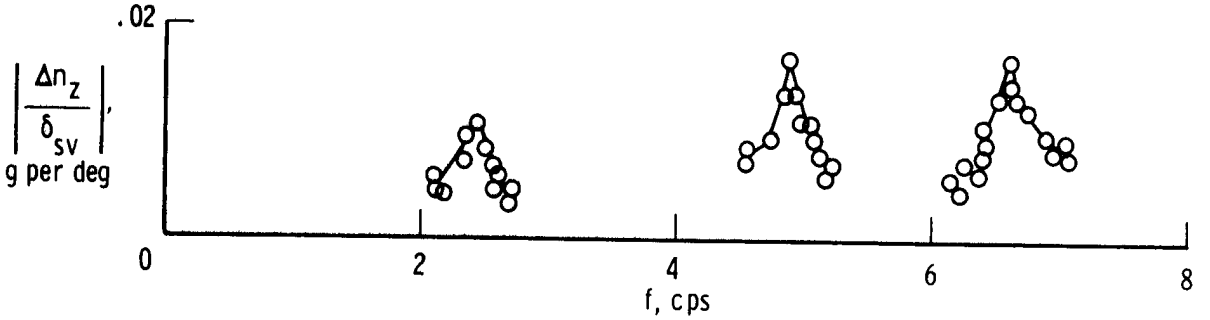

(c) Center of gravity; FS 41.99 m (1653 in.).

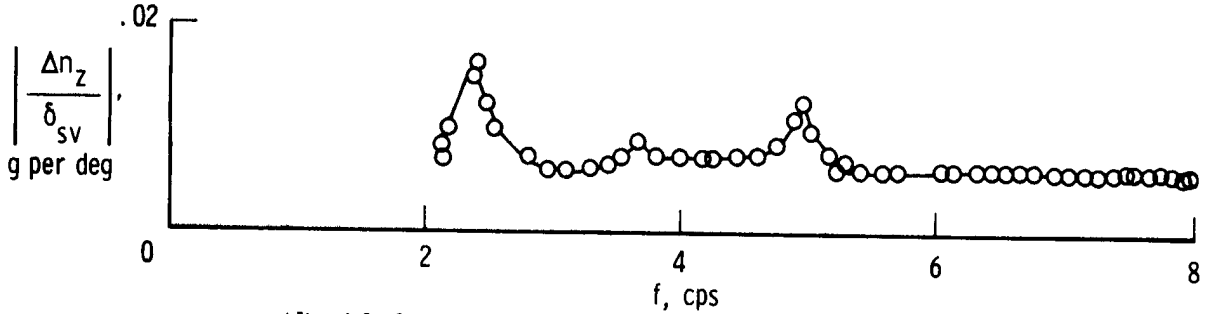

(d) Aft fuselage; FS 51.70 m (2035.5 in.).

Figure 7. Continued.

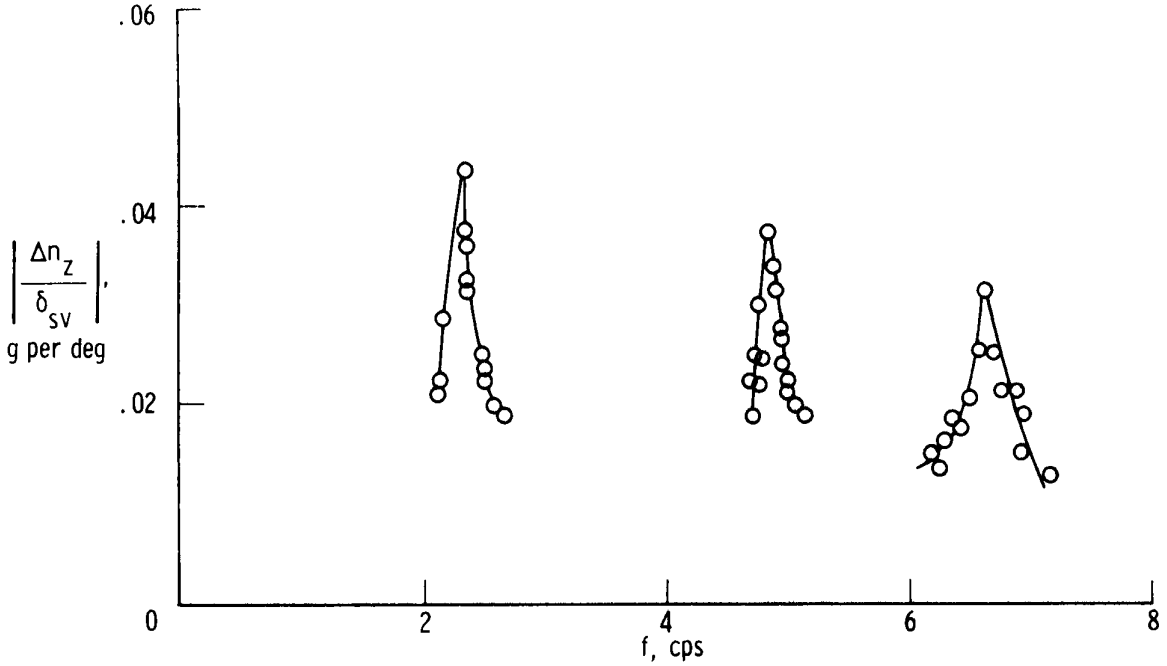

(e) Left wing; FS 56.18 m (2212 in.), BP 7.11 m (280 in.).

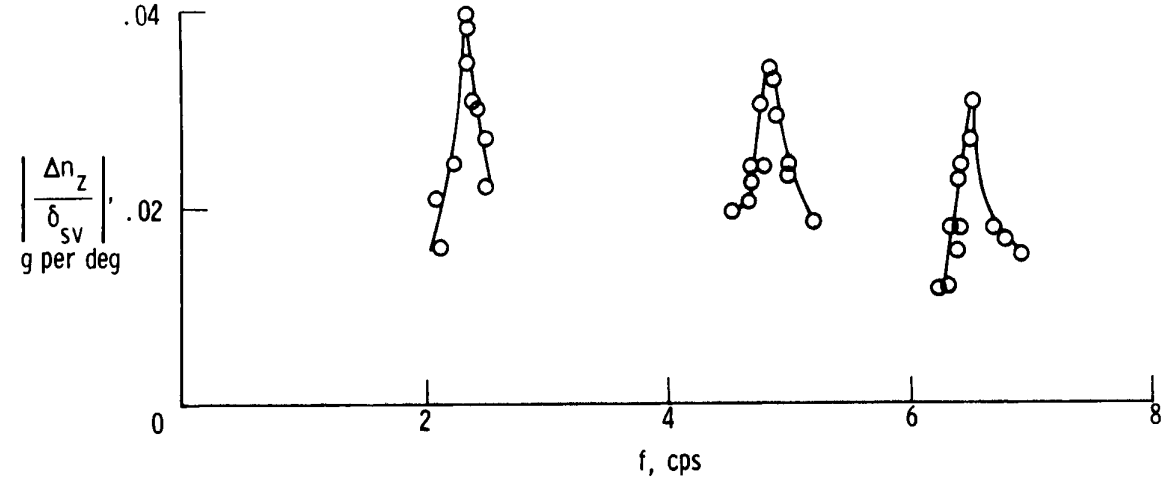

(f) Right wing; FS 56.18 m (2212 in.), BP 7.11 m (280 in.).

Figure 7. Concluded.

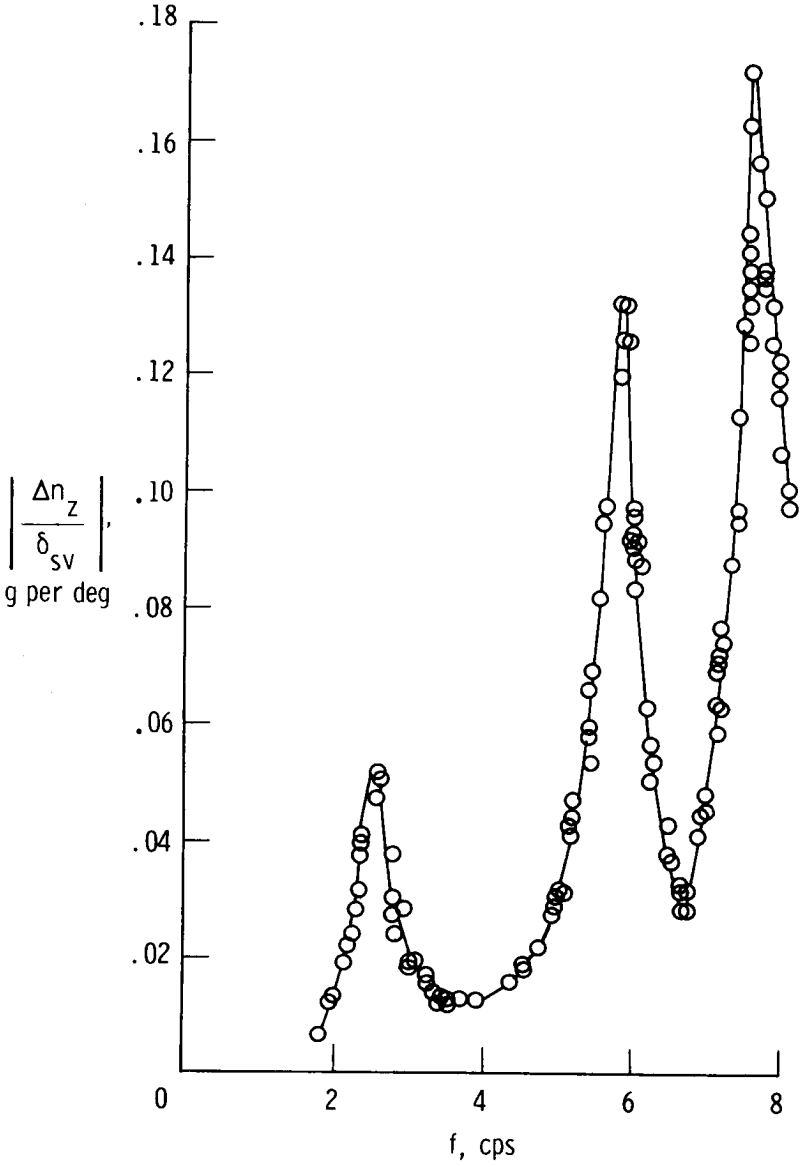

(a) Fuselage nose; FS 4.95 m (194.75 in.).

Figure 8. Flight-measured vertical acceleration response to shaker vane excitation. Lightweight; M = 0.86; h_p = 7620 m (25,000 ft); $\delta_t = 25°$.

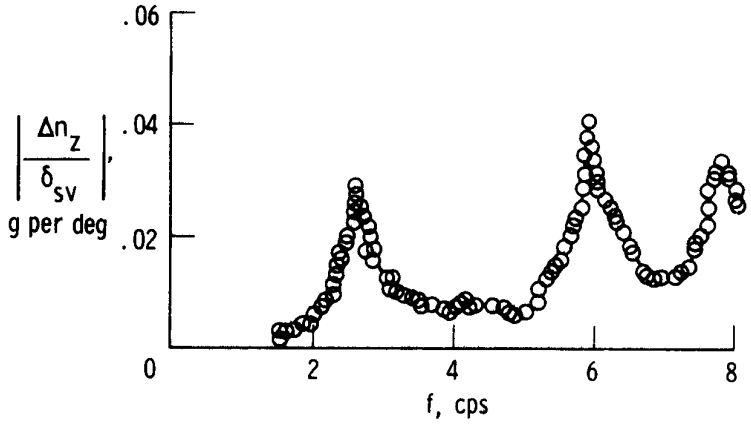

(b) Pilot' s station; FS 11.12 m (438 in.).

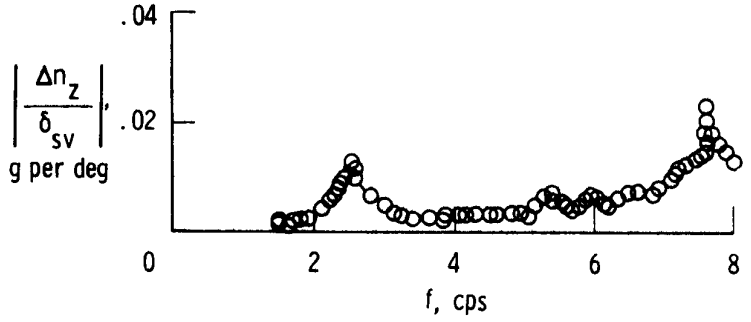

(c) Near center of gravity; FS 37.72 m (1485 in.).

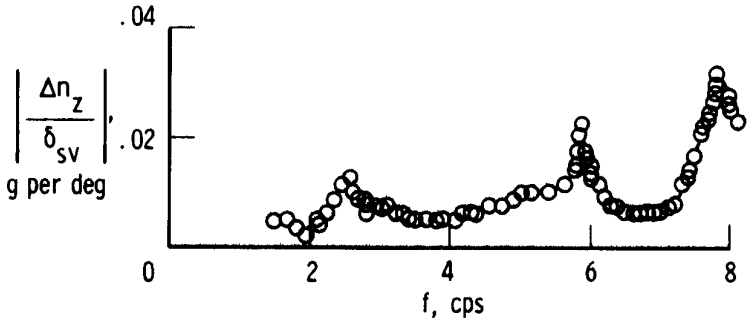

(d) Center of gravity; FS 41.99 m (1653 in.).

Figure 8. Continued.

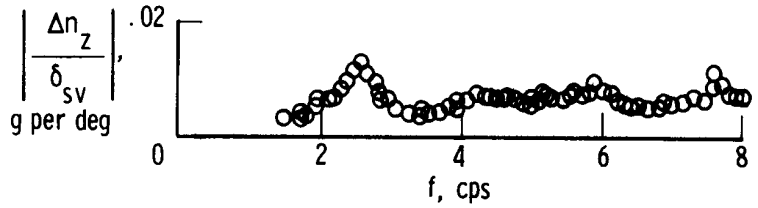

(e) Aft fuselage; FS 51.70 m (2035.5 in.).

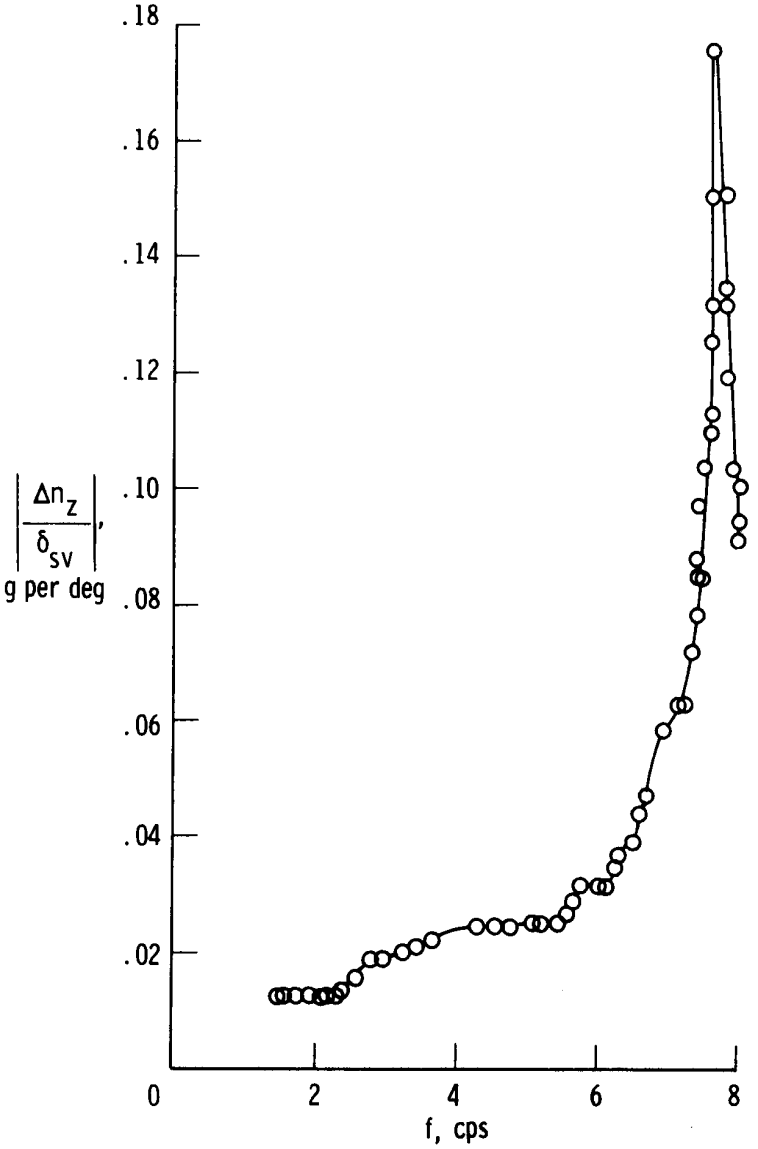

(f) Left canard tip; FS 15.19 m (598 in.); HS 4.32 m (170 in.).

Figure 8. Continued.

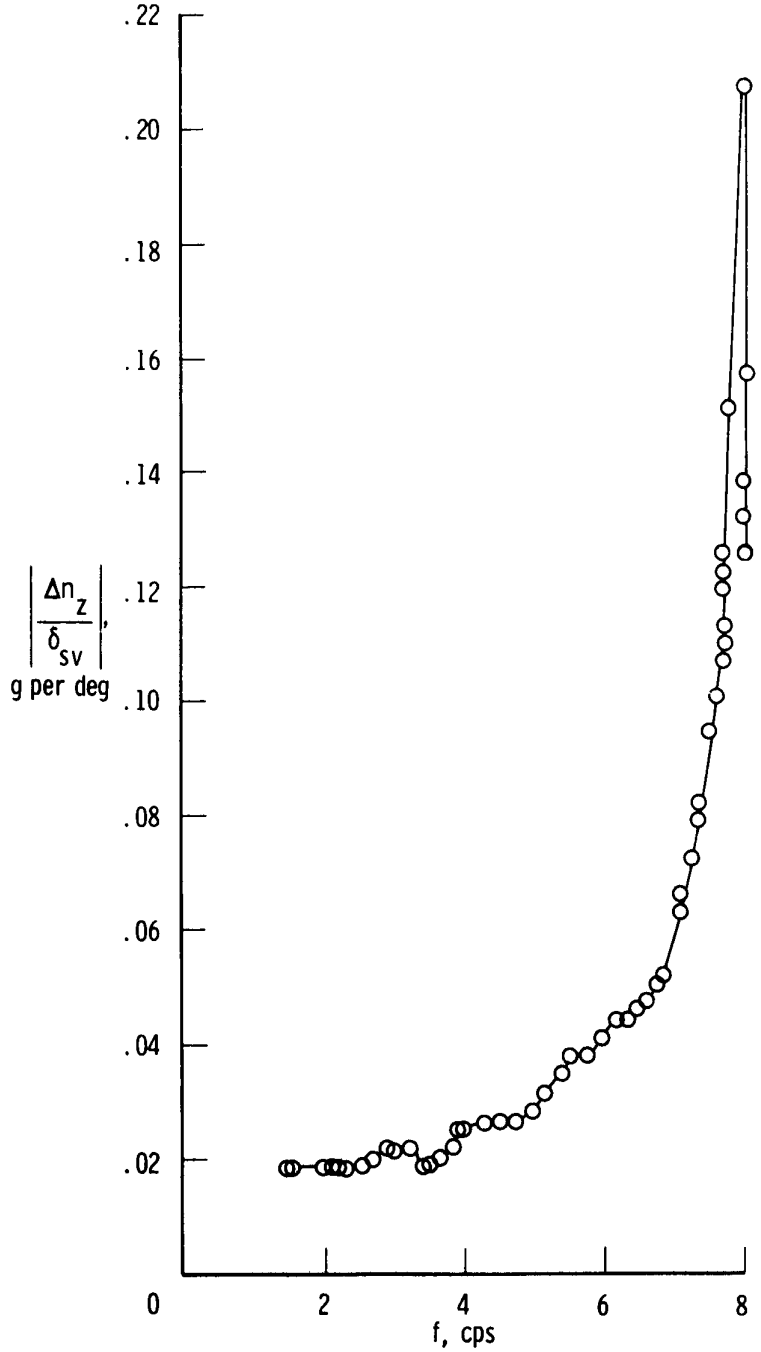

(g) Right canard tip; FS 15.70 m (618 in.); HS 4.32 m (170 in.).

Figure 8. Continued.

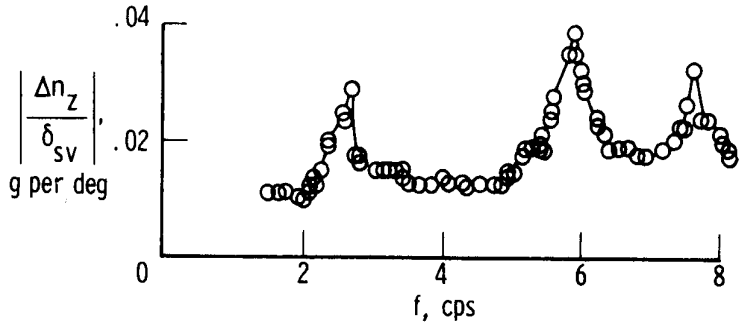

(h) Left wing; FS 56.18 m (2212 in.); BP 7.11 m (280 in.).

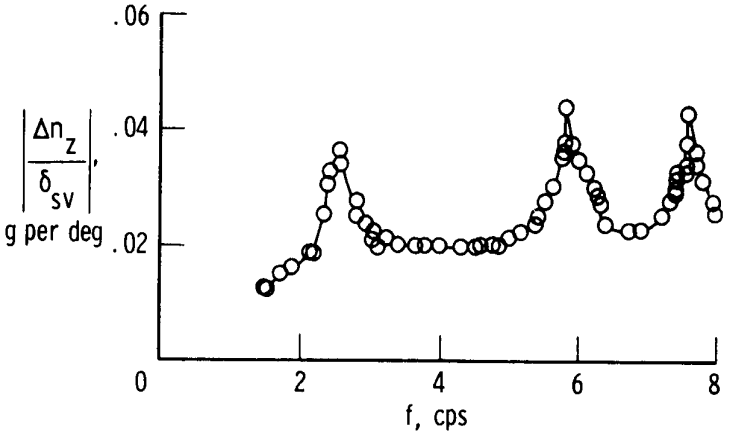

(i) Right wing; FS 56.18 m (2212 in.); BP 7.11 m (280 in.).

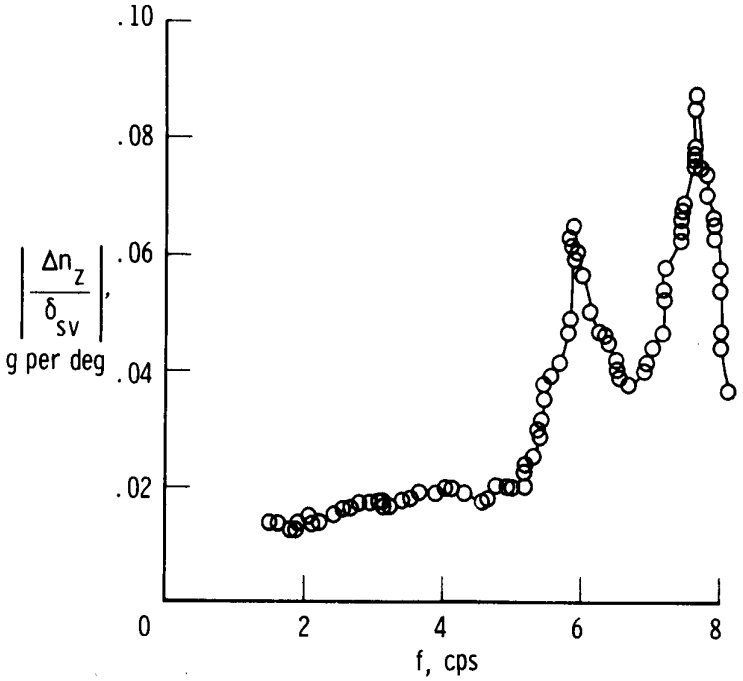

(j) Left wing; FS 46.23 m (1820 in.); BP 9.53 m (375 in.).

Figure 8. Continued.

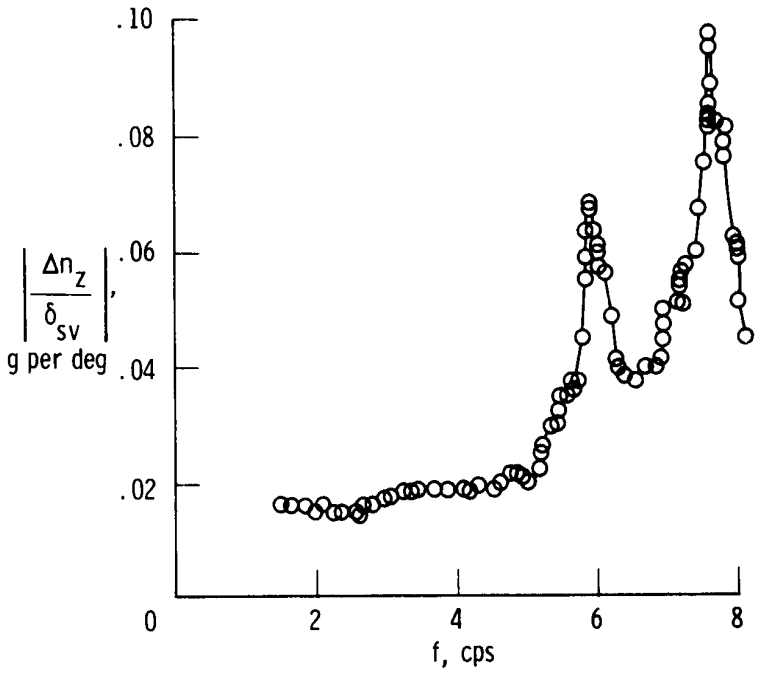

(k) Right wing; FS 46.23 m (1820 in.); BP 9.53 m (375 in.).

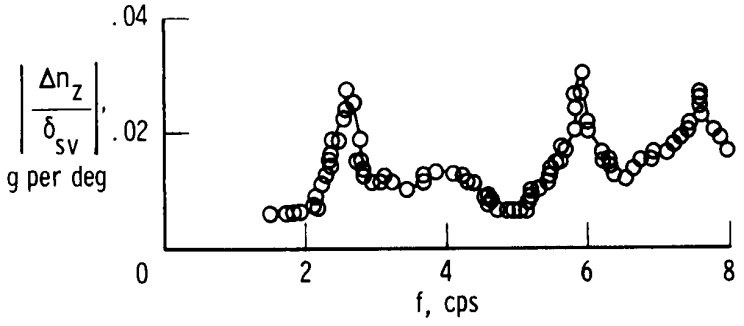

(l) Left wing; FS 55.17 m (2172 in.); BP 9.53 m (375 in.).

Figure 8. Continued.

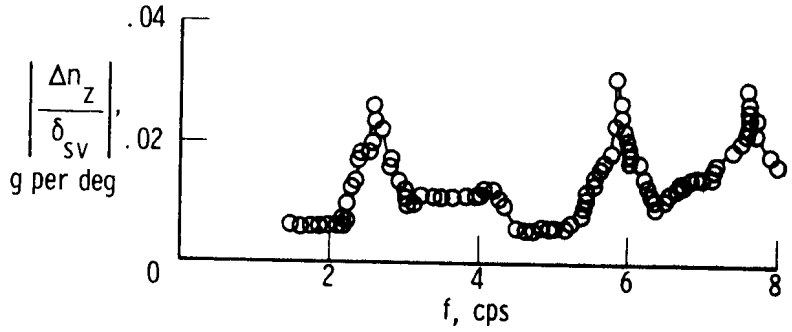

(m) Right wing; FS 55.17 m (2172 in.); BP 9.53 m (375 in.).

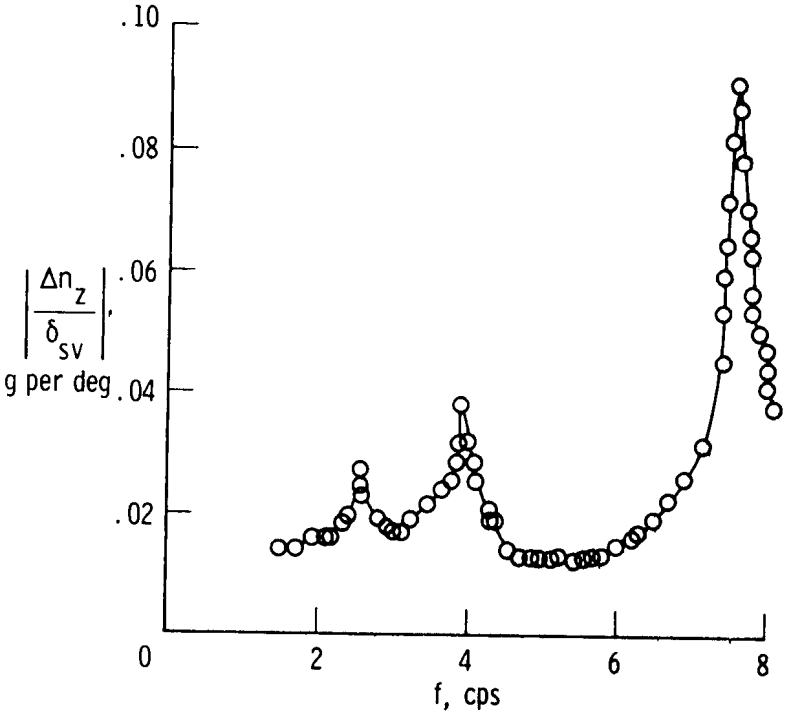

(n) Left wingtip; FS 55.88 m (2200 in.); BP 13.21 m (520 in.).

Figure 8. Concluded.

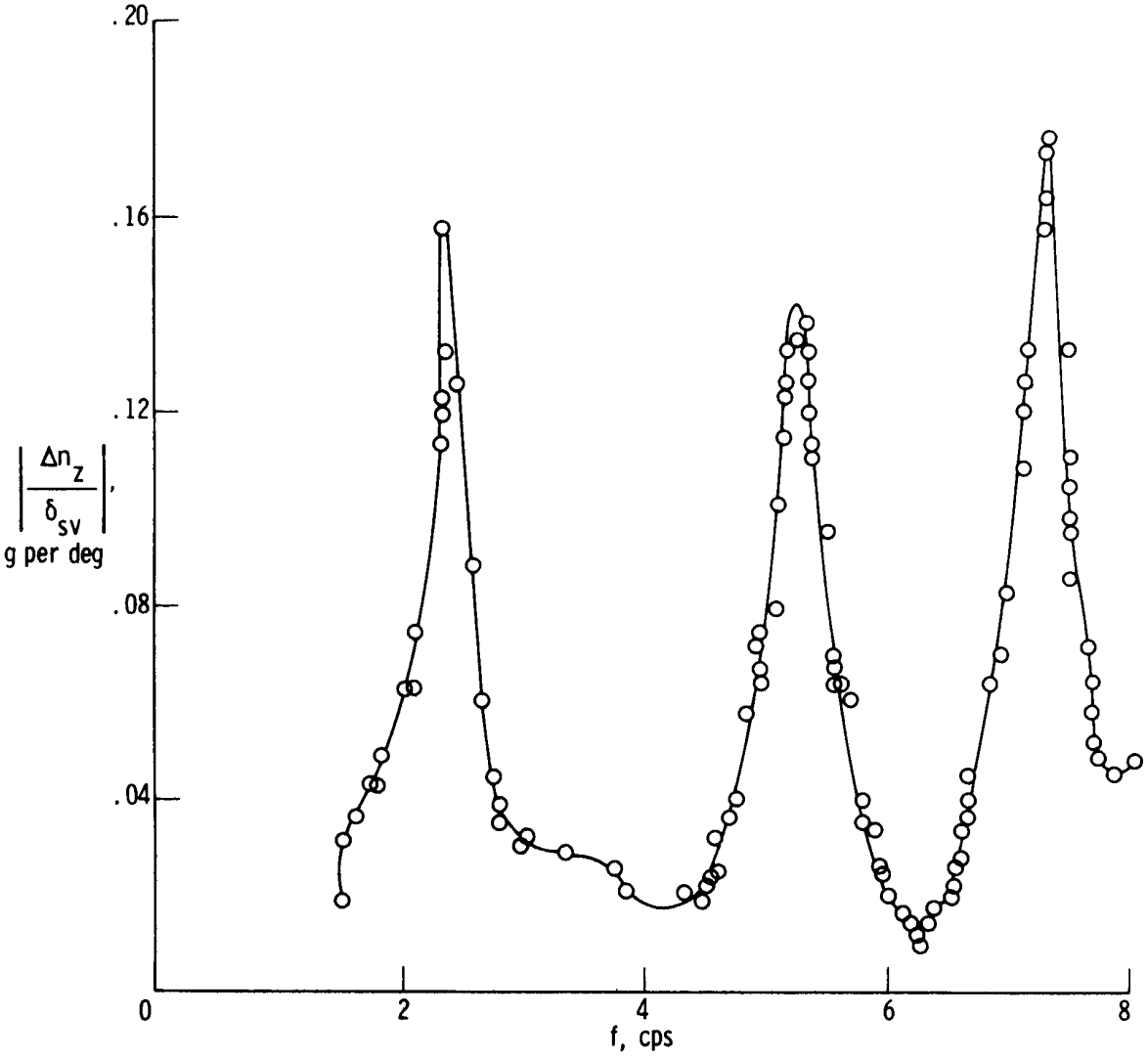

(a) Fuselage nose; FS 4.95 m (194.75 in.).

Figure 9. Flight-measured vertical acceleration response to shaker vane excitation. Mediumweight; M = 1.59; h_p = 11,918 m (39,100 ft); δ_t = 65°.

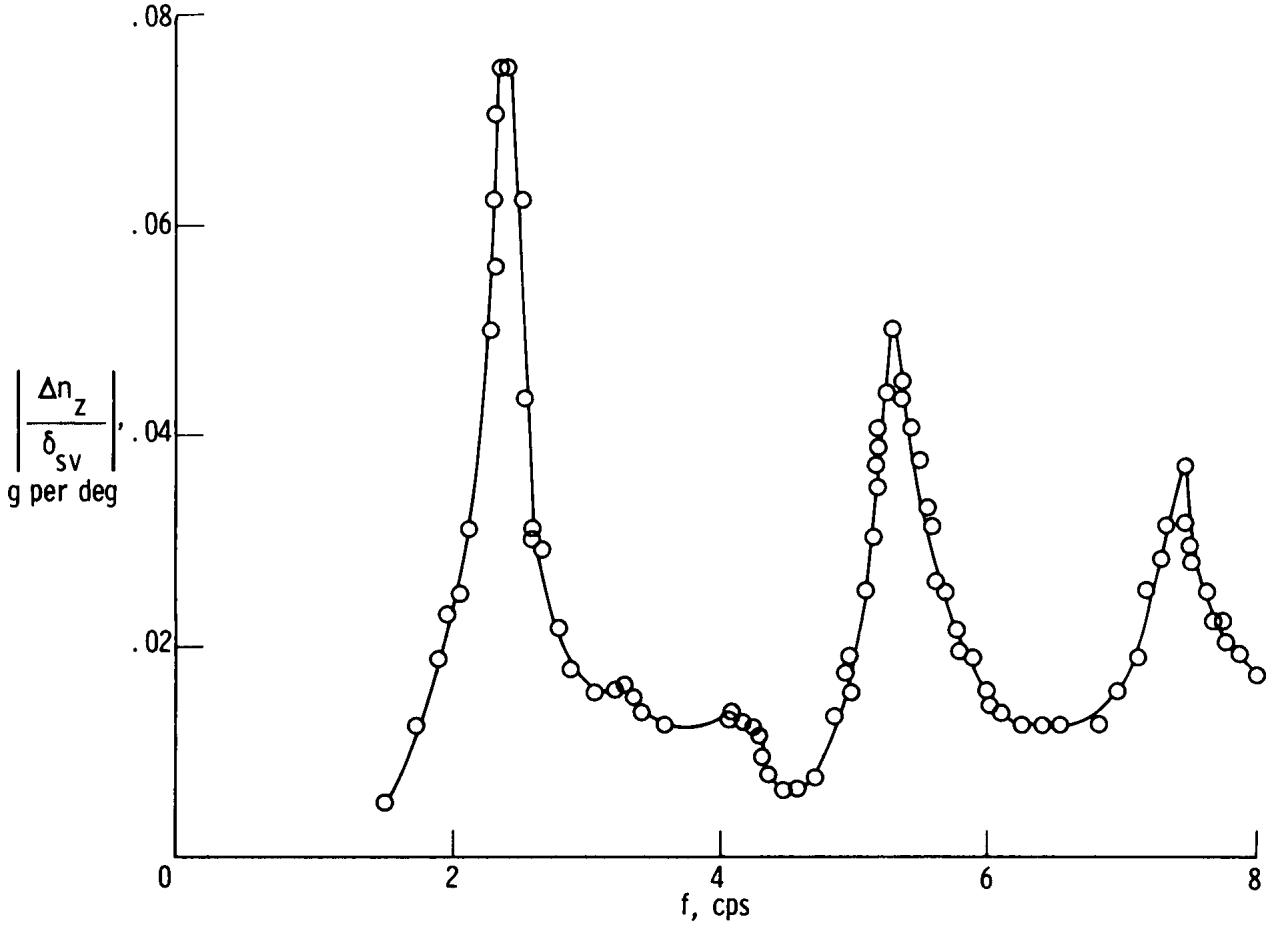

(b) Pilot' s station; FS 11.12 m (438 in.).

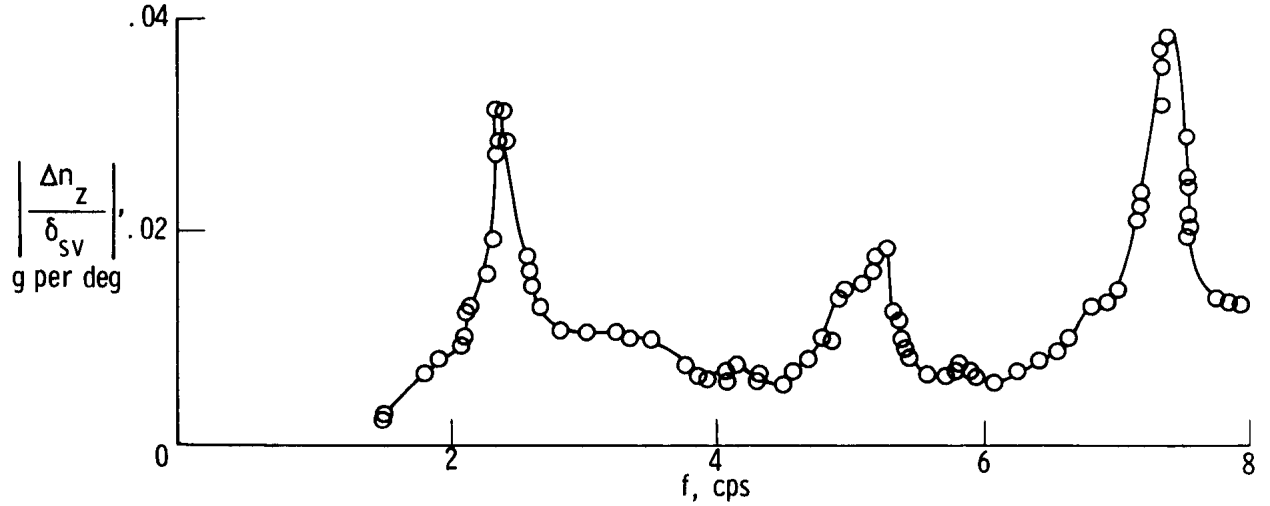

(c) Near center of gravity; FS 37.72 m (1485 in.).

Figure 9. Continued.

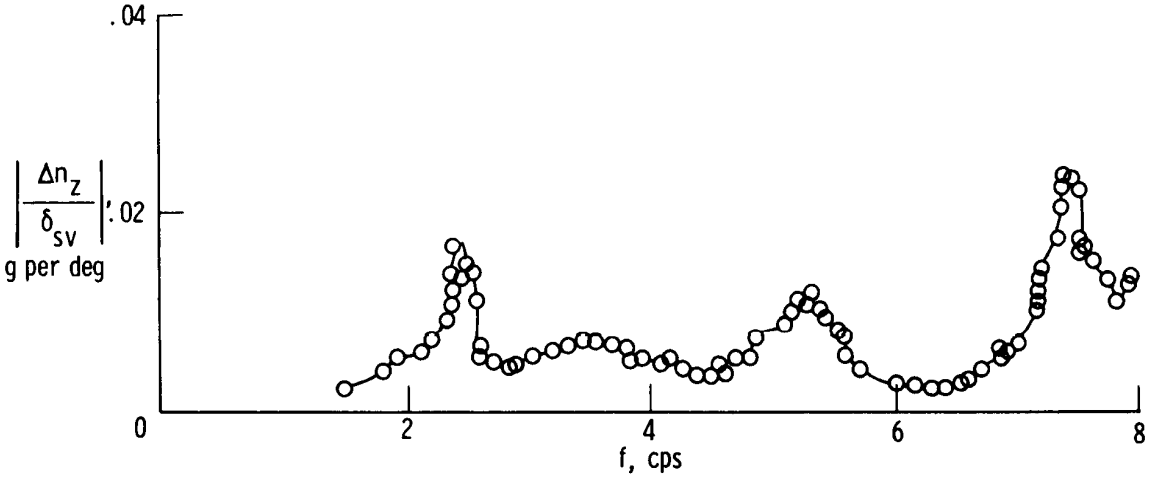

(d) Center of gravity; FS 41.99 m (1653 in.).

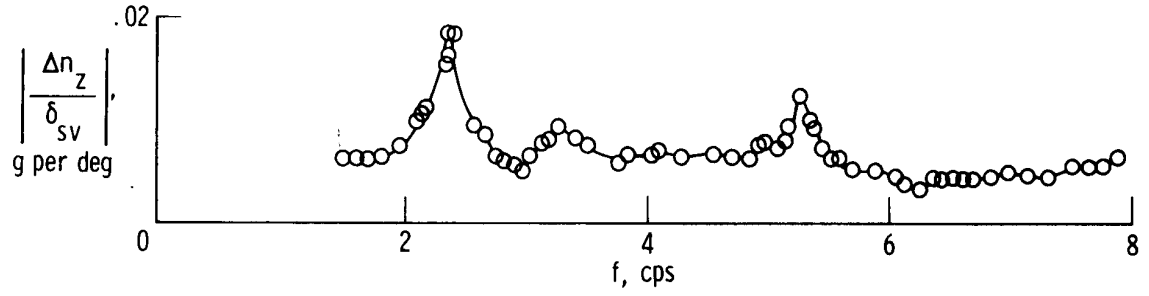

(e) Aft fuselage; FS 51.70 m (2035.5 in.).

Figure 9. Continued.

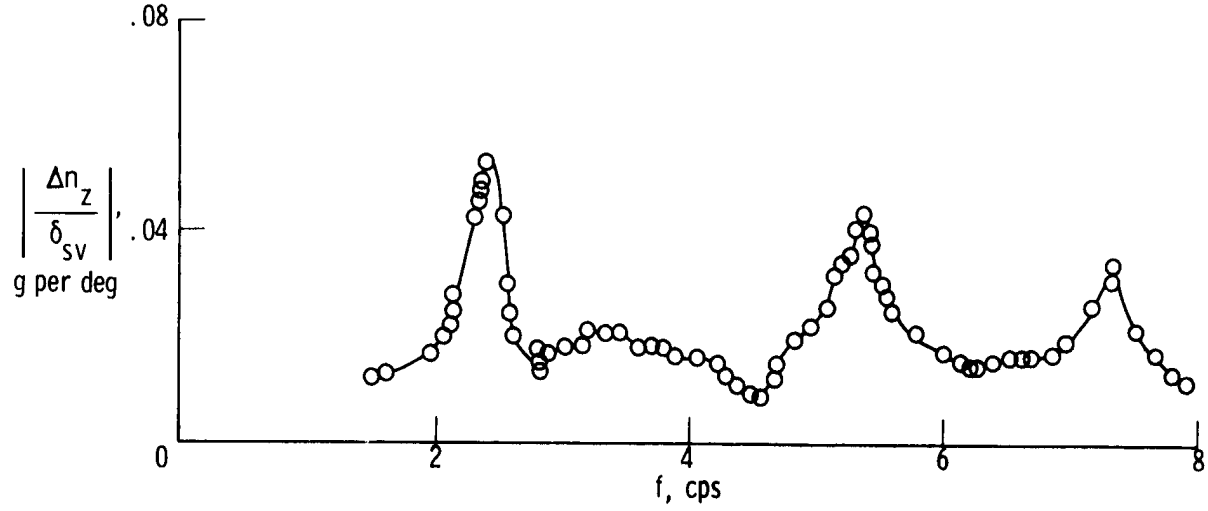

(f) Left wing; FS 56.18 m (2212 in.); BP 7.11 m (280 in.).

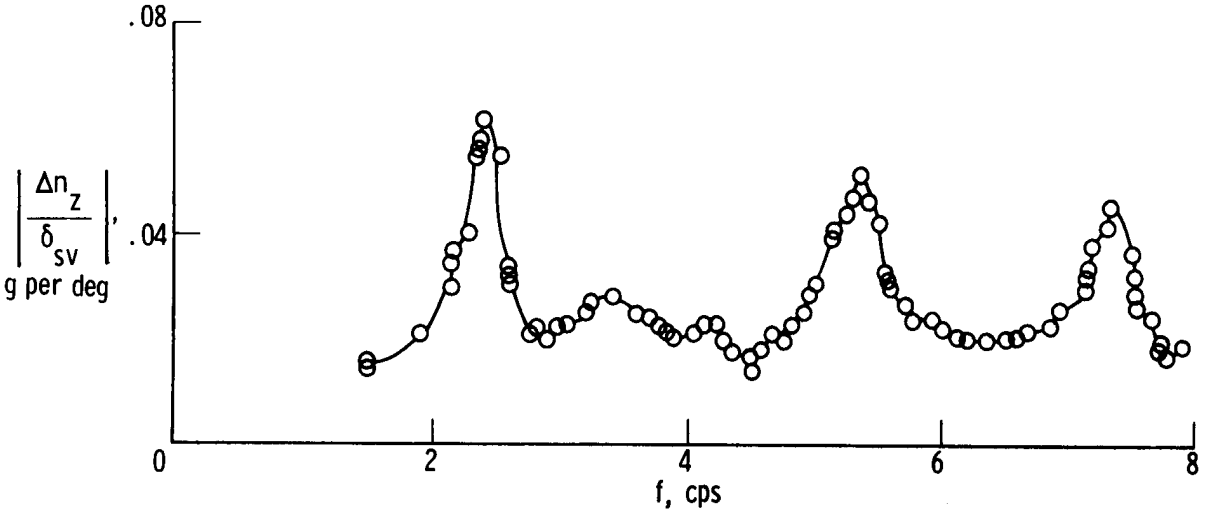

(g) Right wing; FS 56.18 m (2212 in.); BP 7.11 m (280 in.).

Figure 9. Continued.

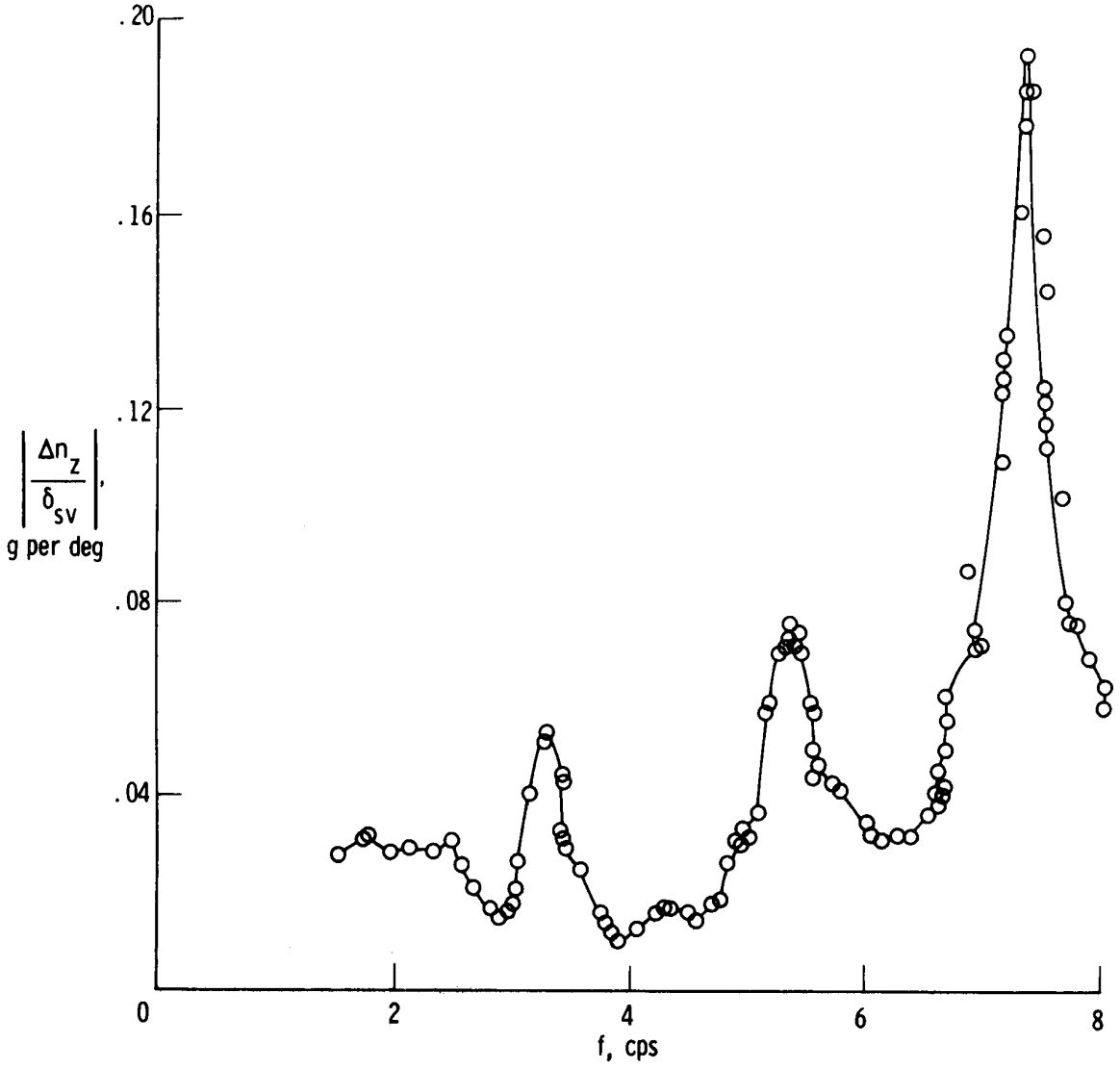

(h) Left wing; FS 46.23 m (1820 in.); BP 9.53 m (375 in.).

Figure 9. Continued.

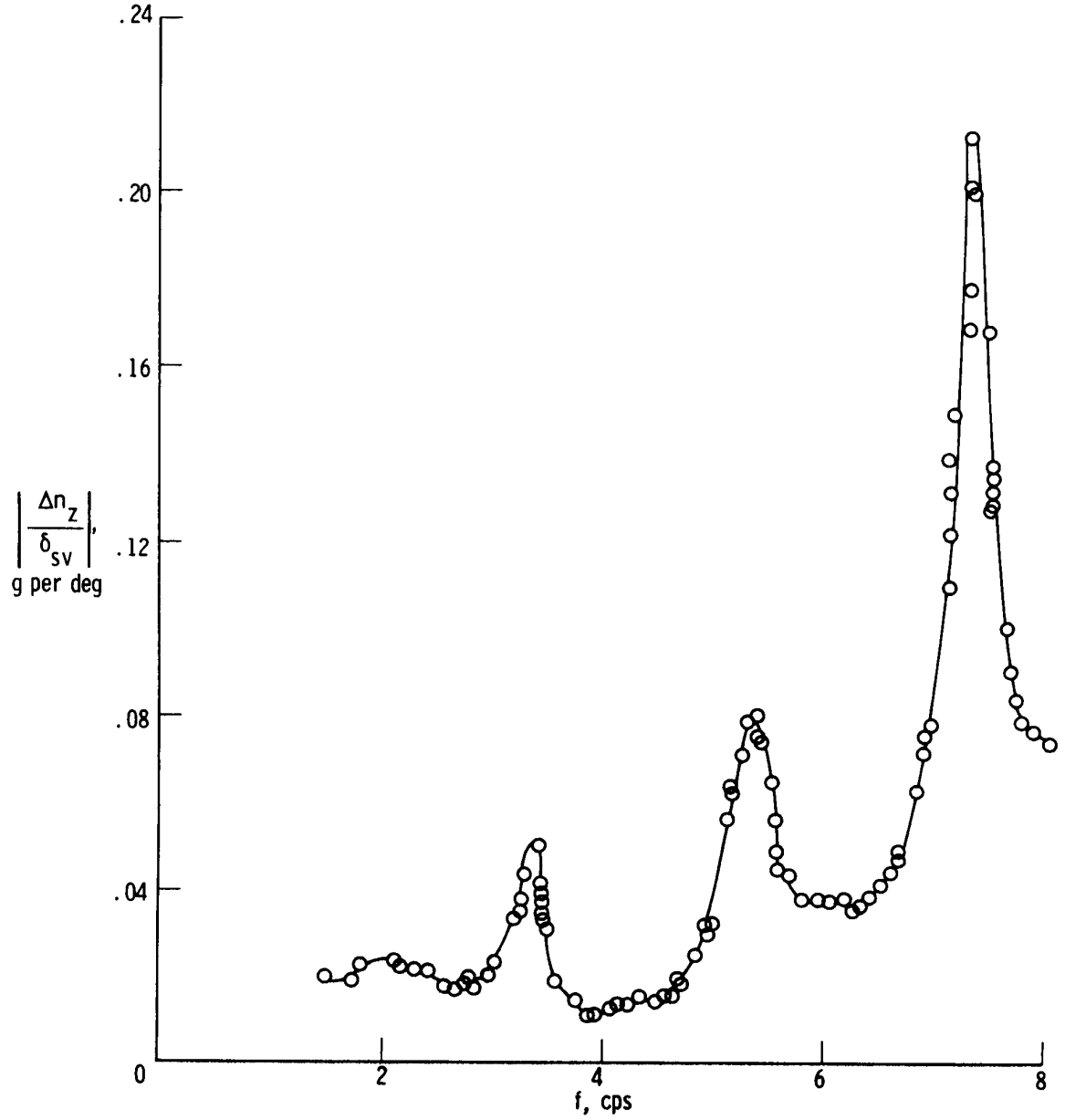

(i) Right wing; FS 46.23 m (1820 in.); BP 9.53 m (375 in.).

Figure 9. Continued.

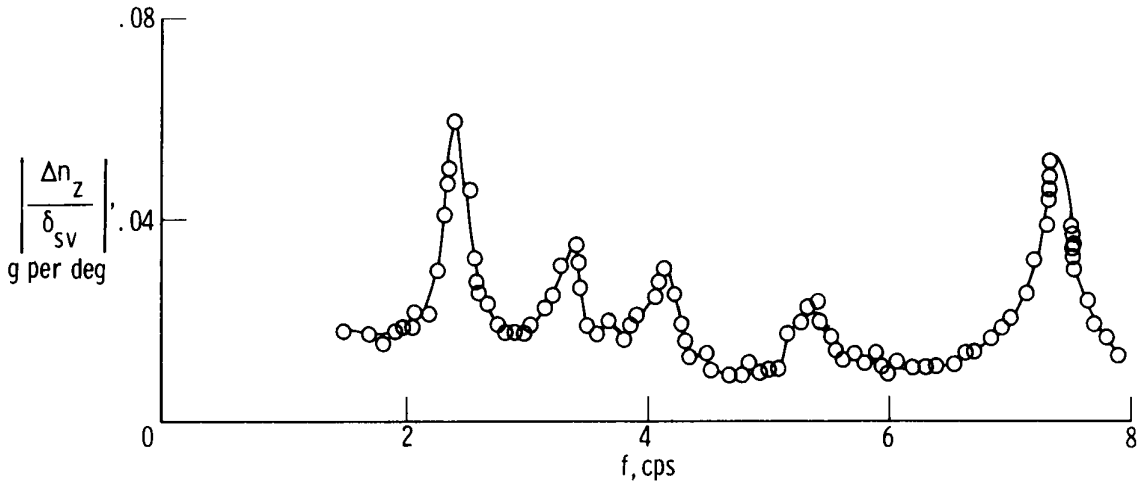

(j) Left wing; FS 55.17 m (2172 in.); BP 9.53 m (375 in.).

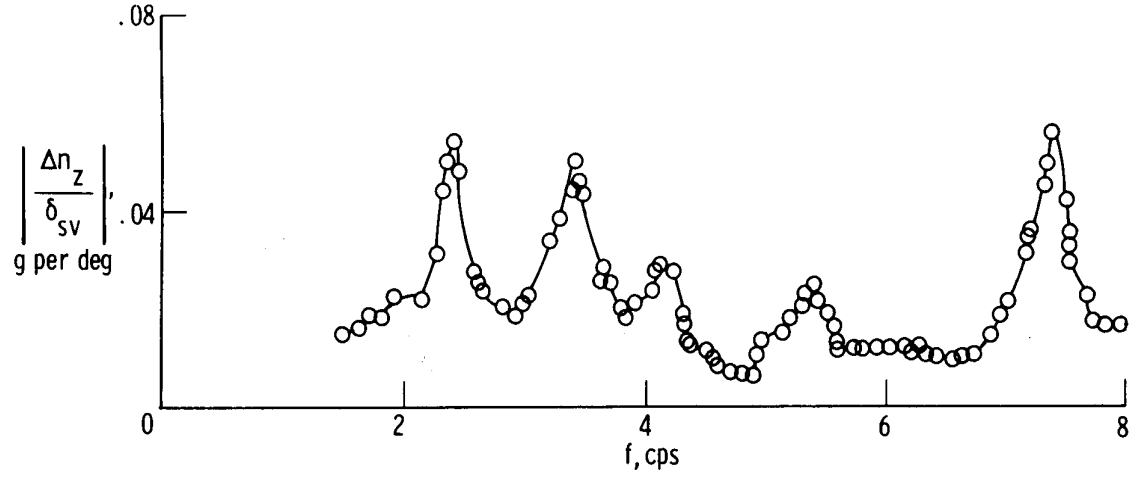

(k) Right wing; FS 55.17 m (2172 in.); BP 9.53 m (375 in.).

Figure 9. Concluded.

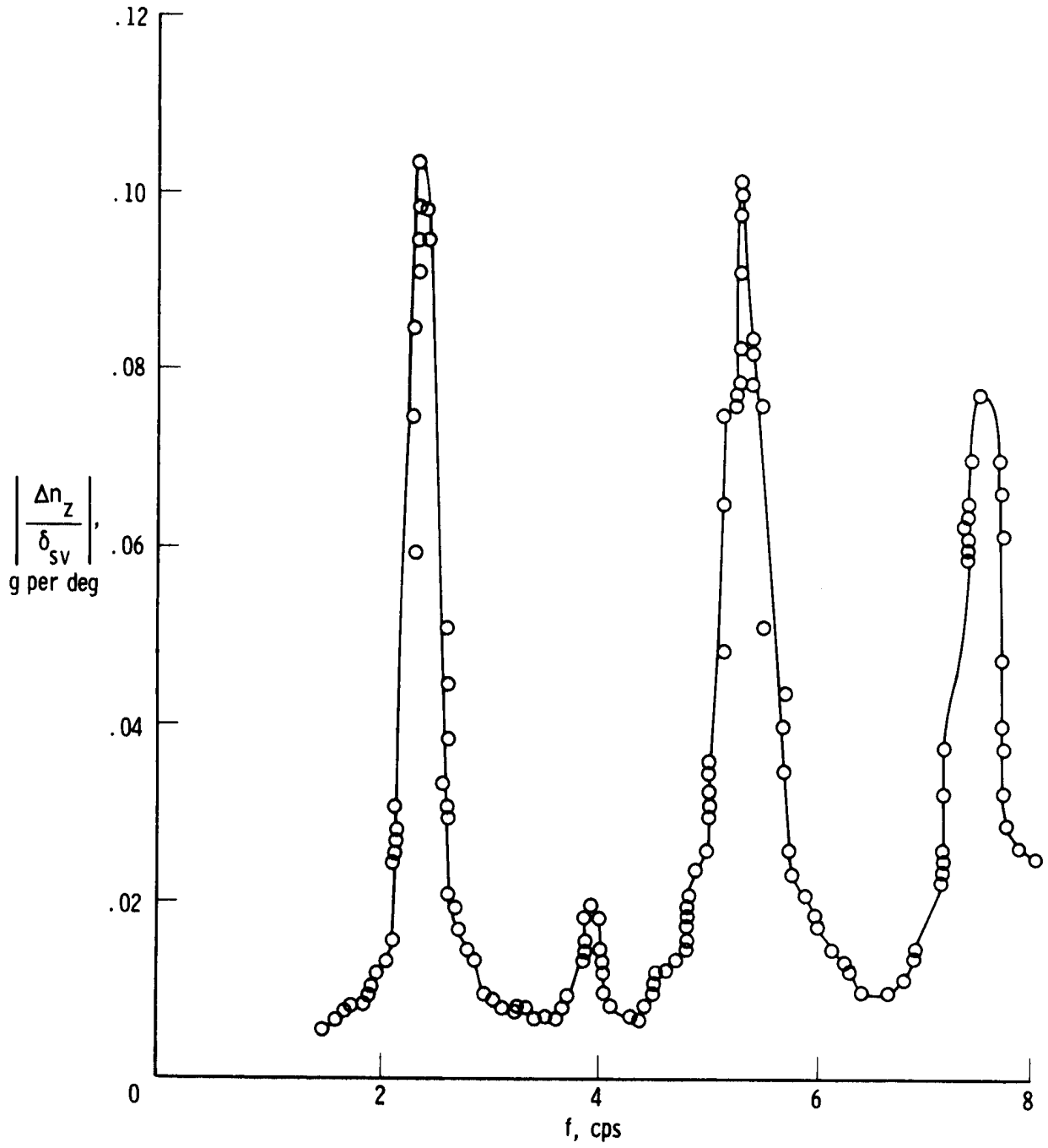

(a) Fuselage nose; FS 4.95 m (194.75 in.).

Figure 10. Flight-measured vertical acceleration response to shaker vane excitation. Mediumweight; M = 2.38; h_p = 18,898 m (62,000 ft); δ_t = 65°.

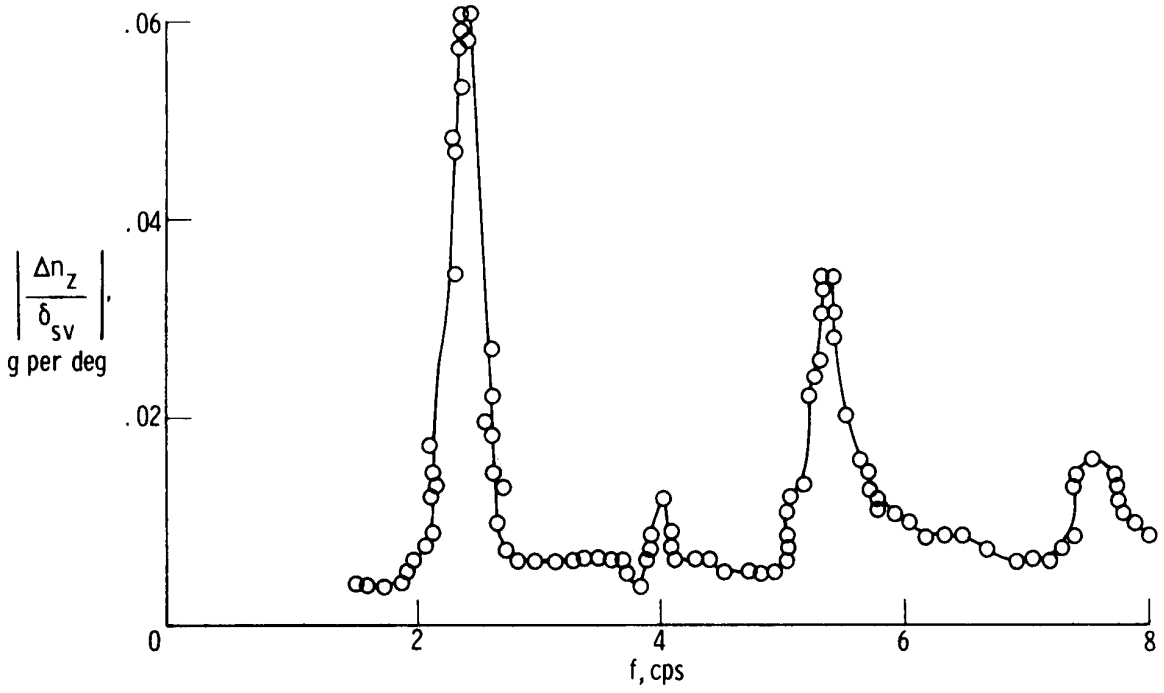

(b) Pilot's station; FS 11.12 m (438 in.).

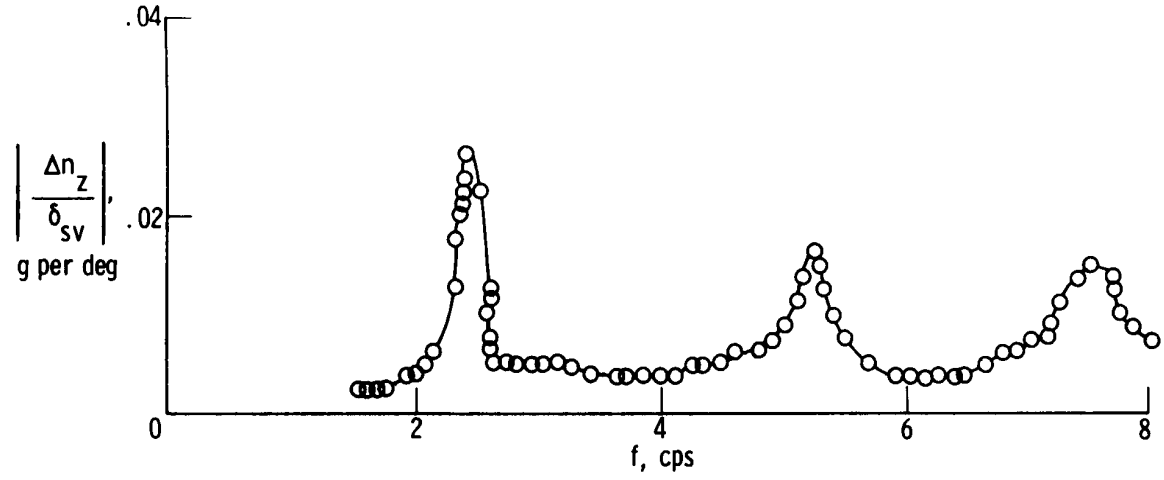

(c) Near center of gravity; FS 37.72 m (1485 in.).

Figure 10. Continued.

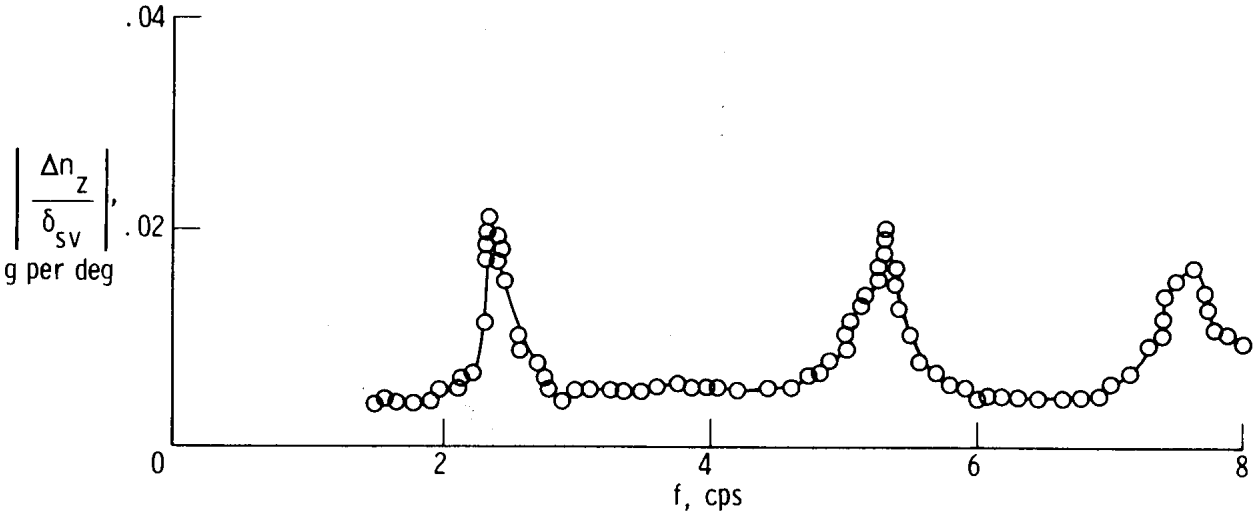

(d) Center of gravity; FS 41.99 m (1653 in.).

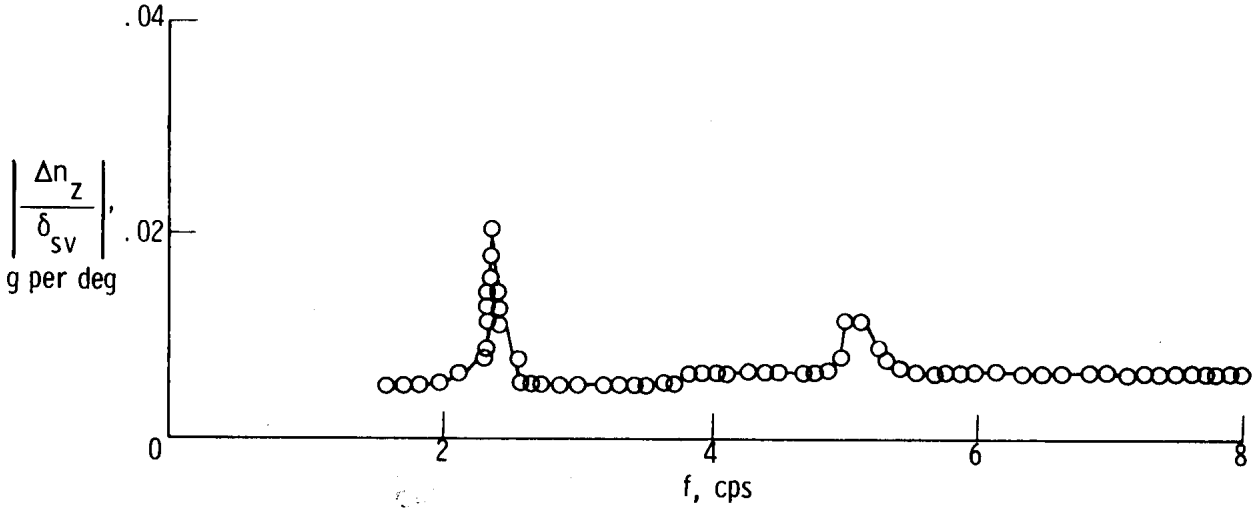

(e) Aft fuselage; FS 51.70 m (2035.5 in.).

Figure 10. Continued.

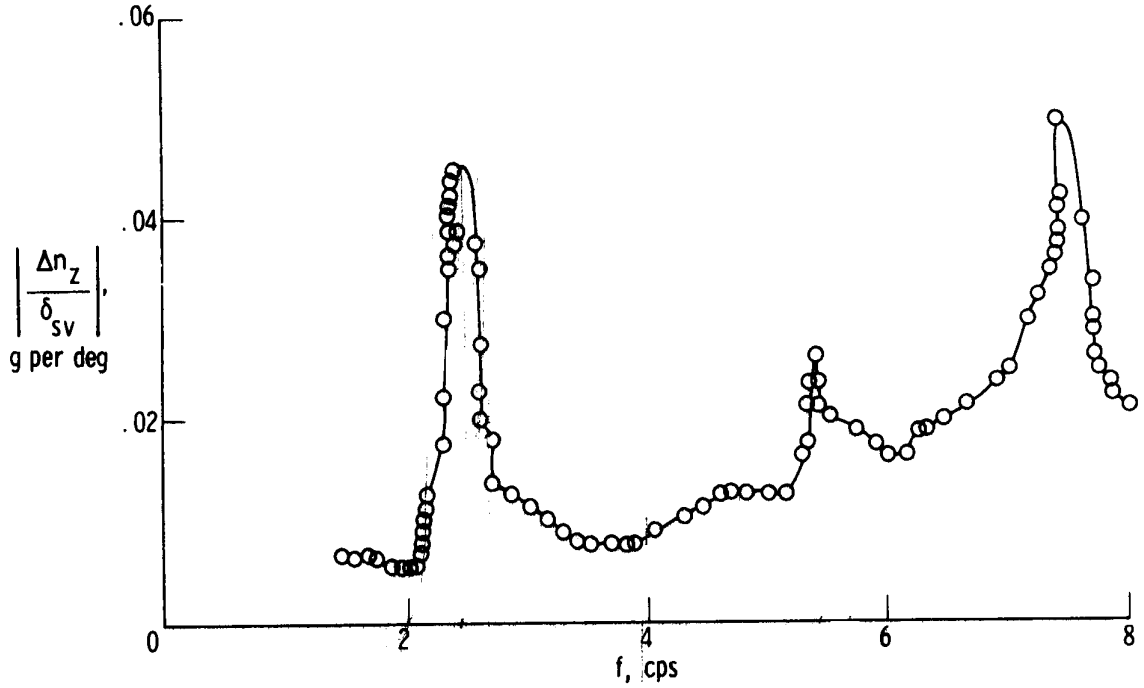

(f) Right canard tip; FS 15.70 m (618 in.); HS 4.32 m (170 in.).

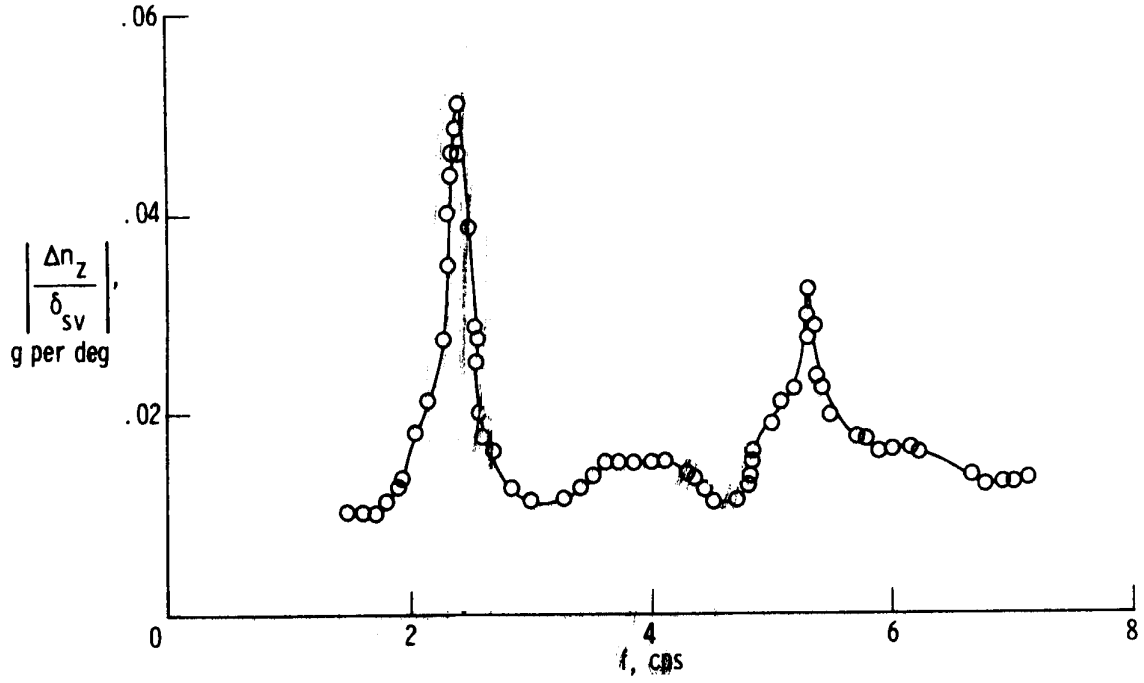

(g) Left wing; FS 56.18 m (2212 in.); BP 7.11 m (280 in.).

Figure 10. Continued.

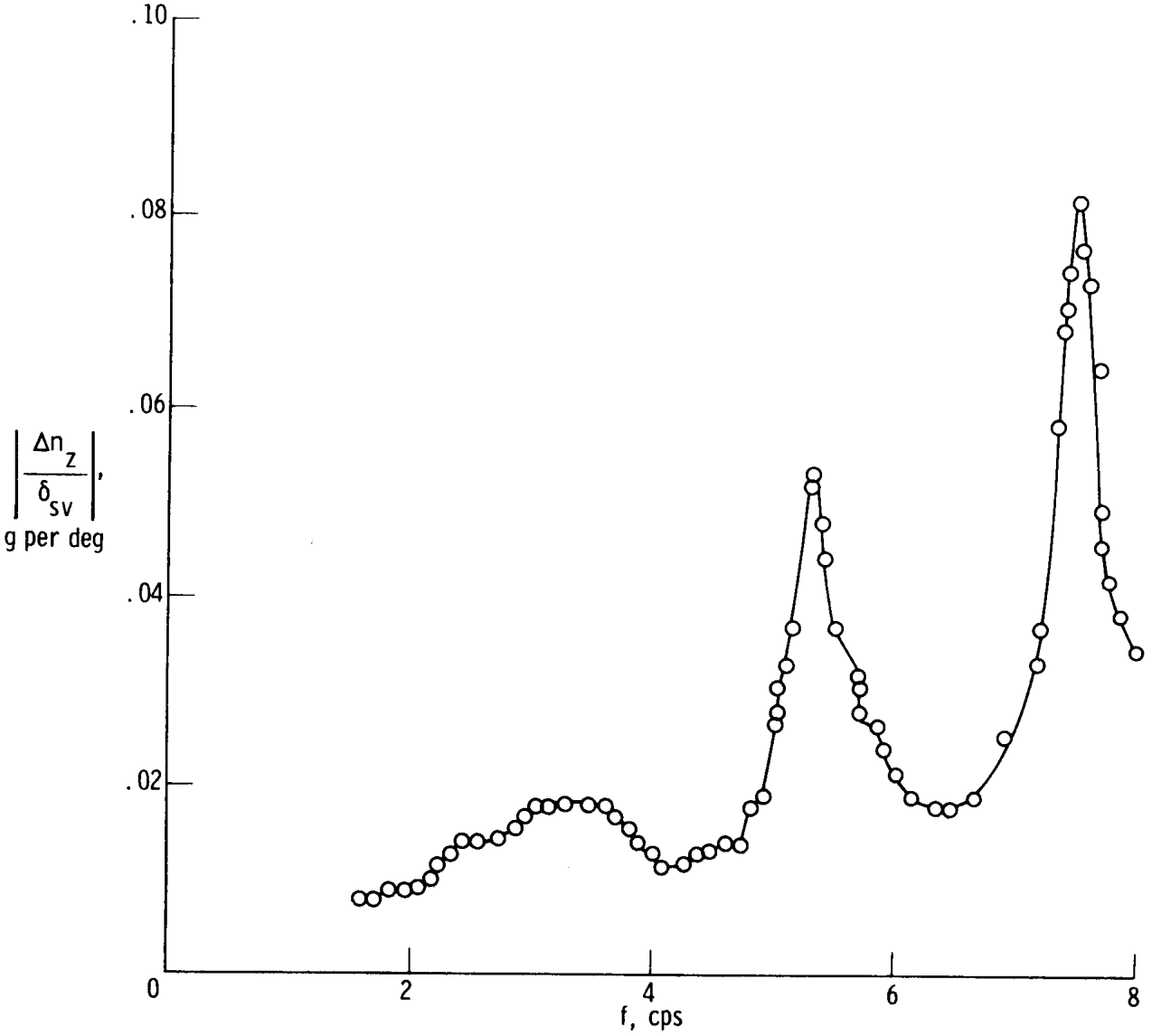

(h) Left wing; FS 46.23 m (1820 in.); BP 9.53 m (375 in.).

Figure 10. Continued.

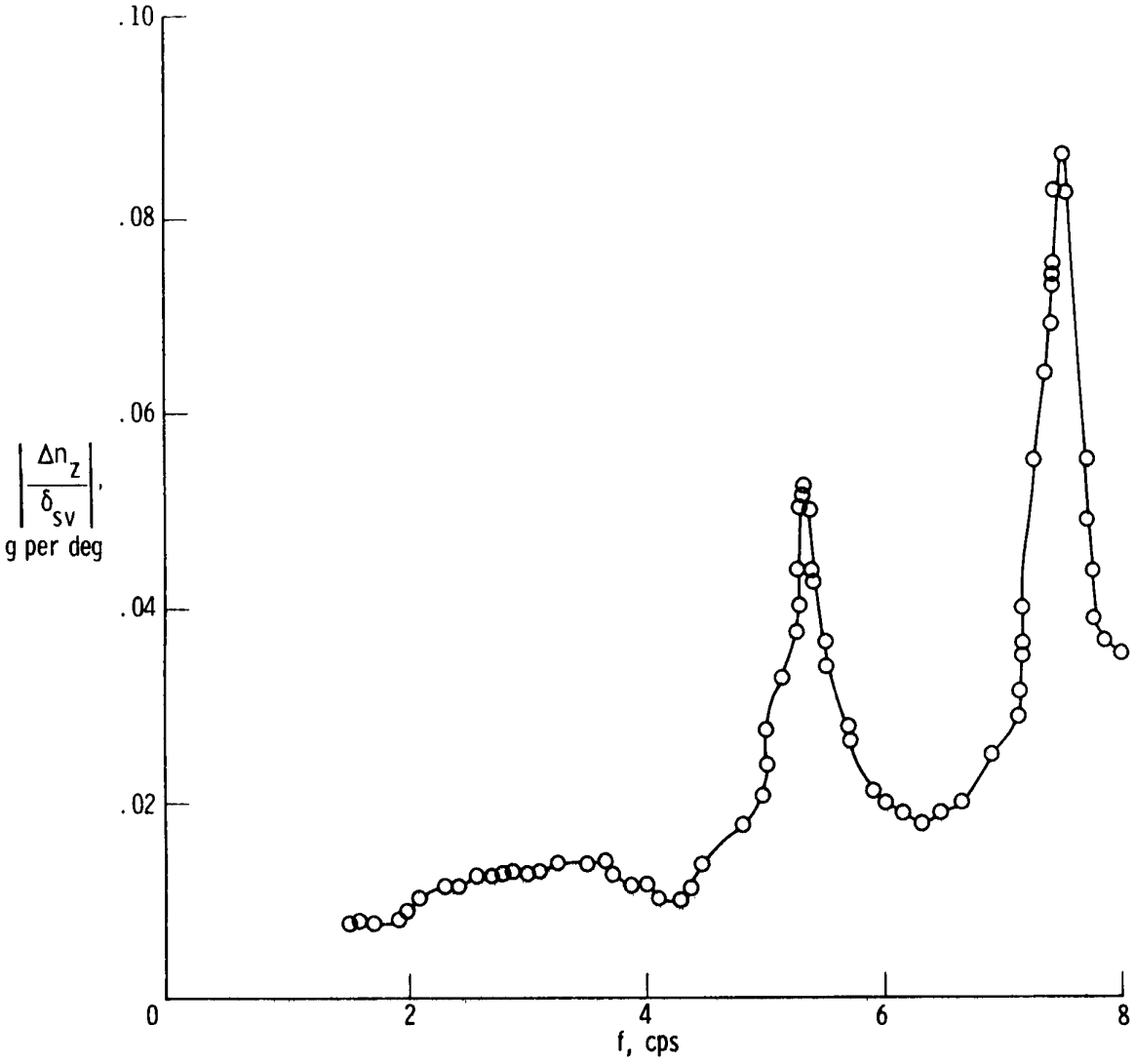

(i) Right wing; FS 46.23 m (1820 in.); BP 9.53 m (375 in.).

Figure 10. Continued.

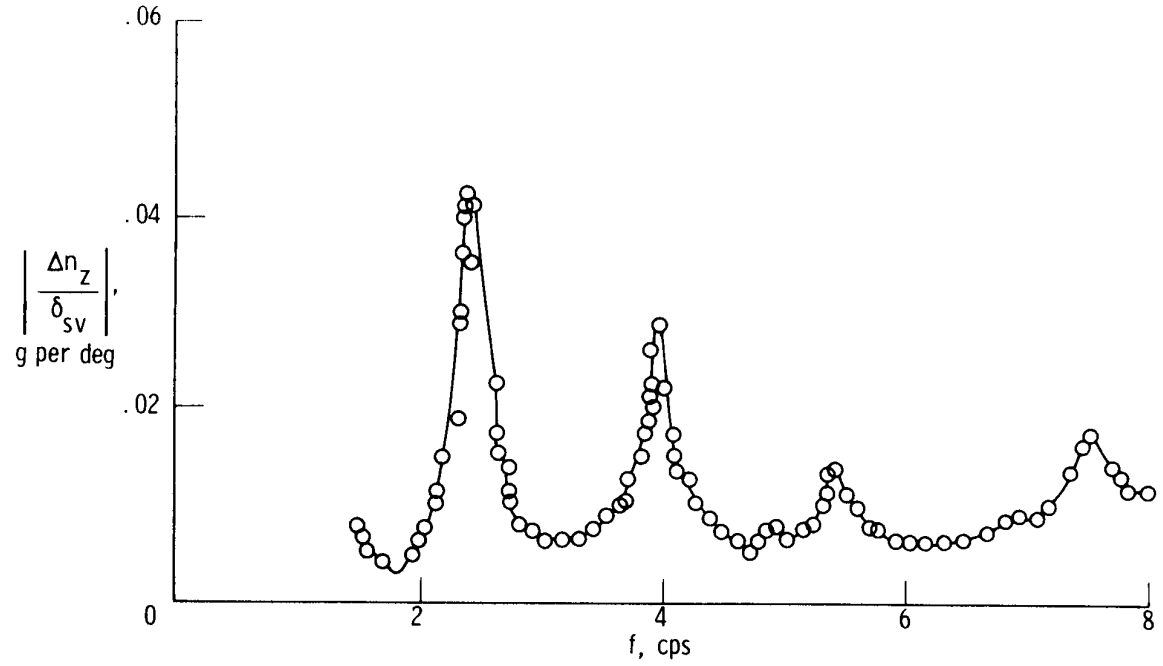

(j) Left wing; FS 55.17 m (2172 in.); BP 9.53 m (375 in.).

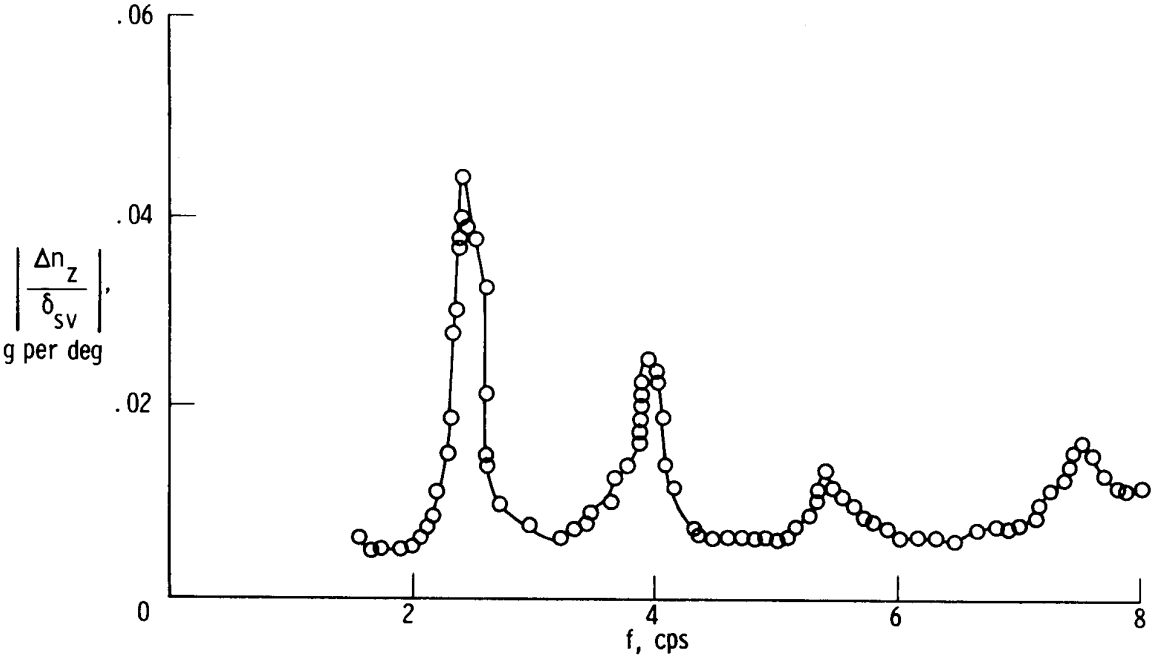

(k) Right wing; FS 55.17 m (2172 in.); BP 9.53 m (375 in.).

Figure 10. Continued.

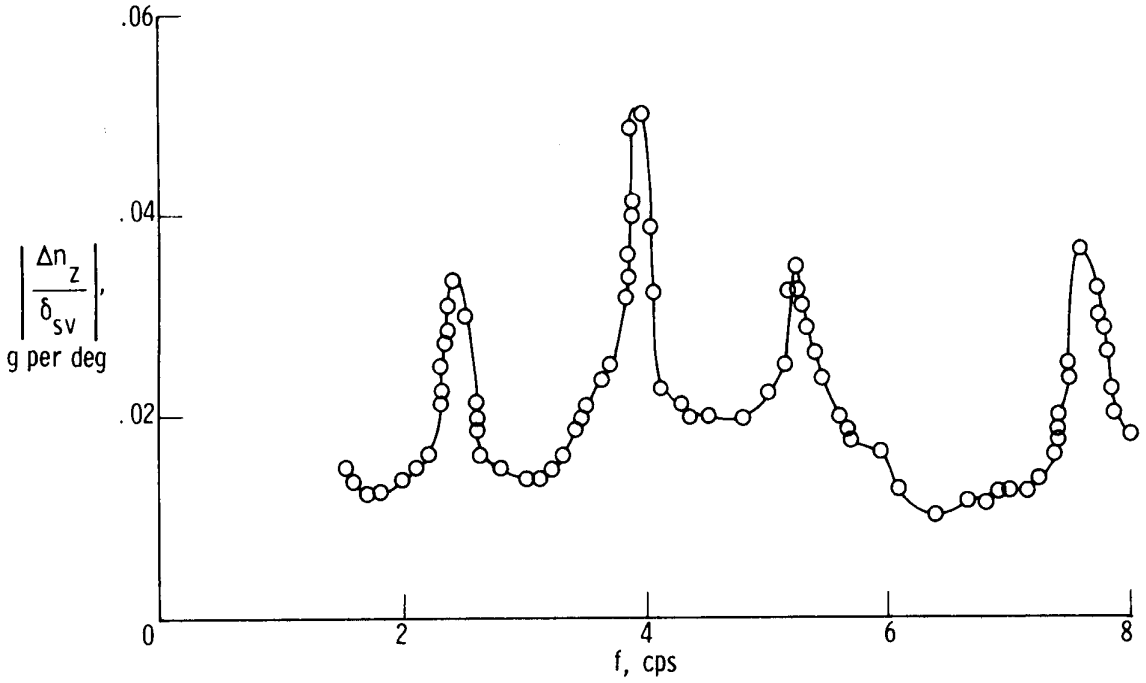

(l) Left wingtip; FS 55.88 m (2200 in.); BP 13.21 m (520 in.).

Figure 10. Concluded.

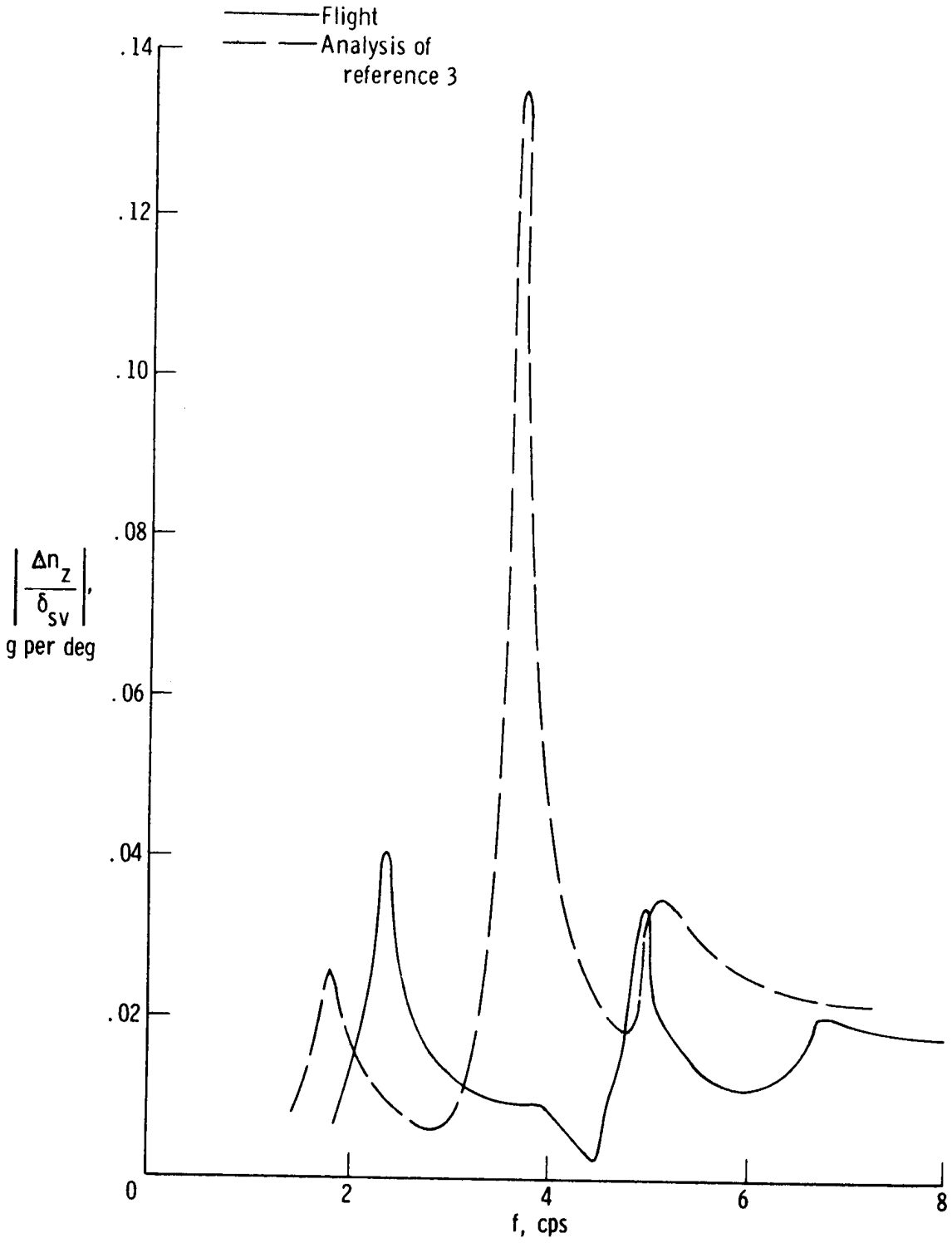

(a) Heavyweight; M = 0.87; h_p = 7620 m (25,000 ft); δ_t = 25°.

Figure 11. Comparison of flight-measured vertical acceleration response to shaker vane excitation with response calculated by using the analysis of reference 3. Pilot's station; FS 11.12 m (438 in.).

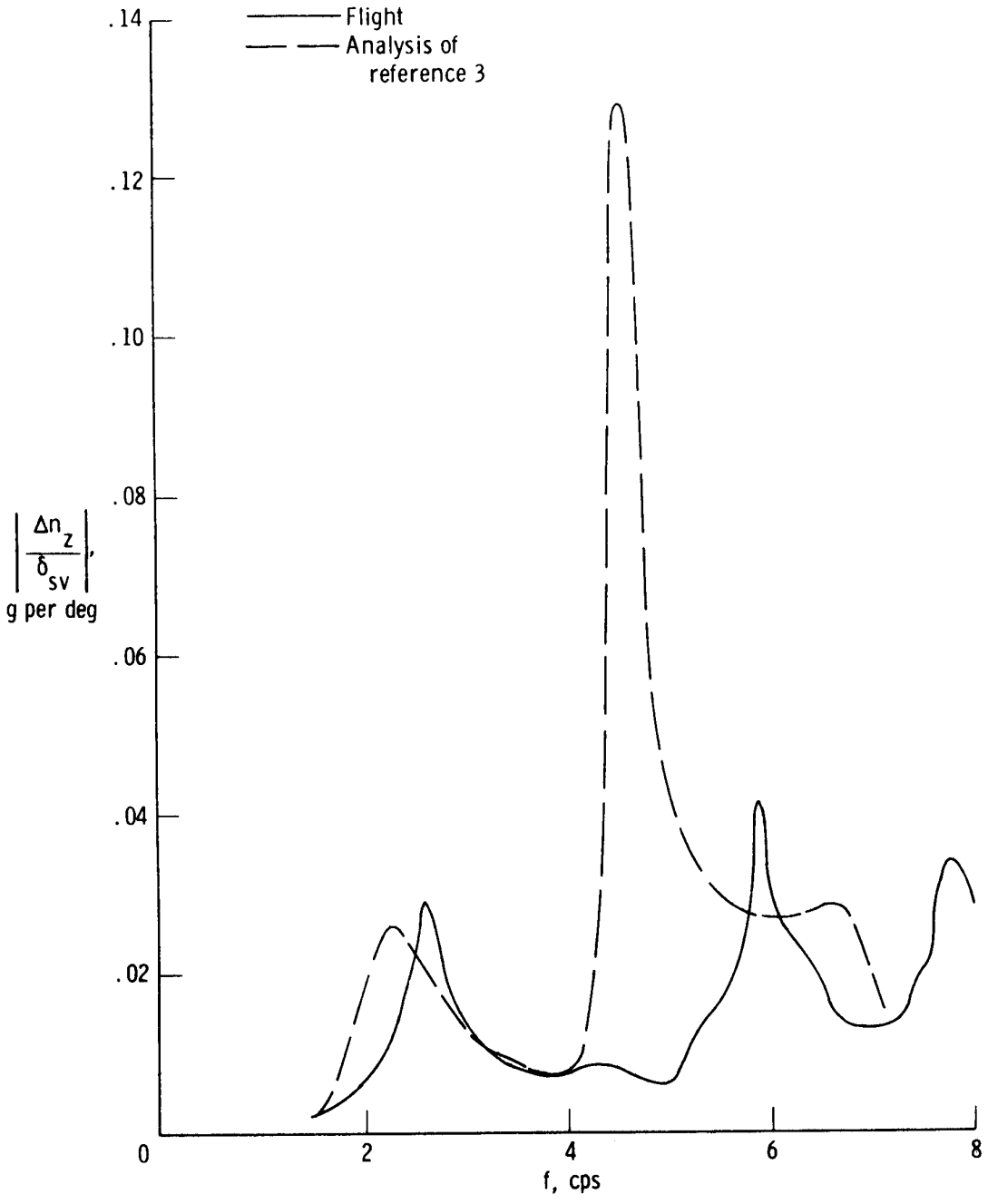

(b) Lightweight; M = 0.86; h_p = 7620 m (25,000 ft); δ_t = 25°.

Figure 11. Continued.

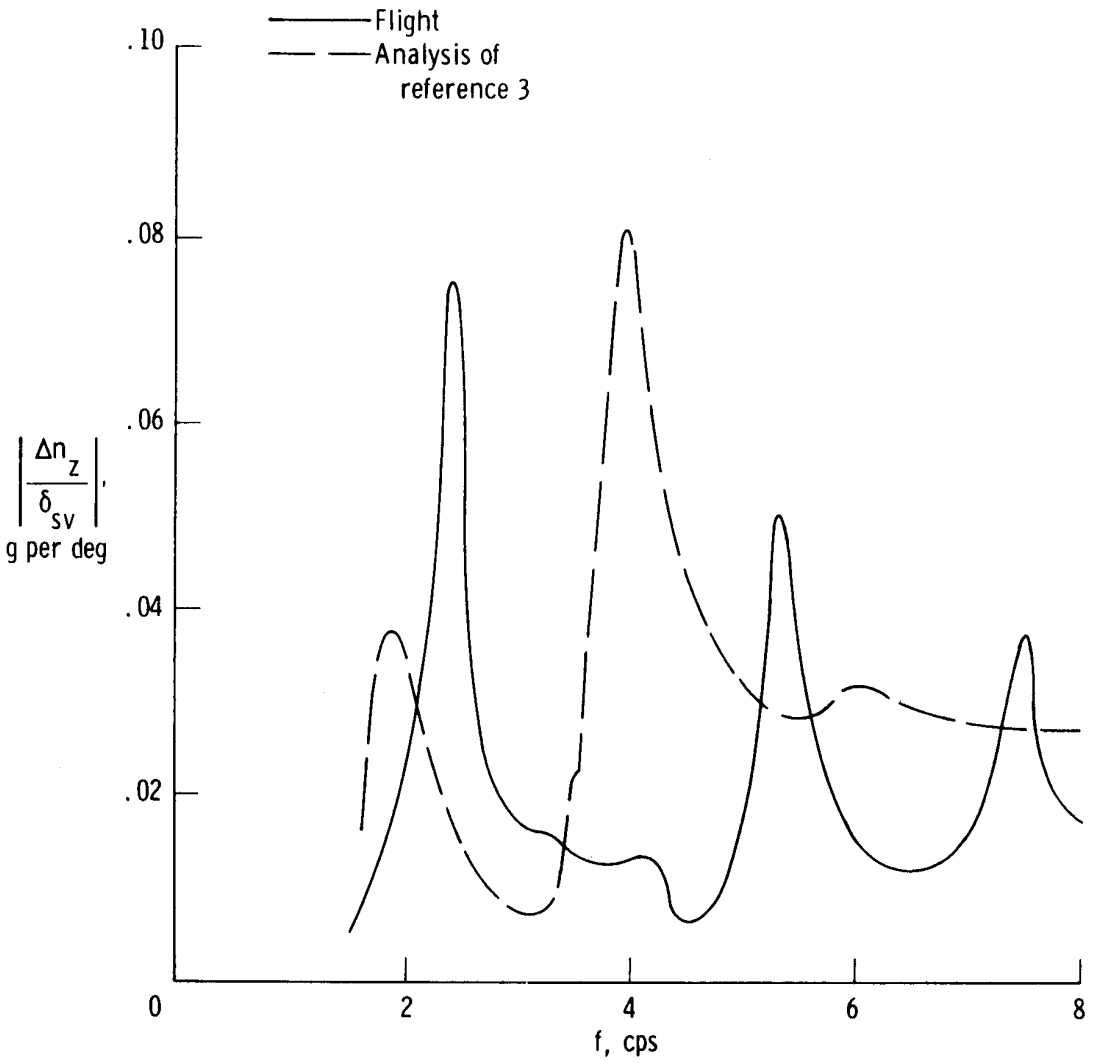

(c) Mediumweight; M = 1.59; h_p = 11,918 m (39,100 ft); δ_t = 65°.

Figure 11. Continued.

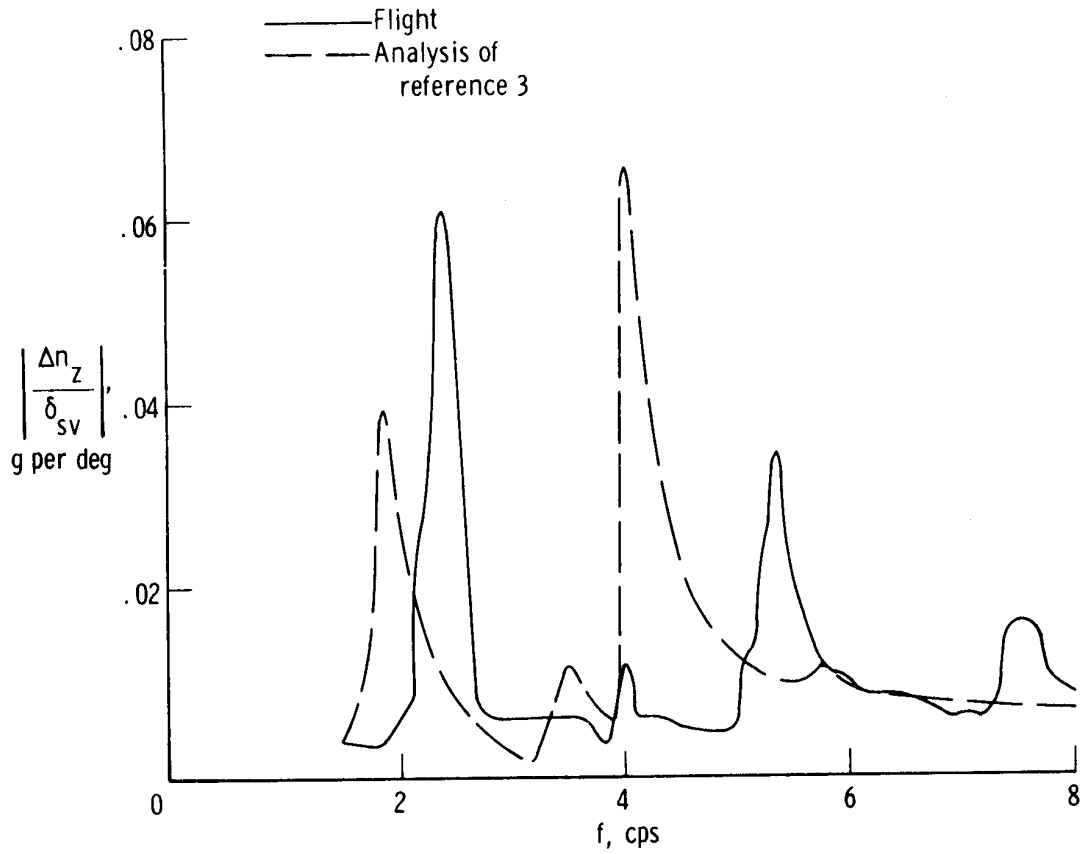

(d) Mediumweight; M = 2.38; h_p = 18,898 m (62,000 ft); $\delta_t = 65°$.

Figure 11. Concluded.

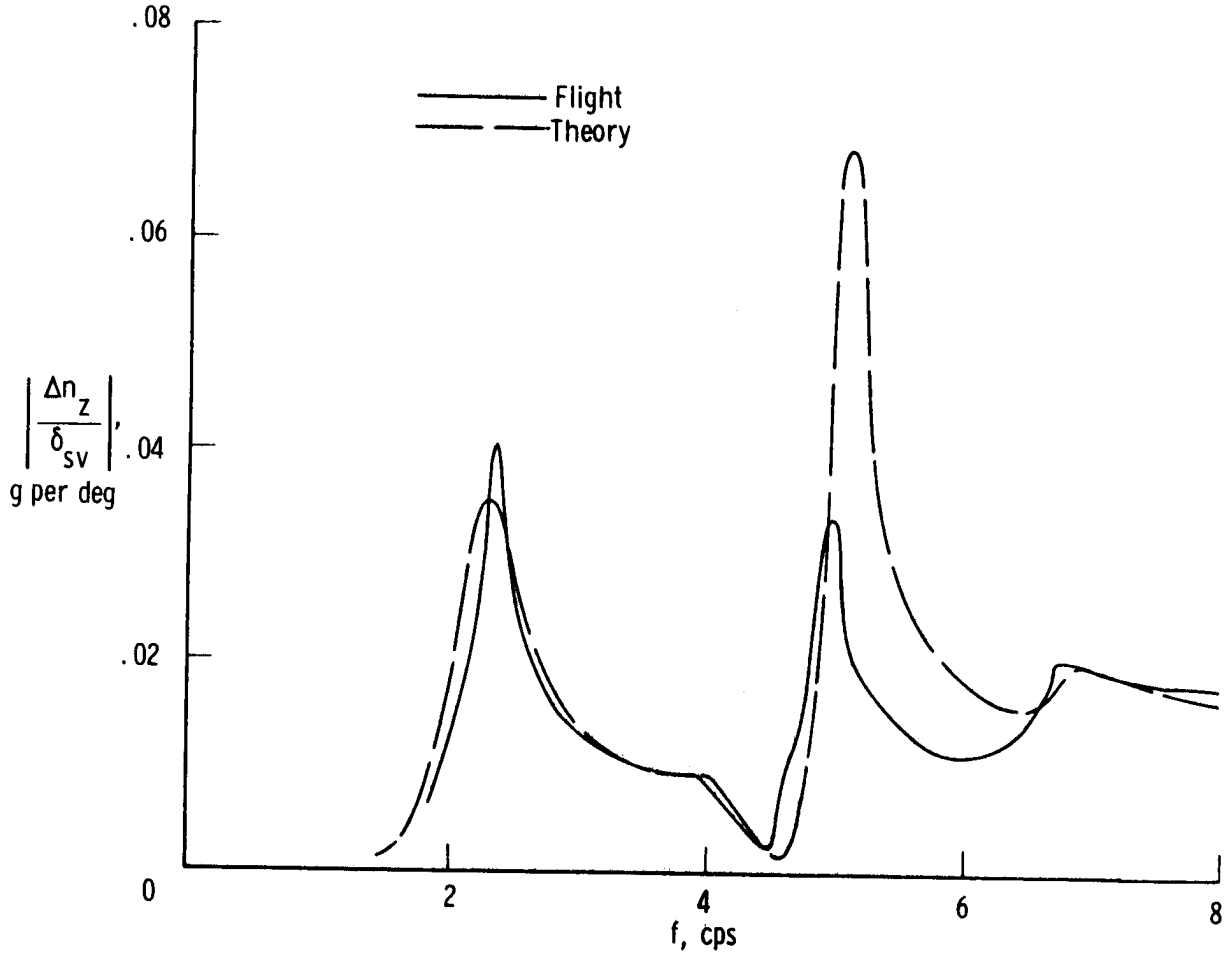

(a) Heavyweight; M = 0.87; h_p = 7620 m (25,000 ft); δ_t = 25°.

Figure 12. Comparison of flight-measured vertical acceleration response to shaker vane excitation with response calculated by using the updated analysis and quasi-steady wing aerodynamic theory. Pilot's station; FS 11.12 m (438 in.).

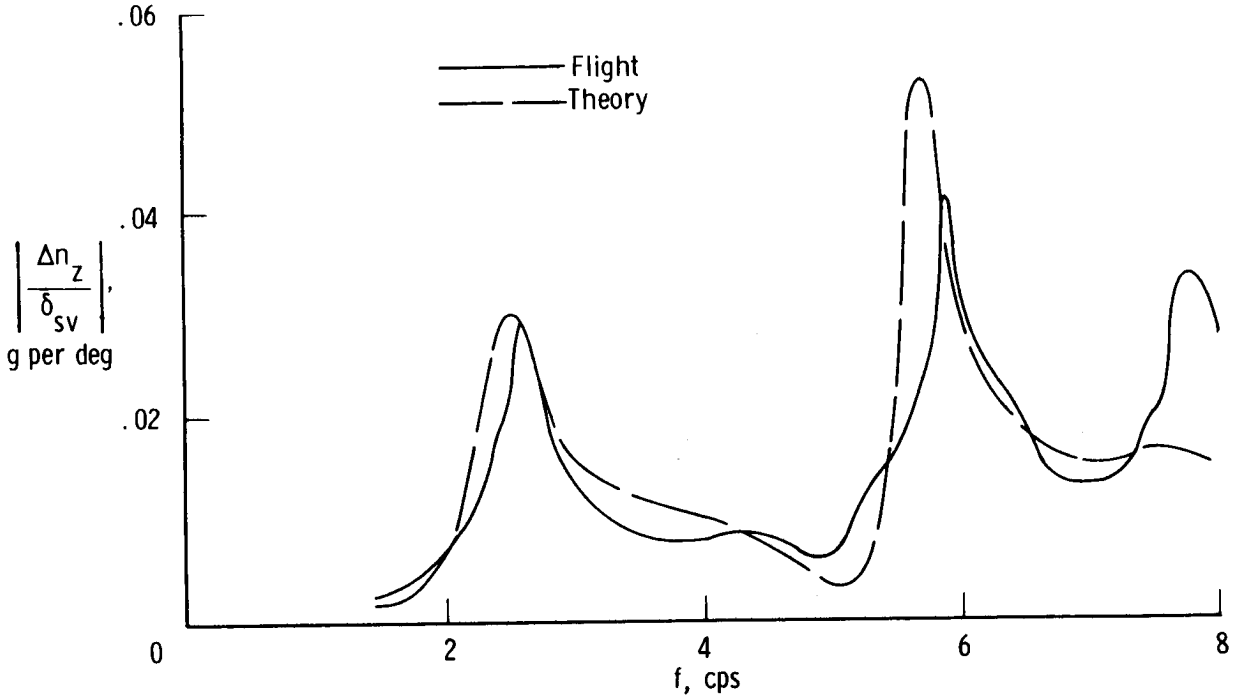

(b) Lightweight; M = 0.86; h_p = 7620 m (25,000 ft); $\delta_t = 25°$.

Figure 12. Continued.

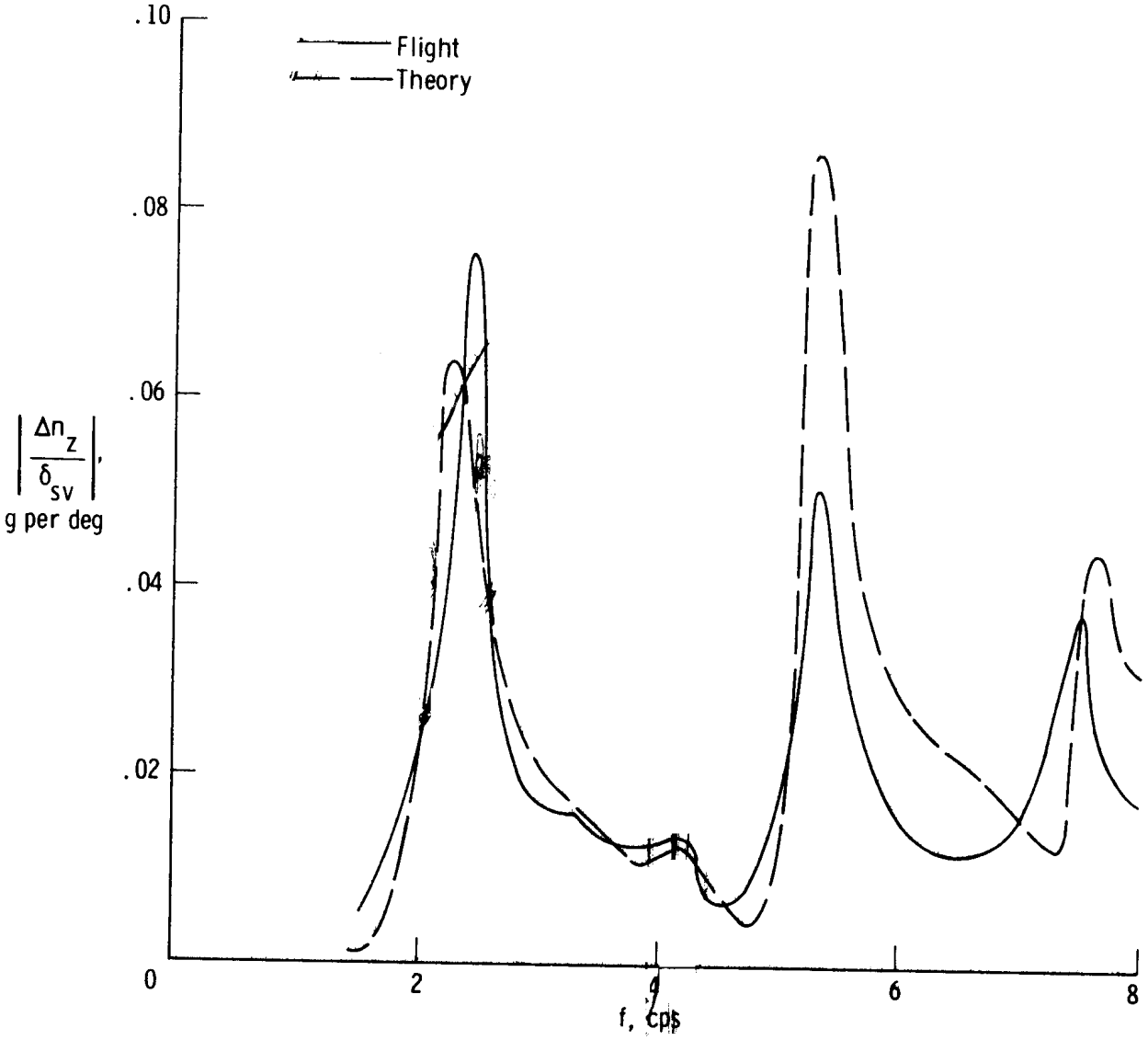

(c) Mediumweight; M = 1.59; h_p = 11,918 m (39,100 ft); δ_t = 65°.

Figure 12. Concluded.

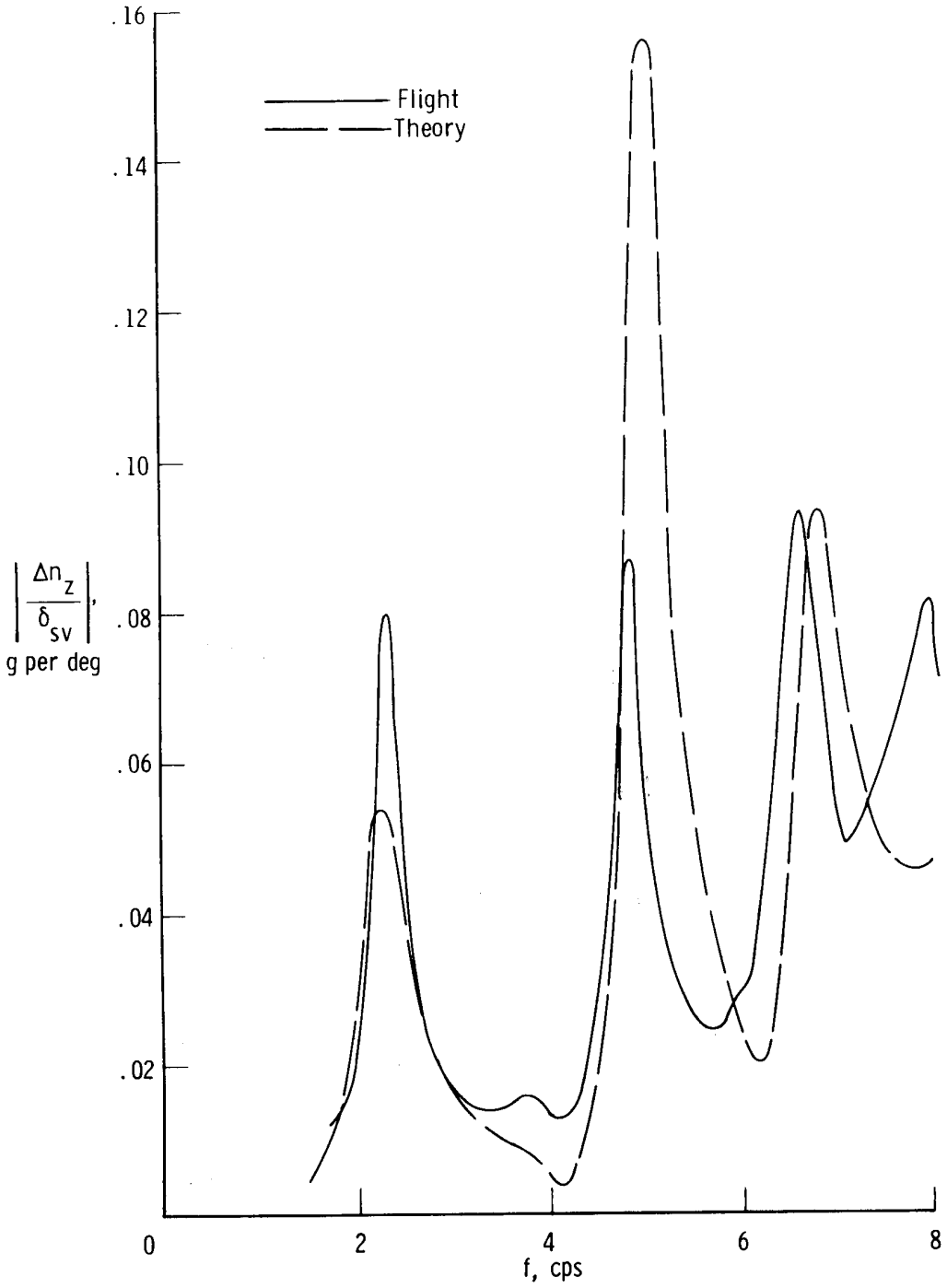

(a) Fuselage nose; FS 4.95 m (194.75 in.)

Figure 13. Comparison of flight-measured vertical acceleration response to shaker vane excitation with response calculated by using the updated analysis and quasi-steady wing aerodynamic theory. Heavyweight; M = 0.87; h_p = 7620 m (25,000 ft); $\delta_t = 25°$.

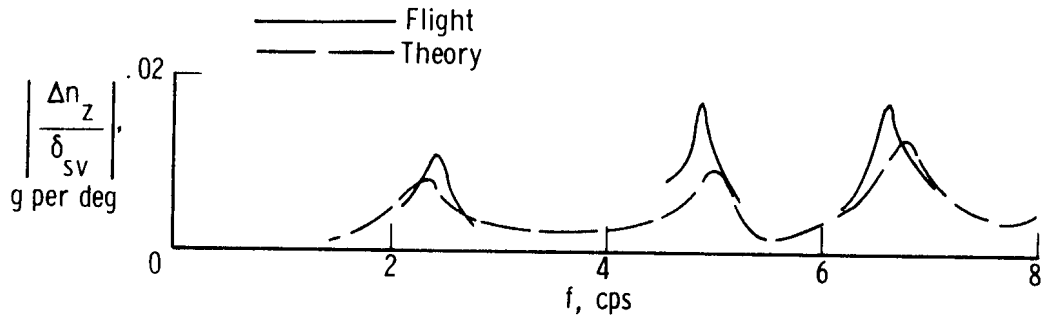

(b) Center of gravity; FS 41.99 m (1653 in.).

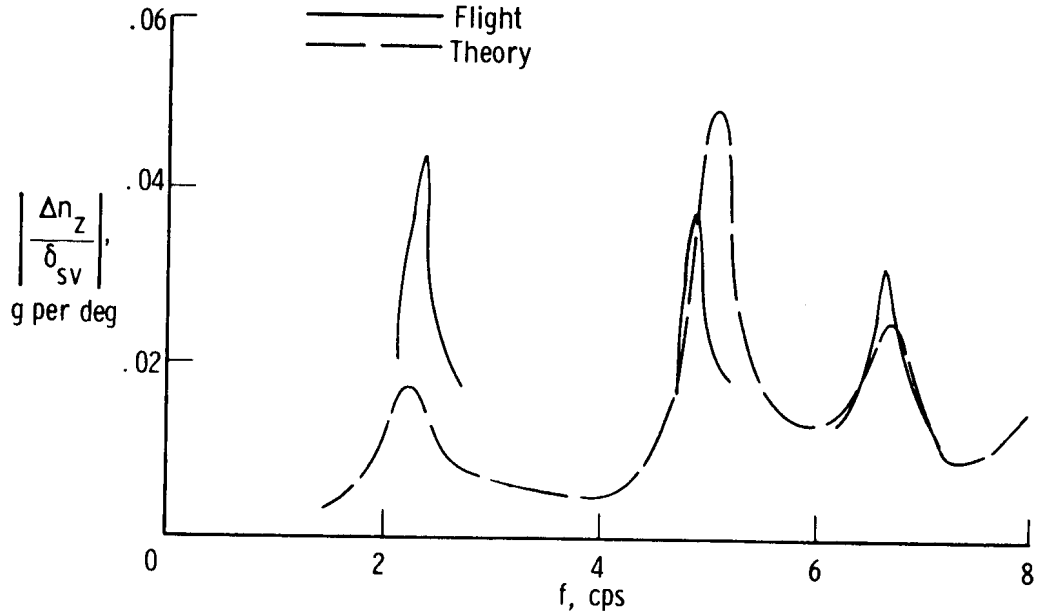

(c) Left wing; FS 56.18 m (2212 in.); BP 7.11 m (280 in.).

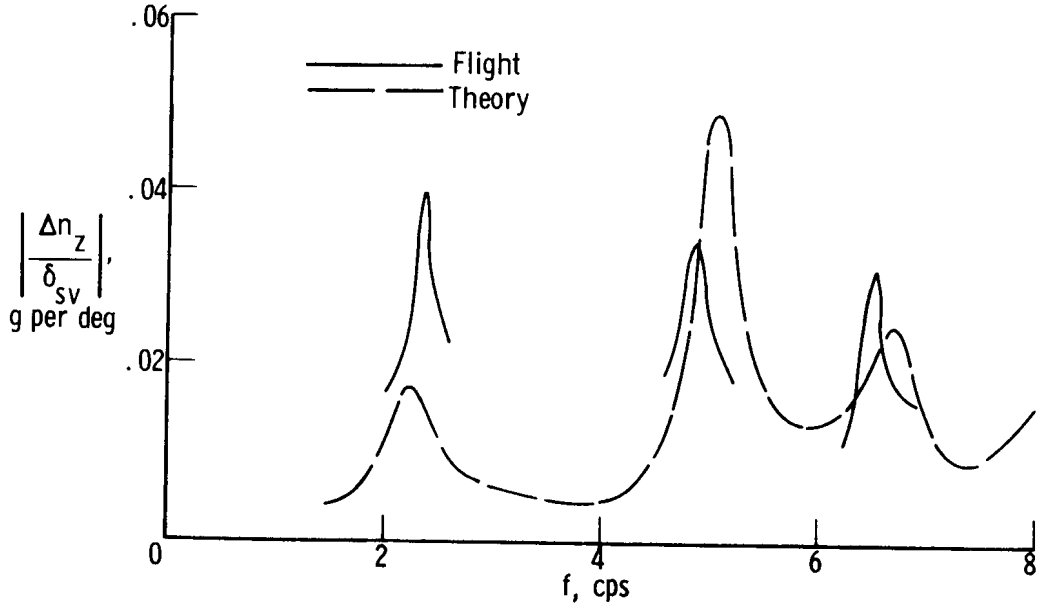

(d) Right wing; FS 56.18 m (2212 in.); BP 7.11 m (280 in.).

Figure 13. Concluded.

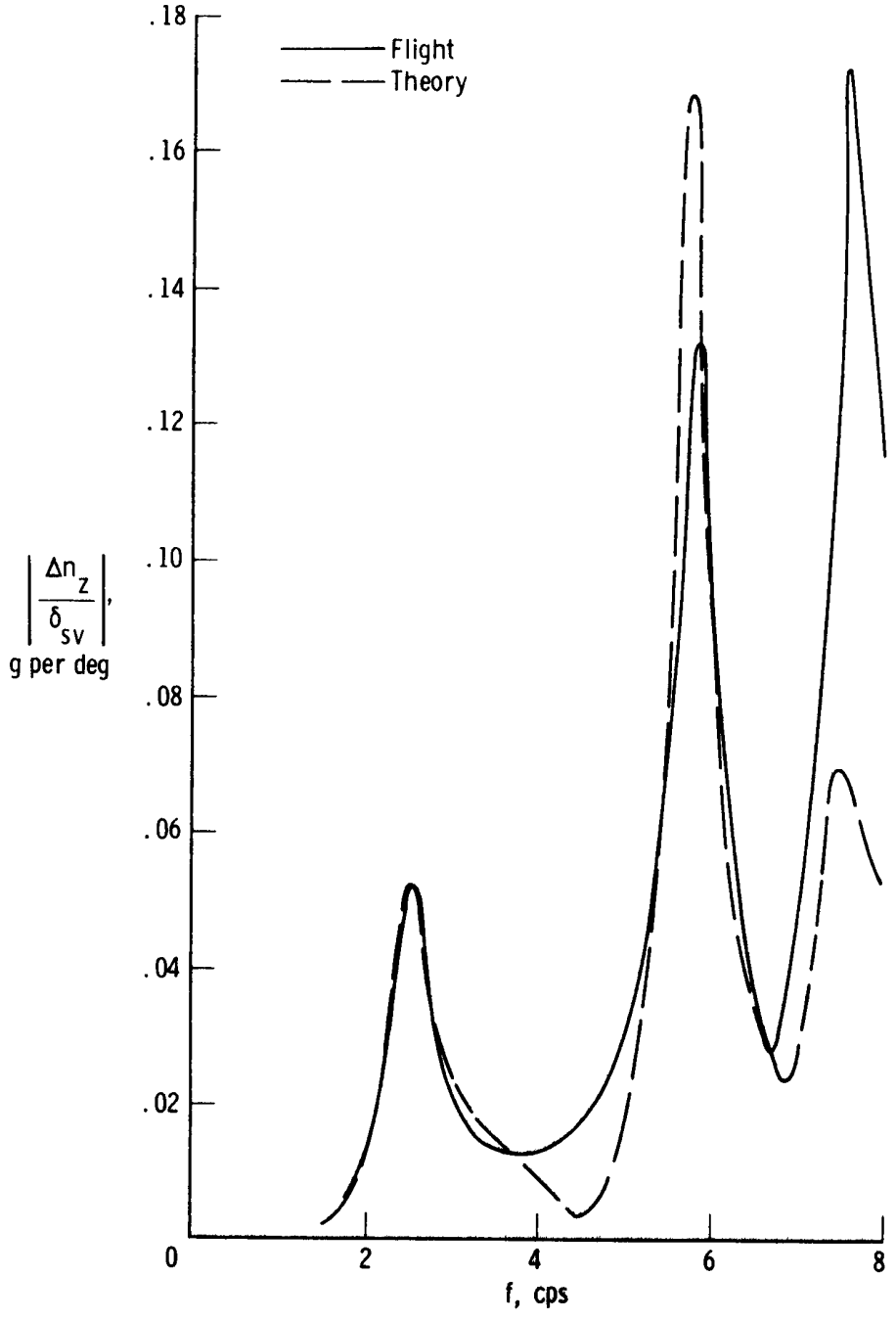

(a) Fuselage nose; FS 4.95 m (194.75 in.).

Figure 14. Comparison of flight-measured vertical acceleration response to shaker vane excitation with response calculated by using the updated analysis and quasi-steady wing aerodynamic theory. Lightweight; M = 0.86; h_p = 7620 m (25,000 ft); δ_t = 25°.

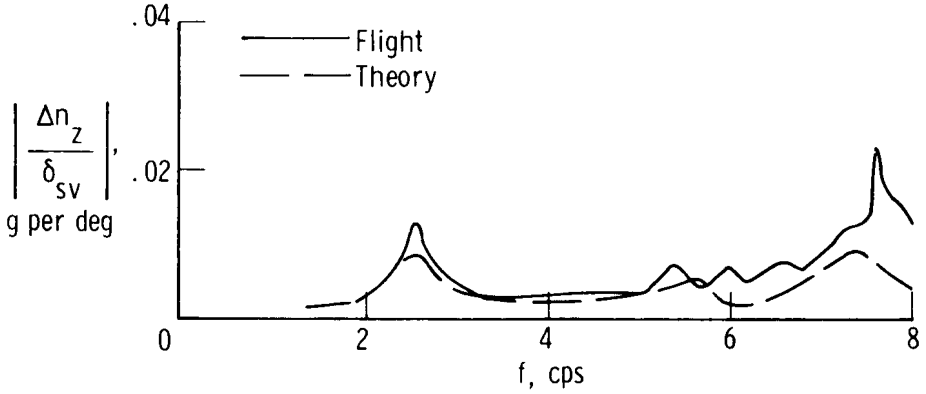

(b) Near center of gravity; FS 37.72 m (1485 in.).

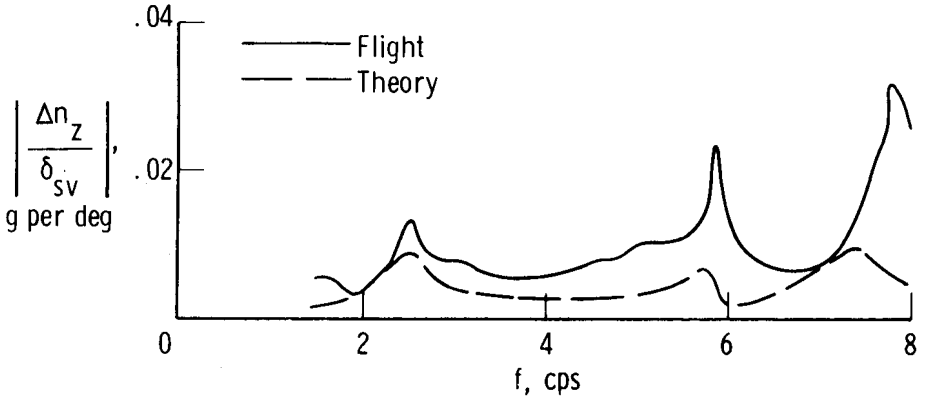

(c) Center of gravity; FS 41.99 m (1653 in.).

Figure 14. Continued.

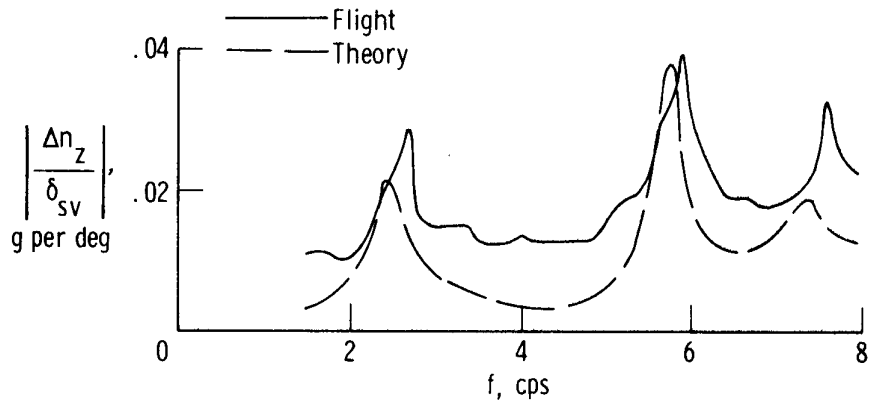

(d) Left wing; FS 56.18 m (2212 in.); BP 7.11 m (280 in.).

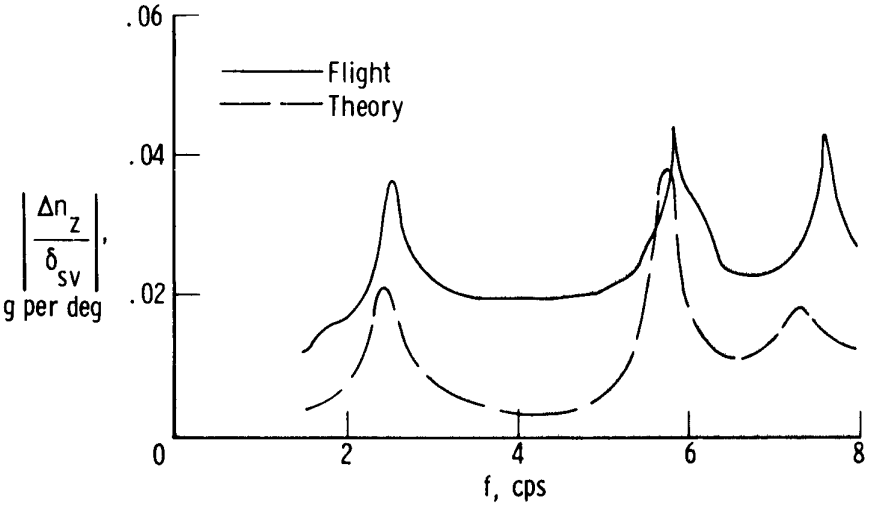

(e) Right wing; FS 56.18 m (2212 in.); BP 7.11 m (280 in.).

Figure 14. Concluded.

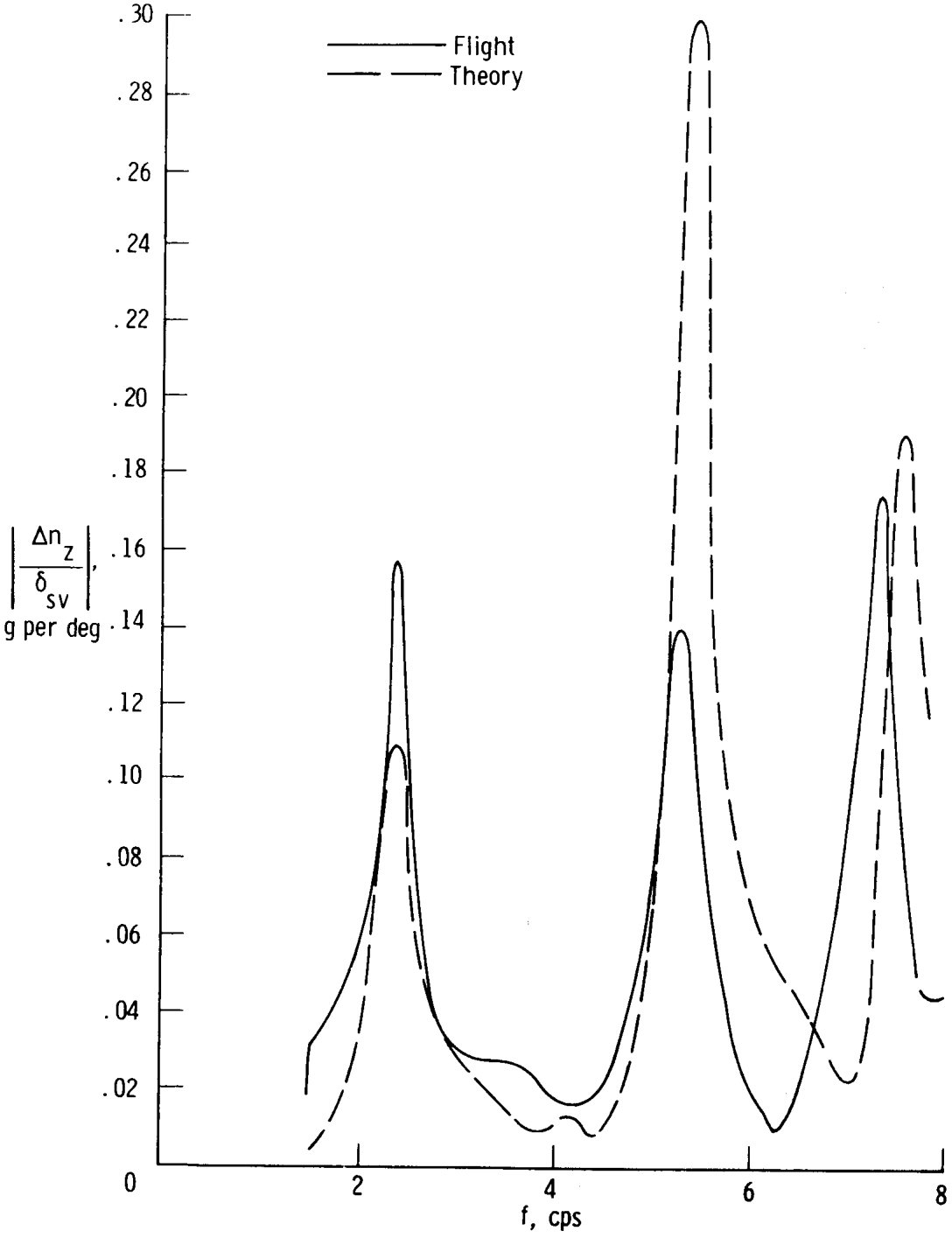

(a) Fuselage nose; FS 4.95 m (194.75 in.).

Figure 15. Comparison of flight-measured vertical acceleration response to shaker vane excitation with response calculated by using the updated analysis and quasi-steady wing aerodynamic theory. Mediumweight; M = 1.59; h_p = 11,918 m (39,100 ft); $\delta_t = 65°$.

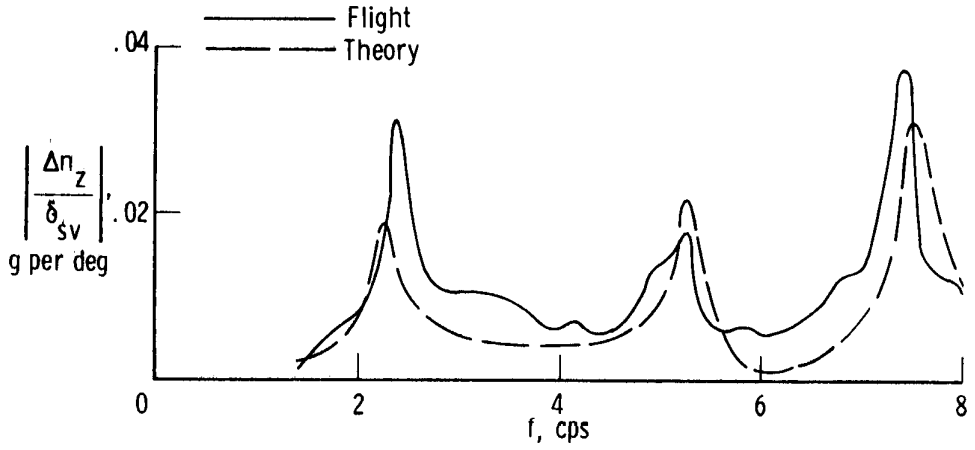

(b) Near center of gravity; FS 37.72 m (1485 in.).

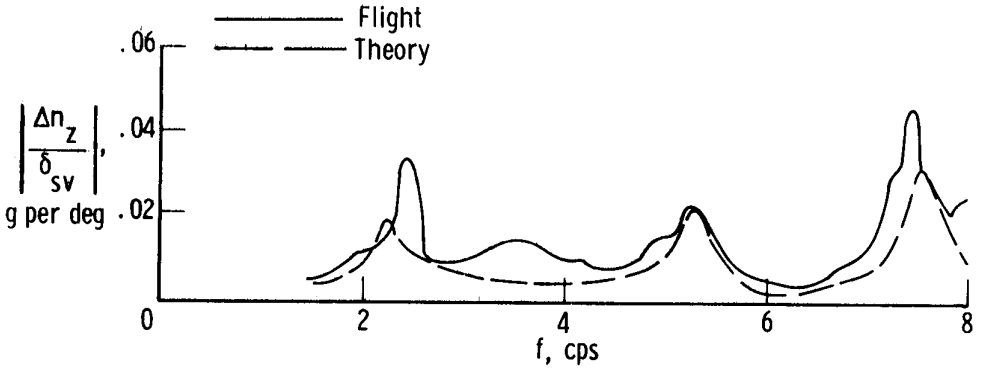

(c) Center of gravity; FS 41.99 m (1653 in.).

Figure 15. Continued.

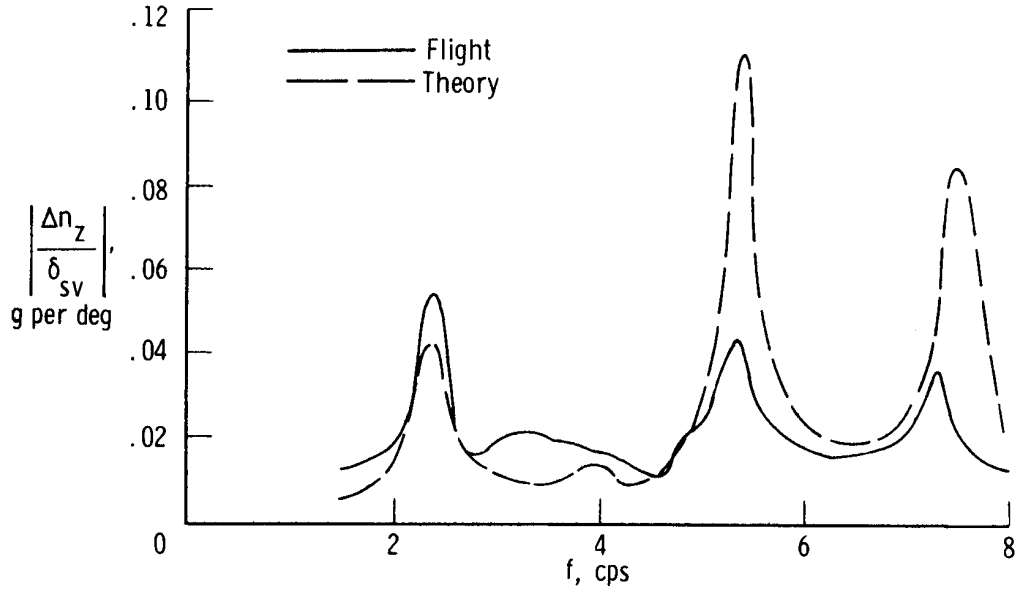

(d) Left wing; FS 56.18 m (2212 in.); BP 7.11 m (280 in.).

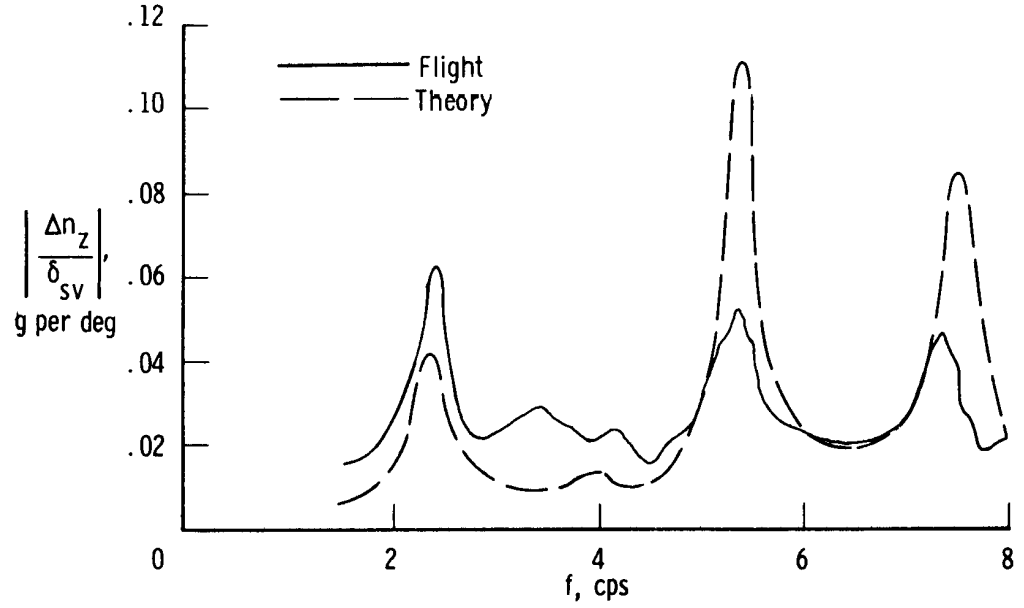

(e) Right wing; FS 56.18 m (2212 in.); BP 7.11 m (280 in.).

Figure 15. Concluded.

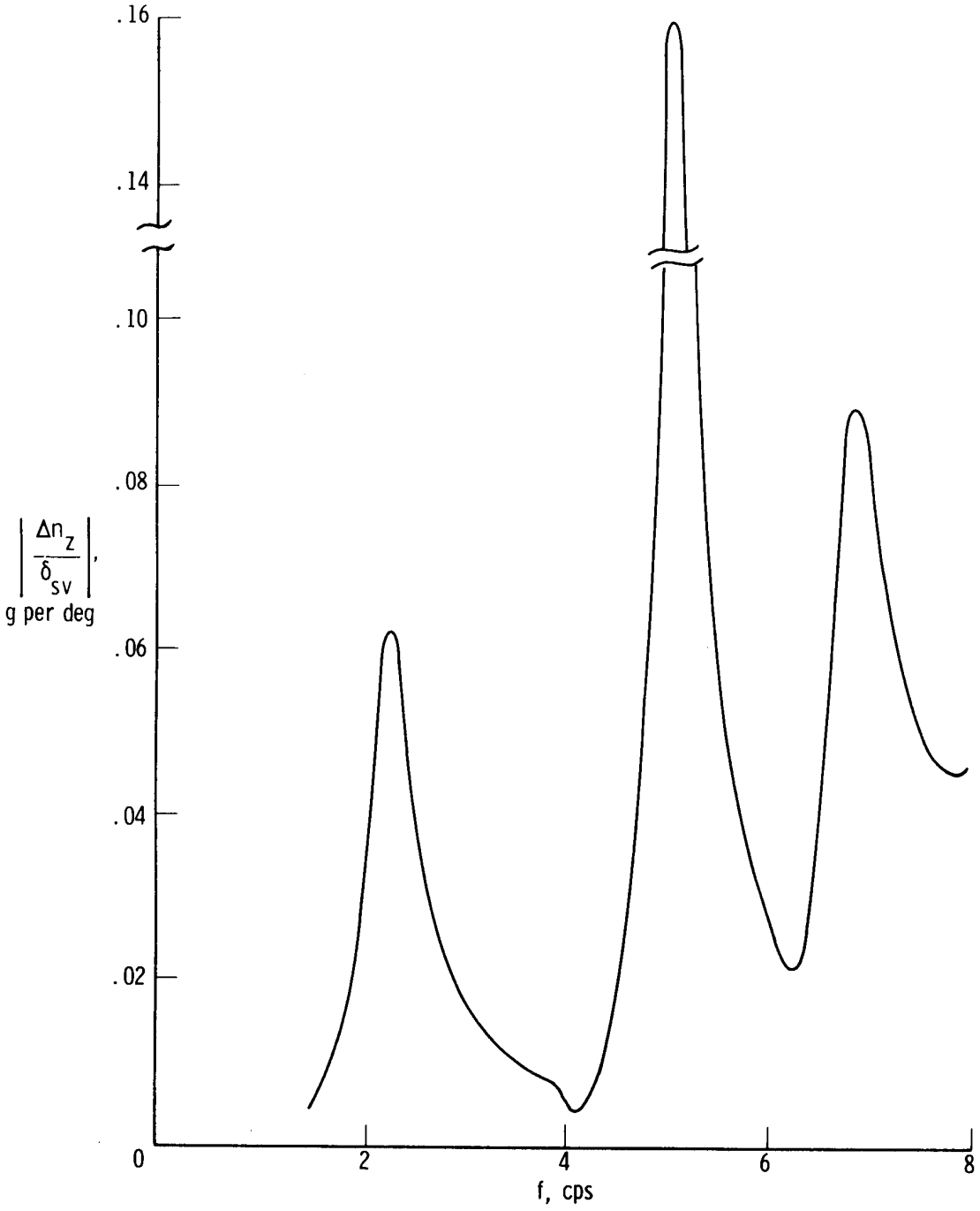

(a) Fuselage nose; FS 4.95 m (194.75 in.).

Figure 16. Vertical acceleration response to shaker vane excitation calculated by using quasi-steady aerodynamic theory without FACS. Updated analysis; heavyweight; M = 0.87; h_p = 7620 m (25,000 ft); $\delta_t = 25°$.

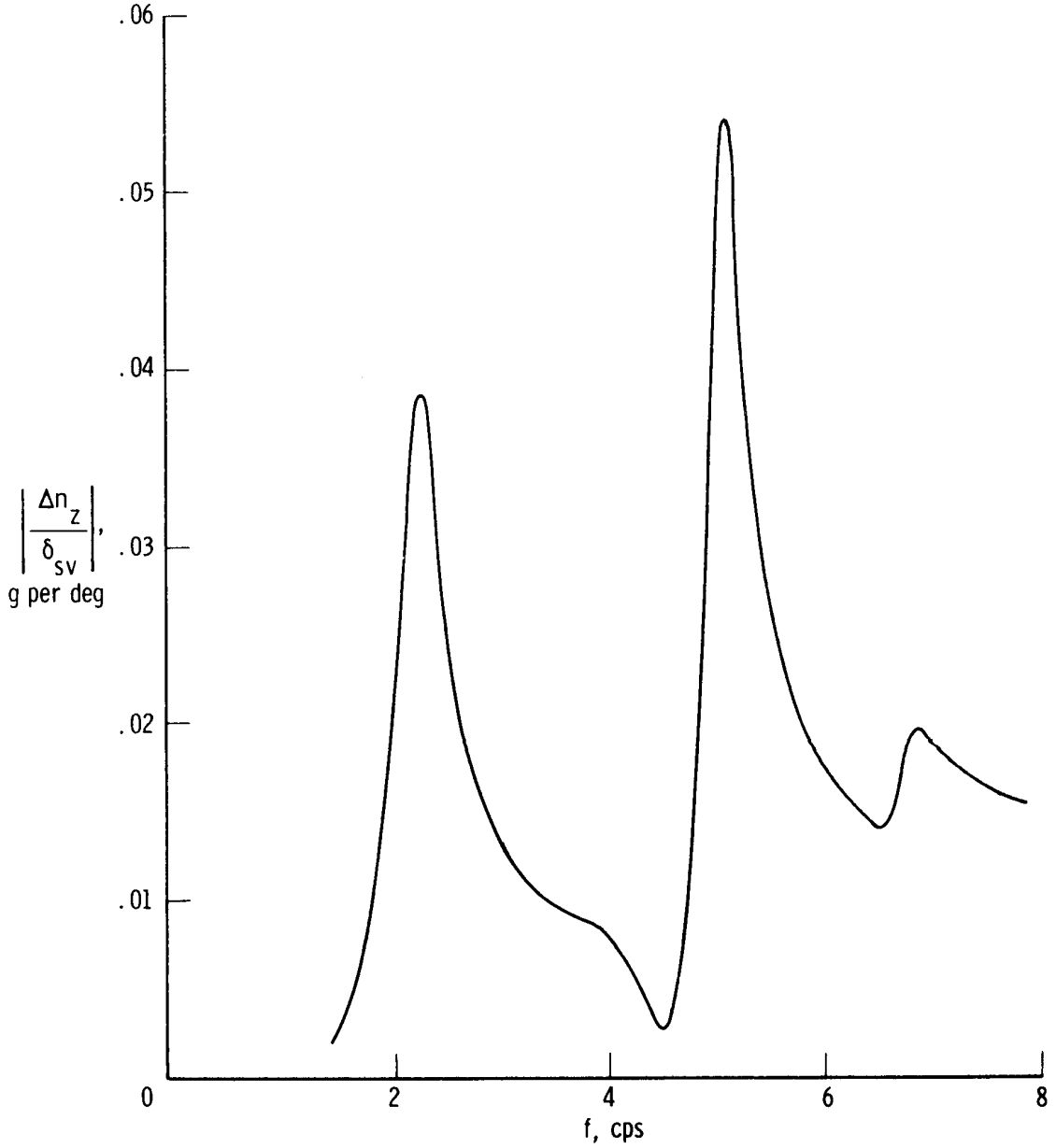

(b) Pilot's station; FS 11.12 m (438 in.).

Figure 16. Continued.

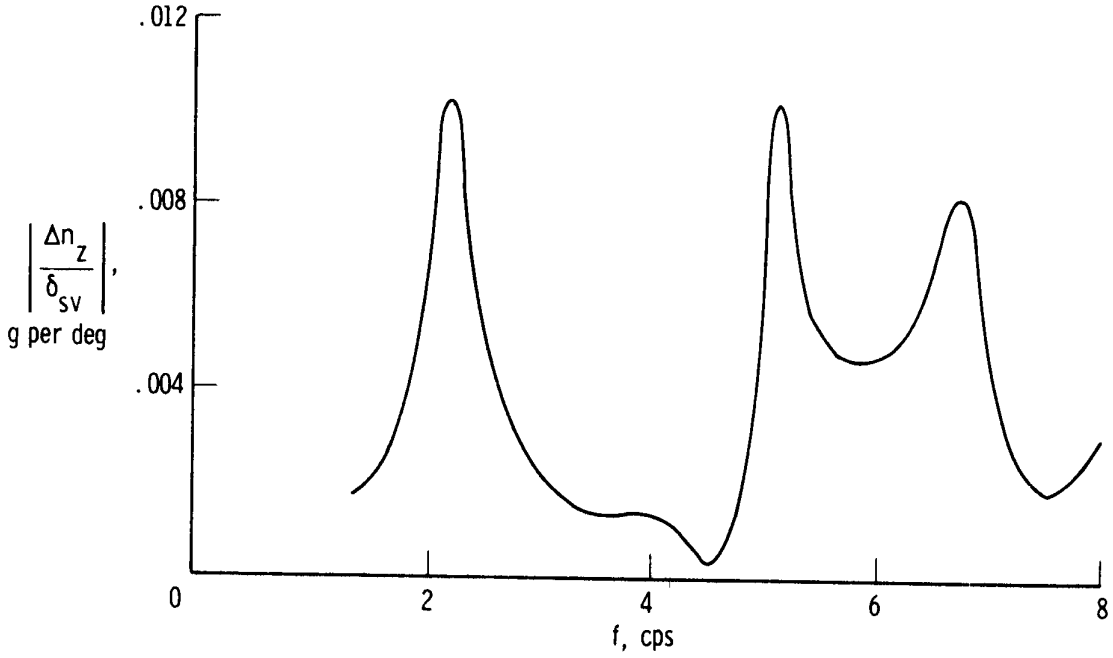

(c) Nosewheel well; FS 32.61 m (1284 in.).

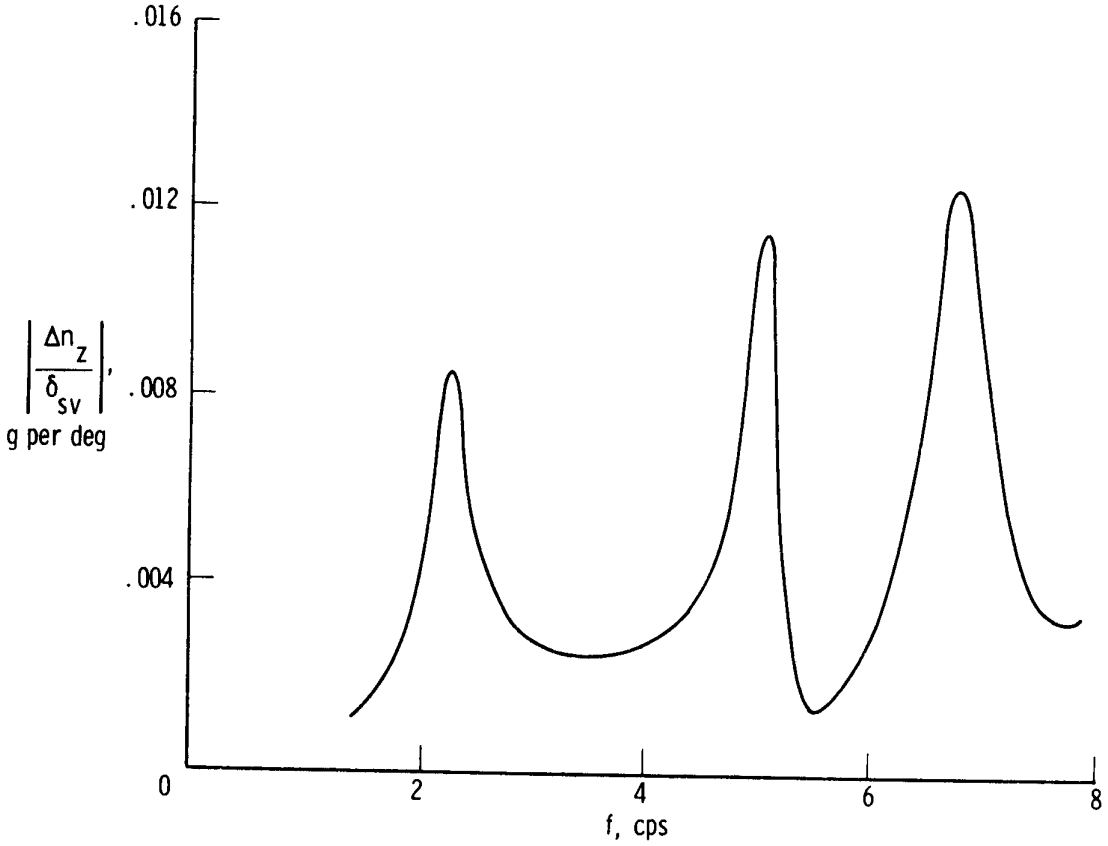

(d) Near center of gravity; FS 37.72 m (1485 in.).

Figure 16. Continued.

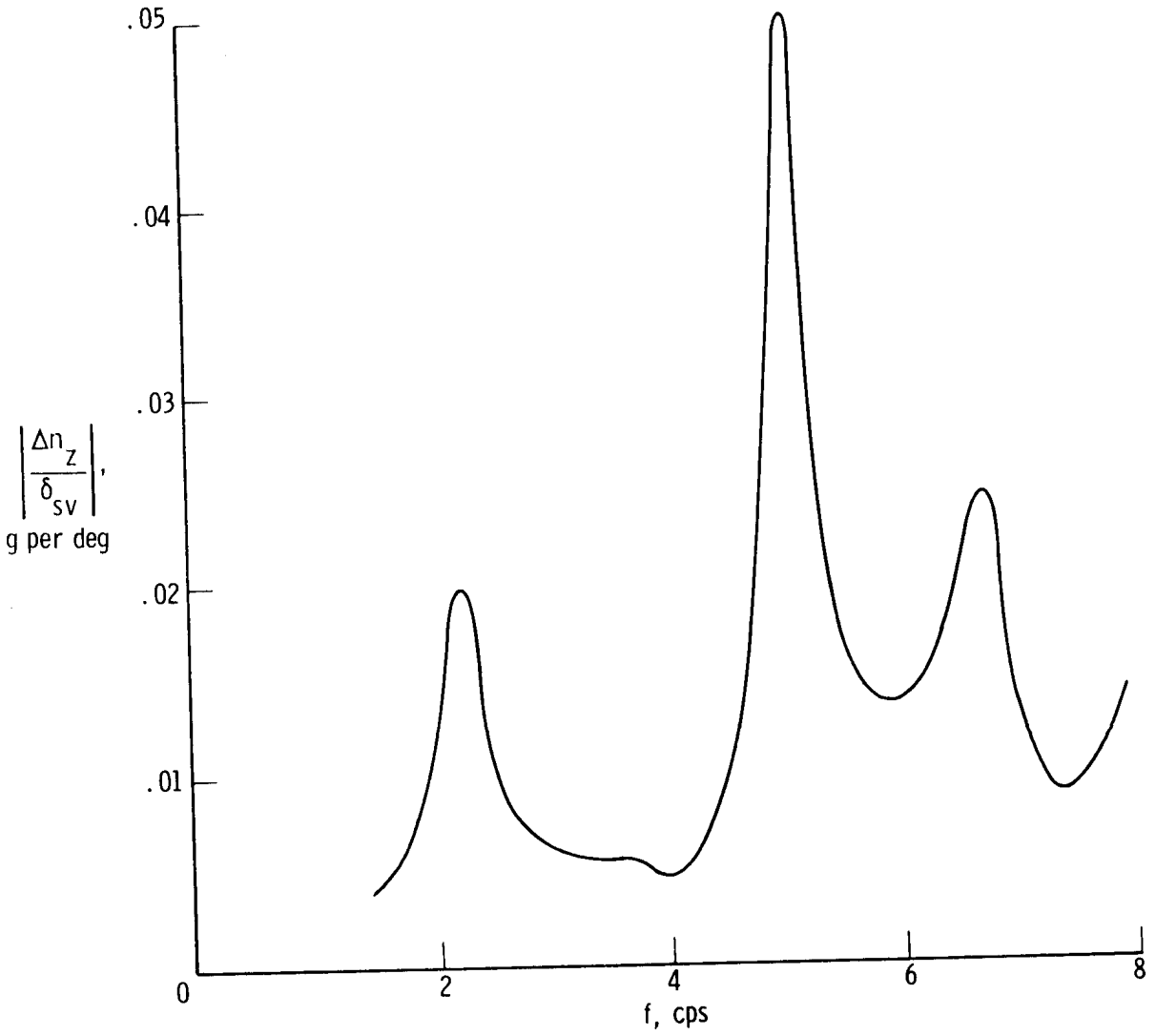

(e) Wing accelerometer; FS 56.18 m (2212 in.); BP 7.11 m (280 in.).

Figure 16. Concluded.

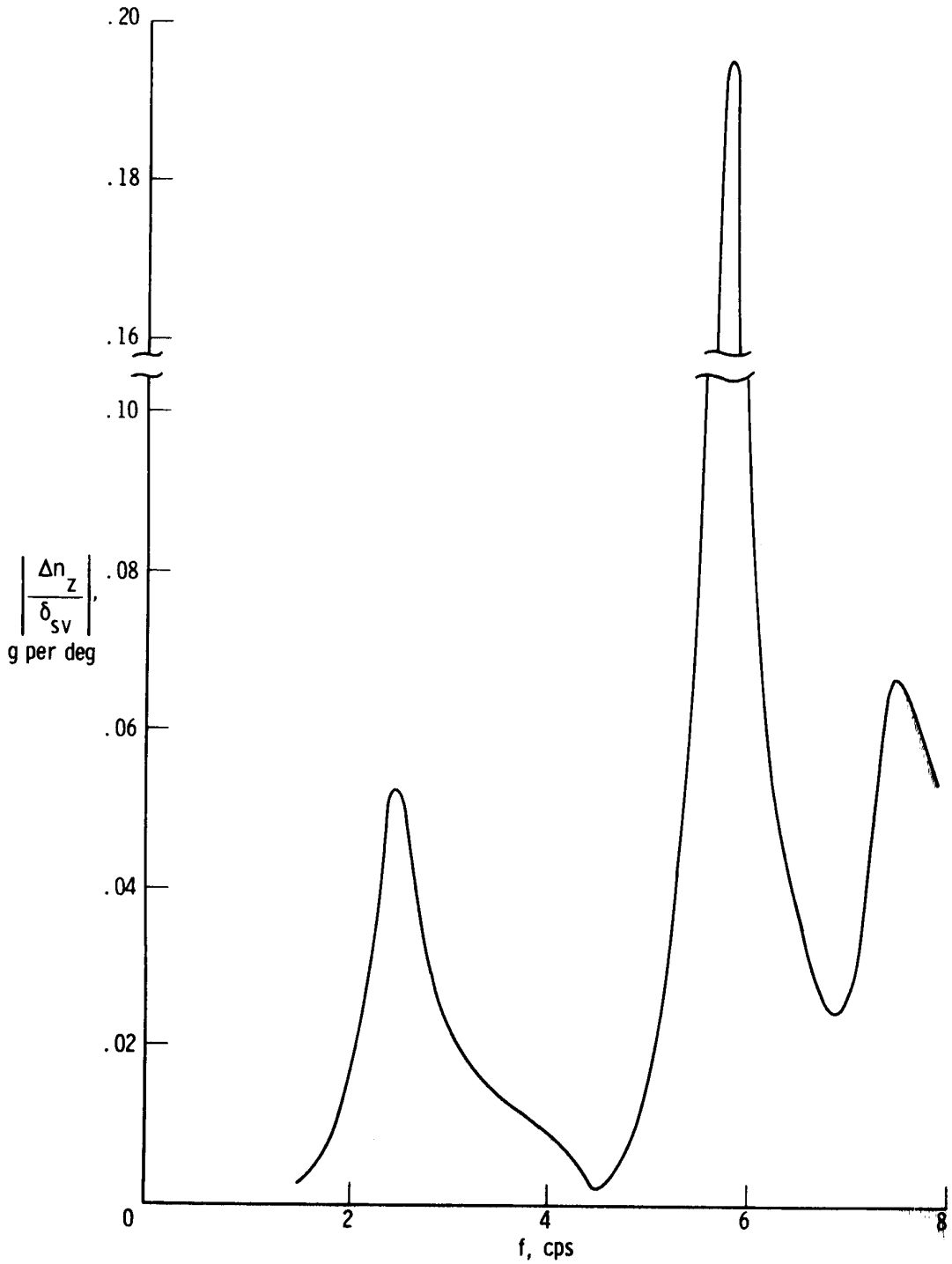

(a) Fuselage nose; FS 3.68 m (145 in.).

Figure 17. Vertical acceleration response to shaker vane excitation calculated by using quasi-steady aerodynamic theory without FACS. Updated analysis; lightweight; $M = 0.86$; $h_p = 7620$ m (25,000 ft); $\delta_t = 25°$.

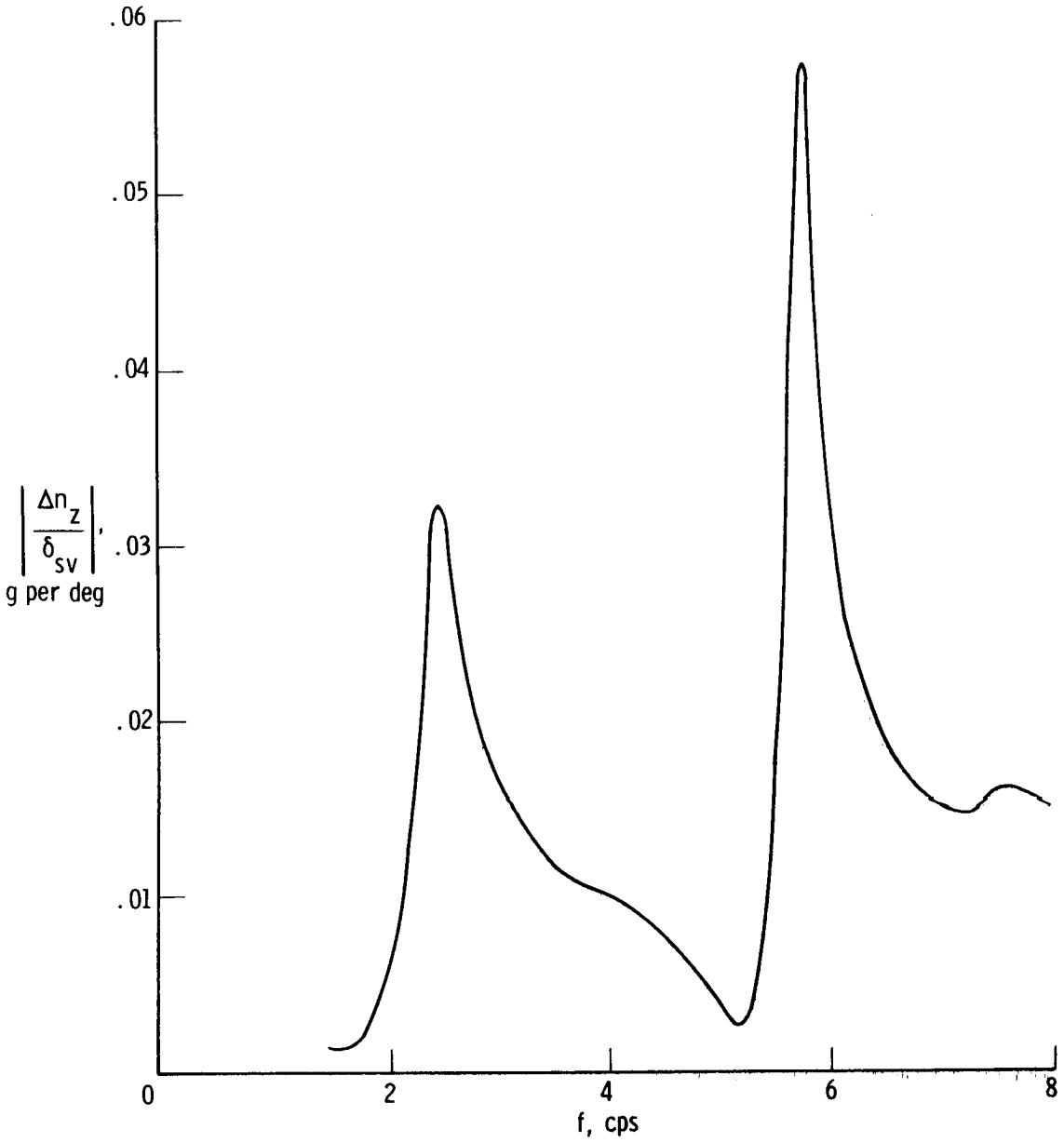

(b) Pilot' s station; FS 11.12 m (438 in.).

Figure 17. Continued.

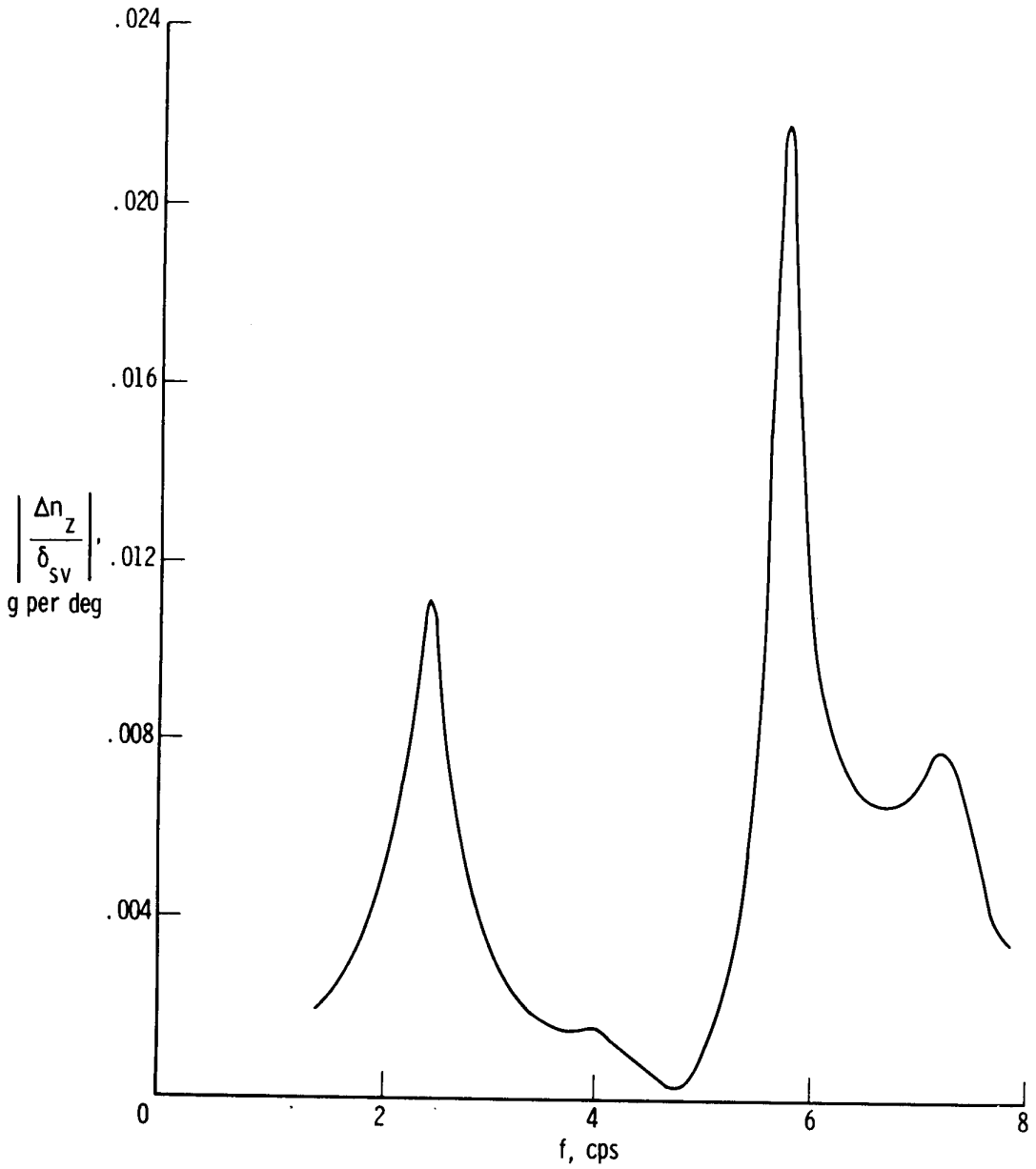

(c) Nosewheel well; FS 32.61 m (1284 in.).

Figure 17. Continued.

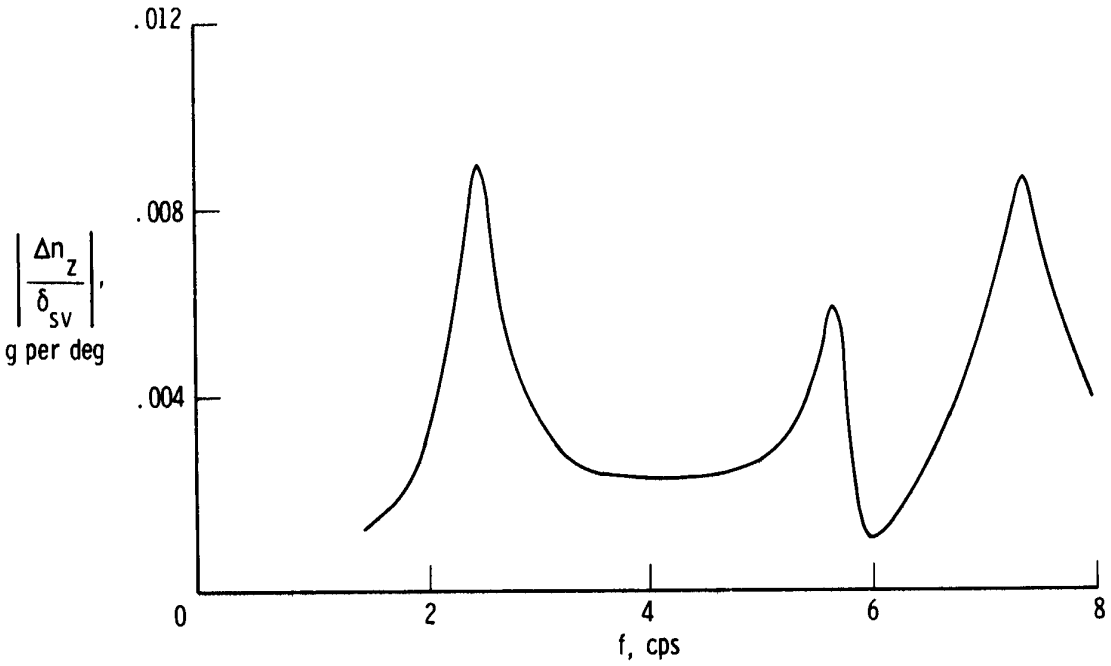

(d) Near center of gravity; FS 37.72 m (1485 in.).

Figure 17. Continued.

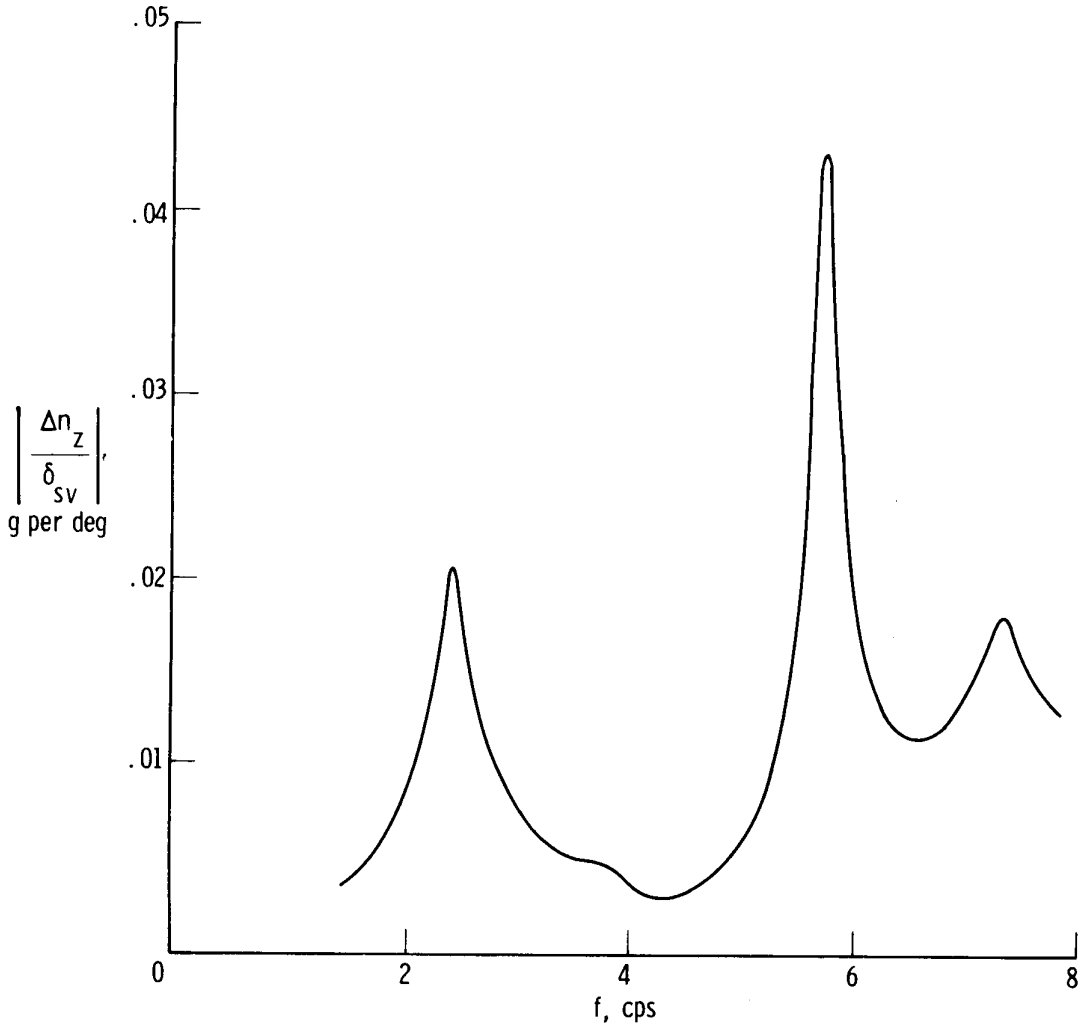

(e) Wing accelerometer; FS 56.18 m (2212 in.); BP 7.11 m (280 in.).

Figure 17. Concluded.

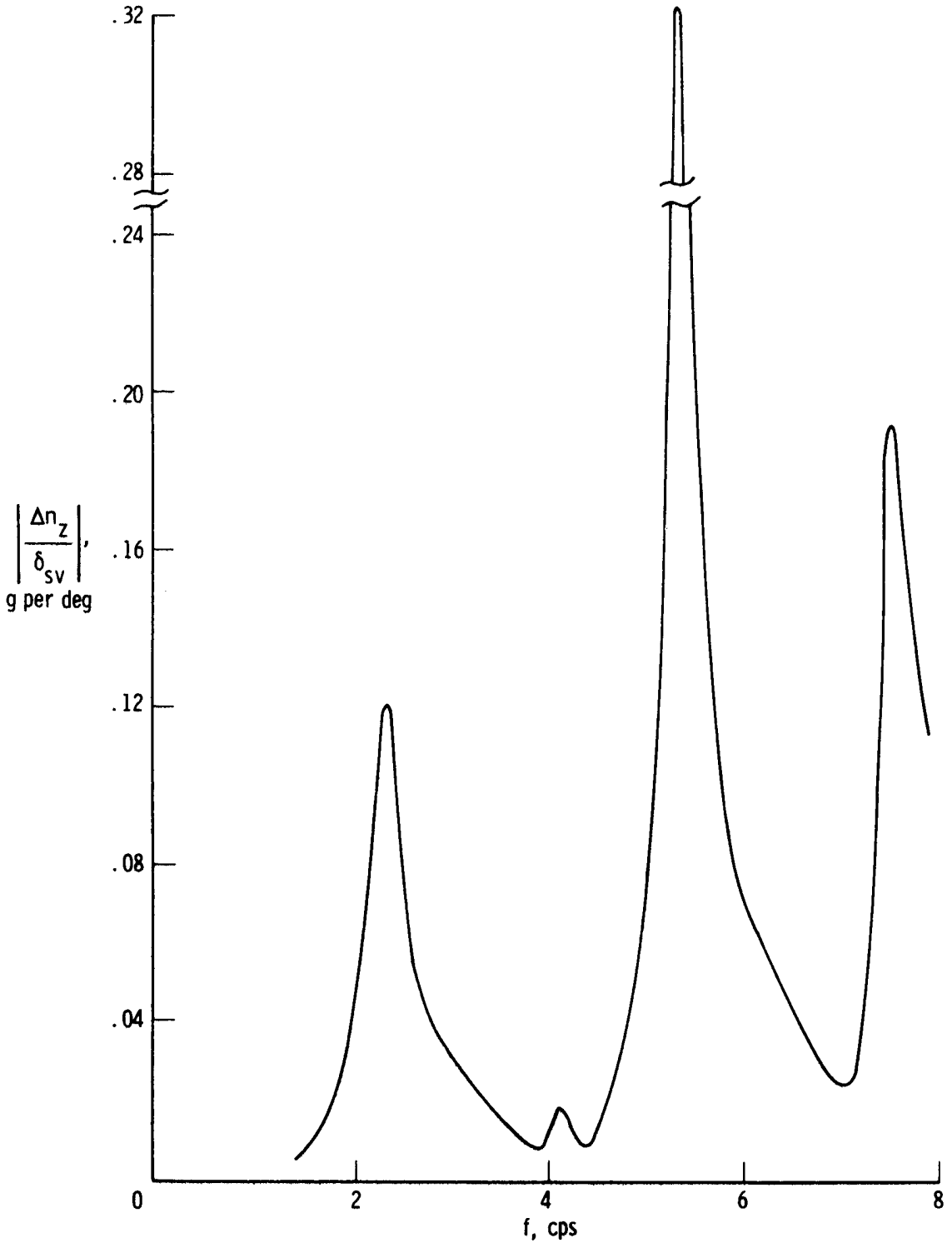

(a) Fuselage nose; FS 4.95 m (194.75 in.).

Figure 18. Vertical acceleration response to shaker vane excitation calculated by using quasi-steady aerodynamic theory without FACS. Updated analysis; medium-weight; M = 1.59; h_p = 11,918 m (39,100 ft); δ_t = 65°.

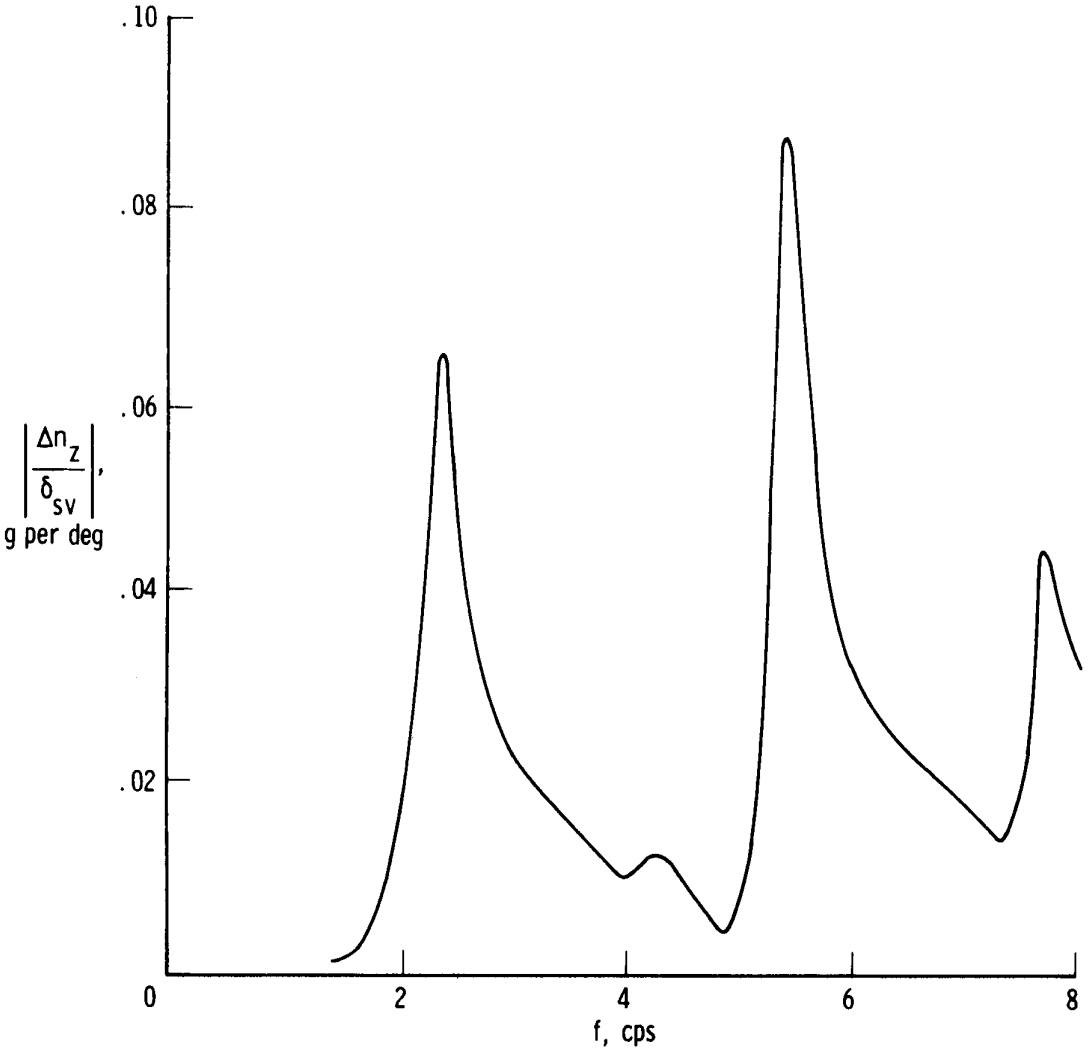

(b) Pilot's station; FS 11.12 m (438 in.).

Figure 18. Continued.

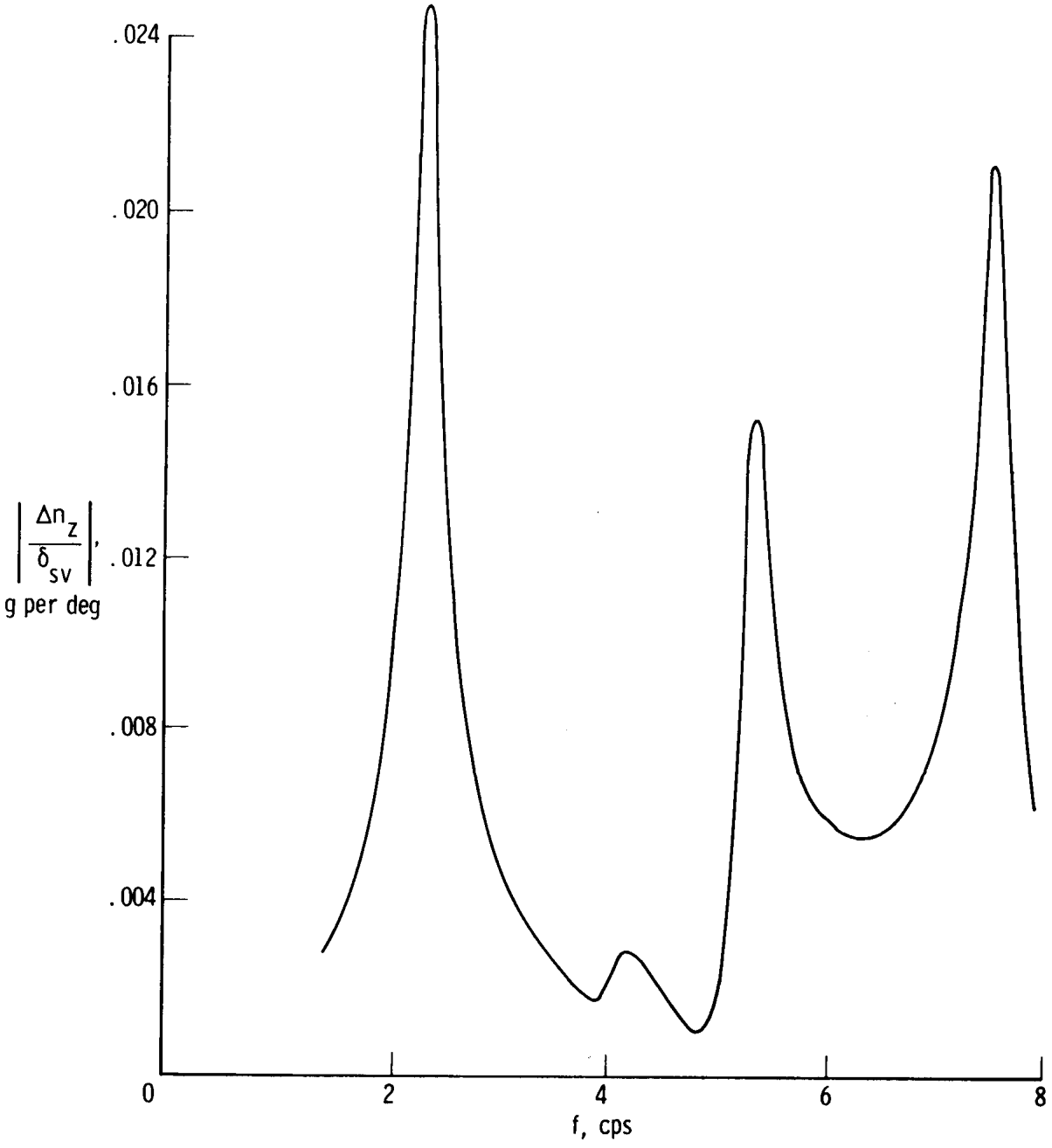

(c) Nosewheel well; FS 32.61 m (1284 in.).

Figure 18. Continued.

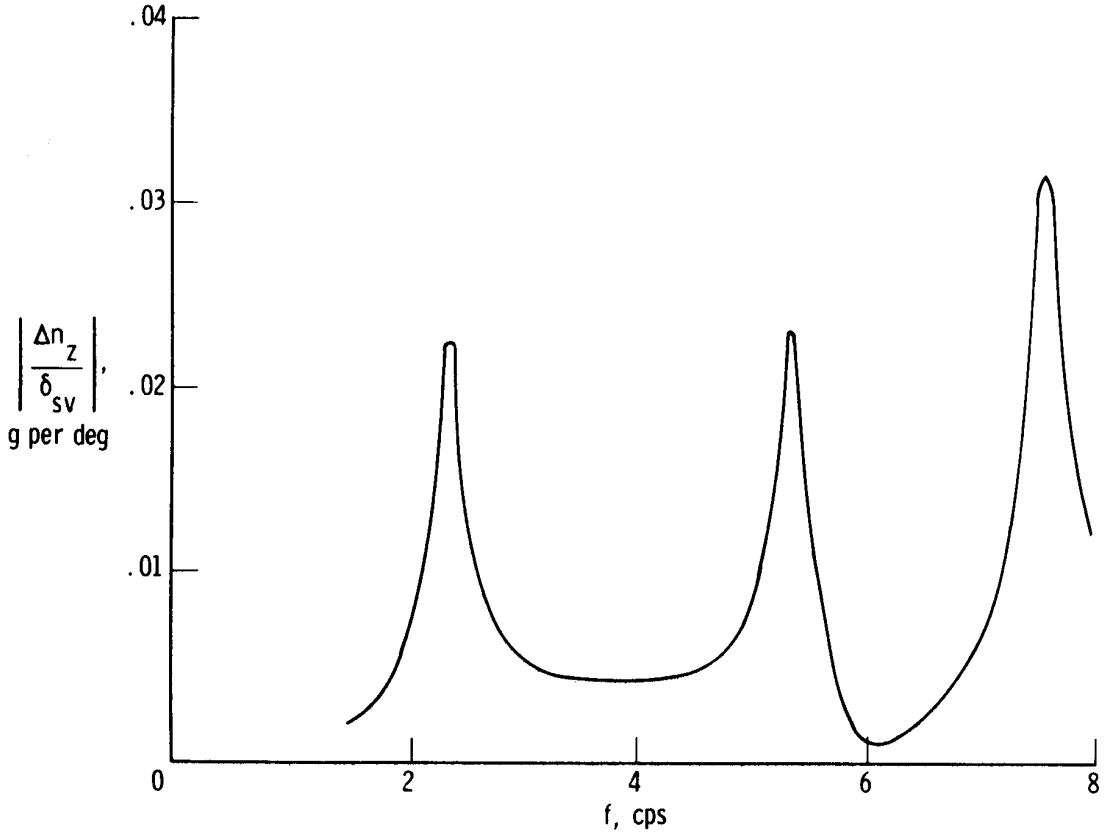

(d) Near center of gravity; FS 37.72 m (1485 in.).

Figure 18. Continued.

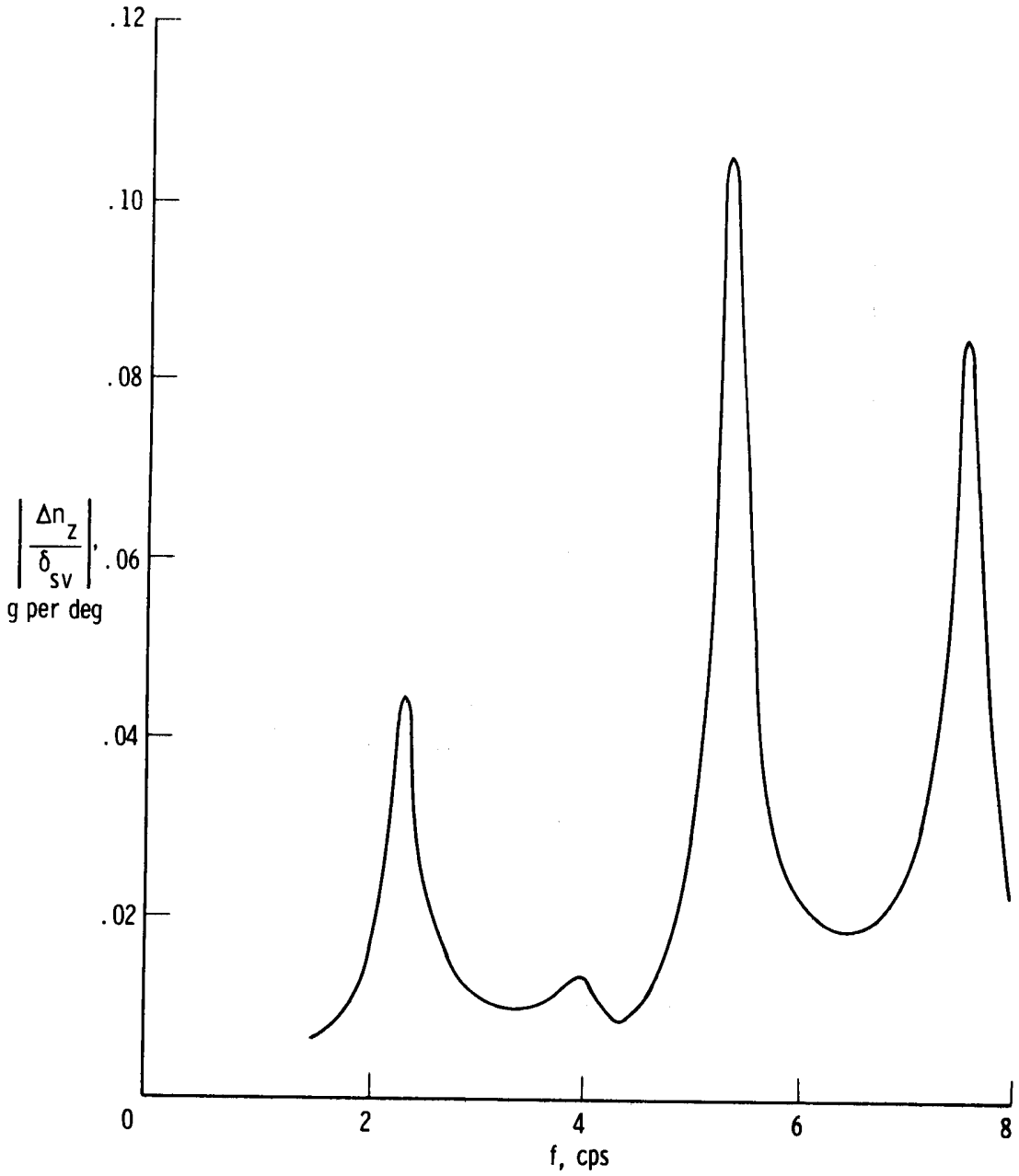

(e) Wing accelerometer; FS 56.18 m (2212 in.); BP 7.11 m (280 in.).

Figure 18. Concluded.

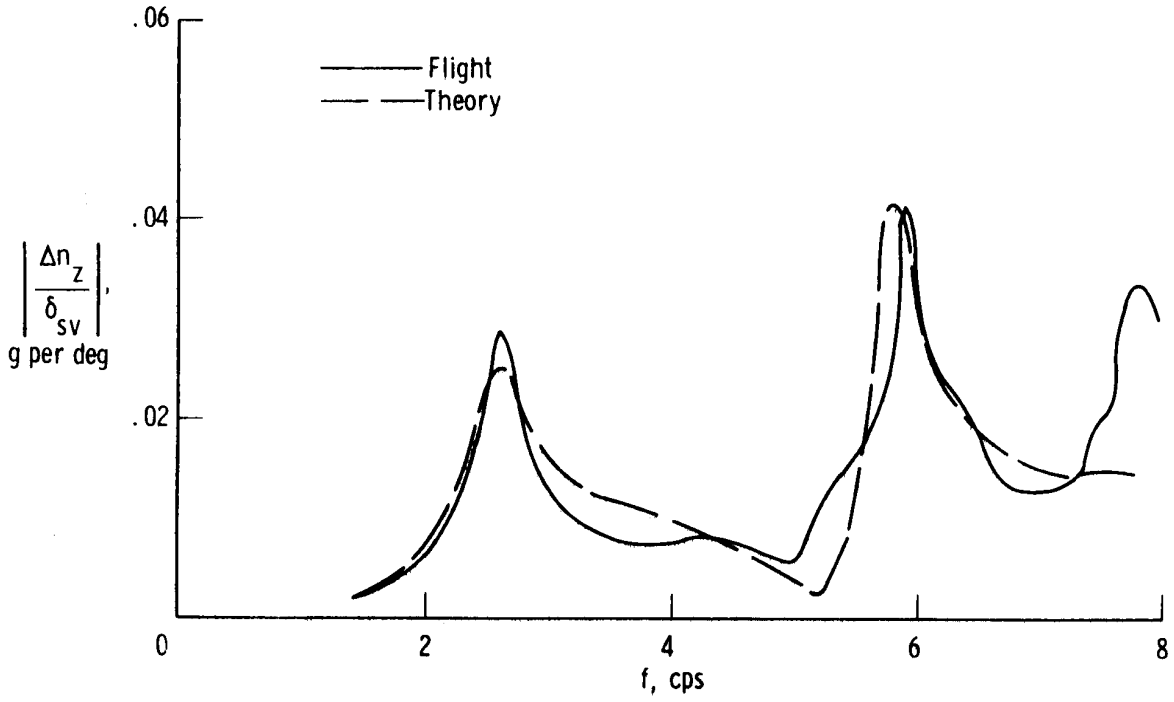

Figure 19. Comparison of flight-measured vertical acceleration response to shaker vane excitation with response calculated by using unsteady wing aerodynamic theory. Updated analysis; lightweight; M = 0.86; h_p = 7620 m (25,000 ft); δ_t = 25°; pilot' s station; FS 11.12 m (438 in.).

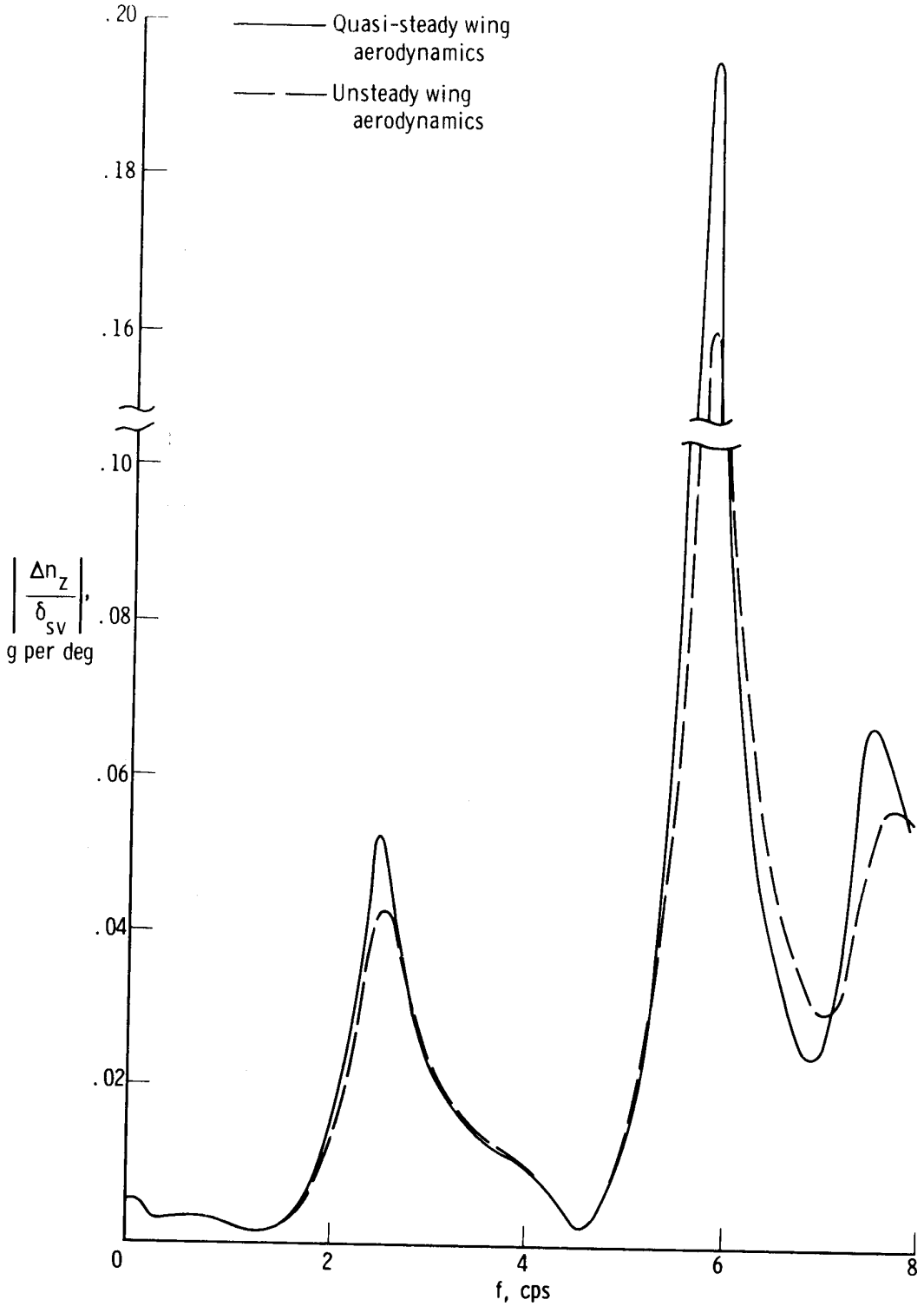

(a) Fuselage nose; FS 4.95 m (194.75 in.).

Figure 20. Comparison of vertical acceleration response to shaker vane excitation calculated by using quasi-steady and unsteady wing aerodynamics without FACS. Updated analysis; lightweight; M = 0.86; h_p = 7620 m (25,000 ft); $\delta_t = 25°$.

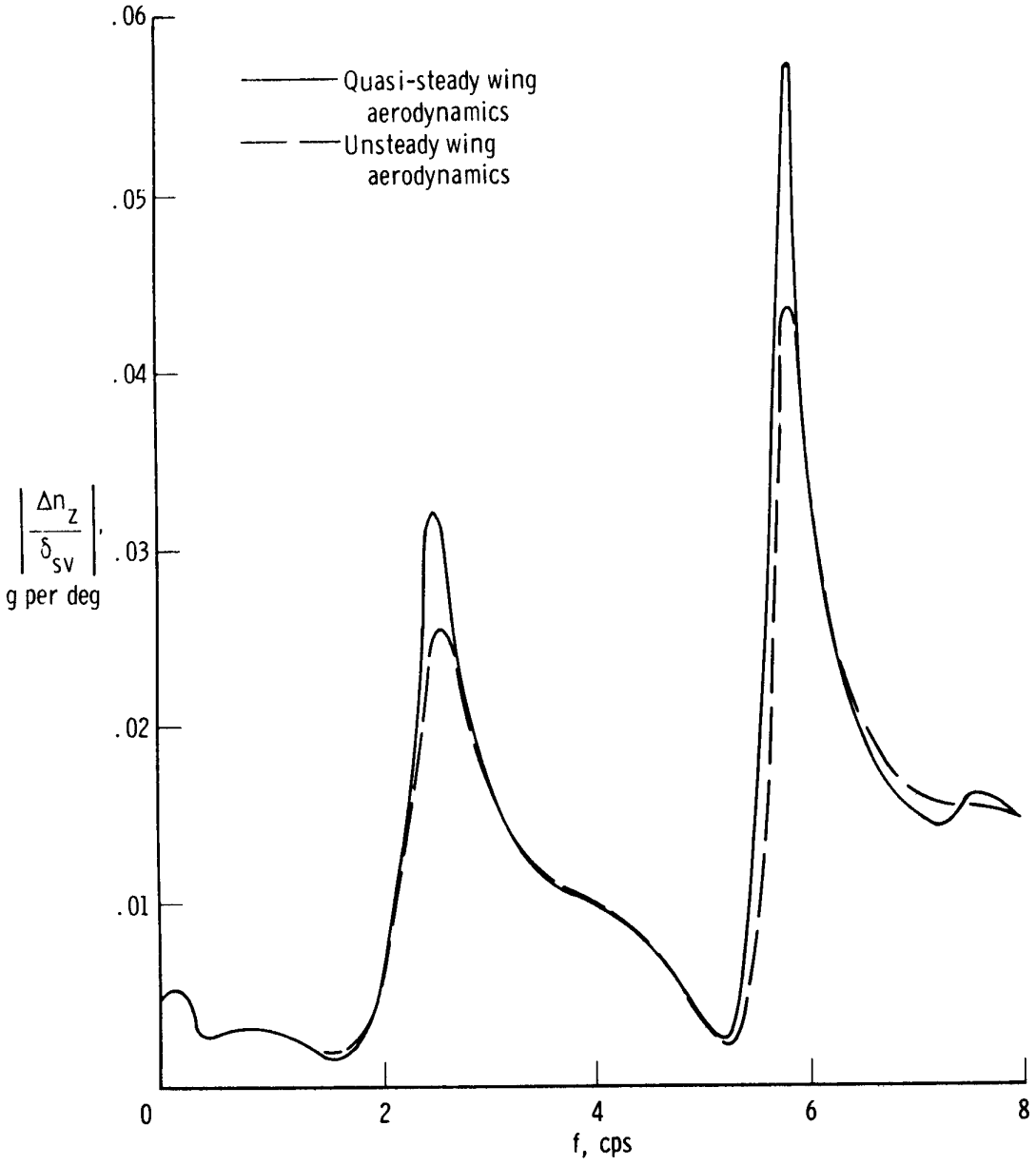

(b) Pilot's station; FS 11.12 m (438 in.).

Figure 20. Continued.

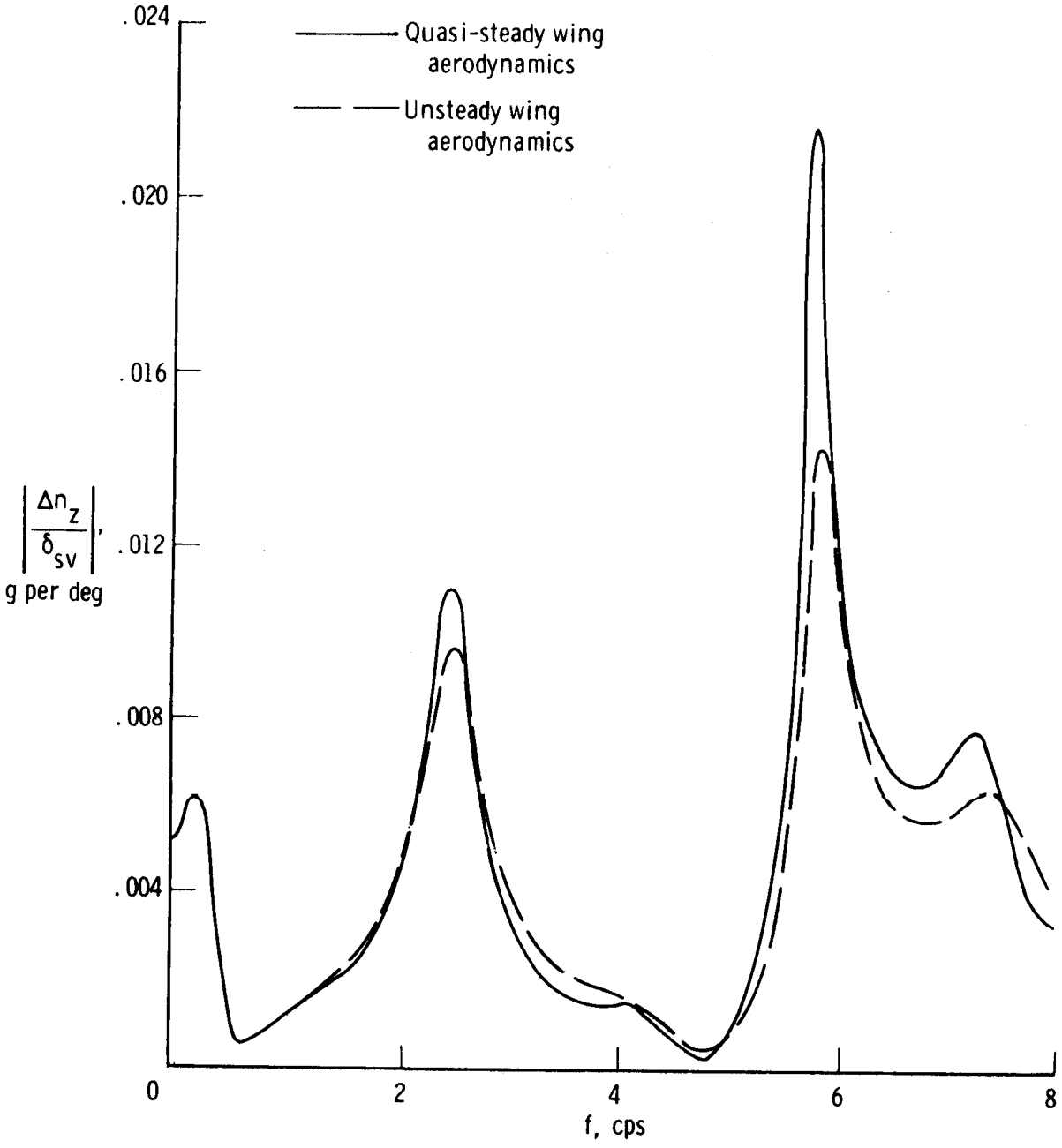

(c) Nosewheel well; FS 32.61 m (1284 in.).

Figure 20. Continued.

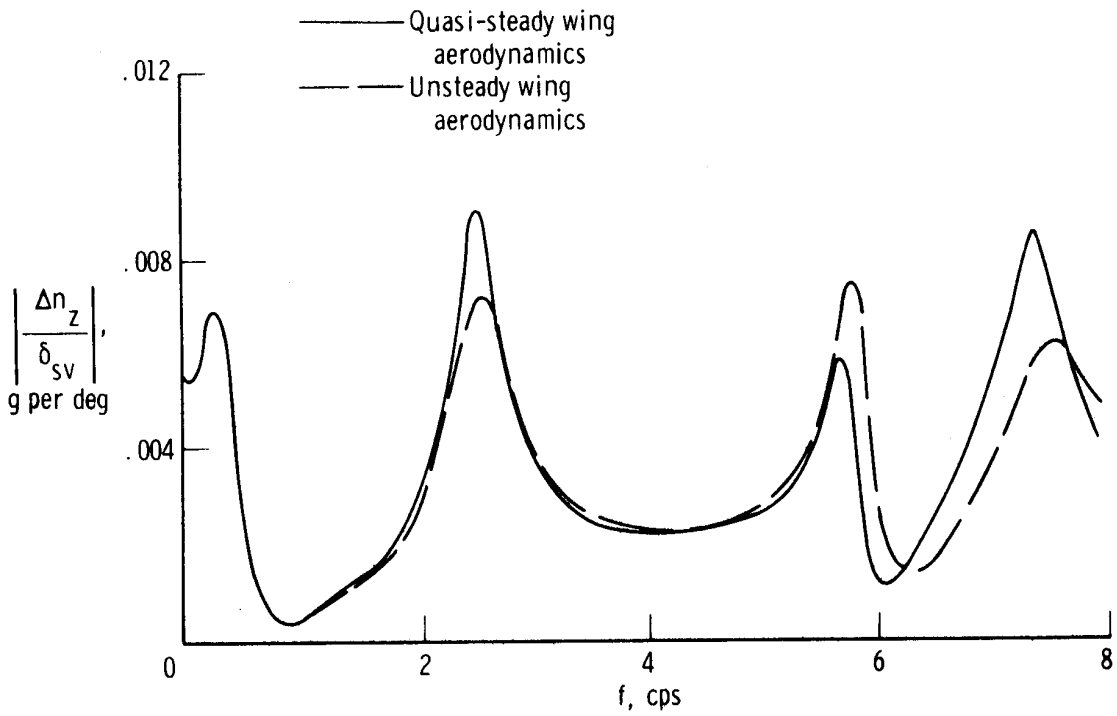

(d) Near center of gravity; FS 37.72 m (1485 in.).

Figure 20. Continued.

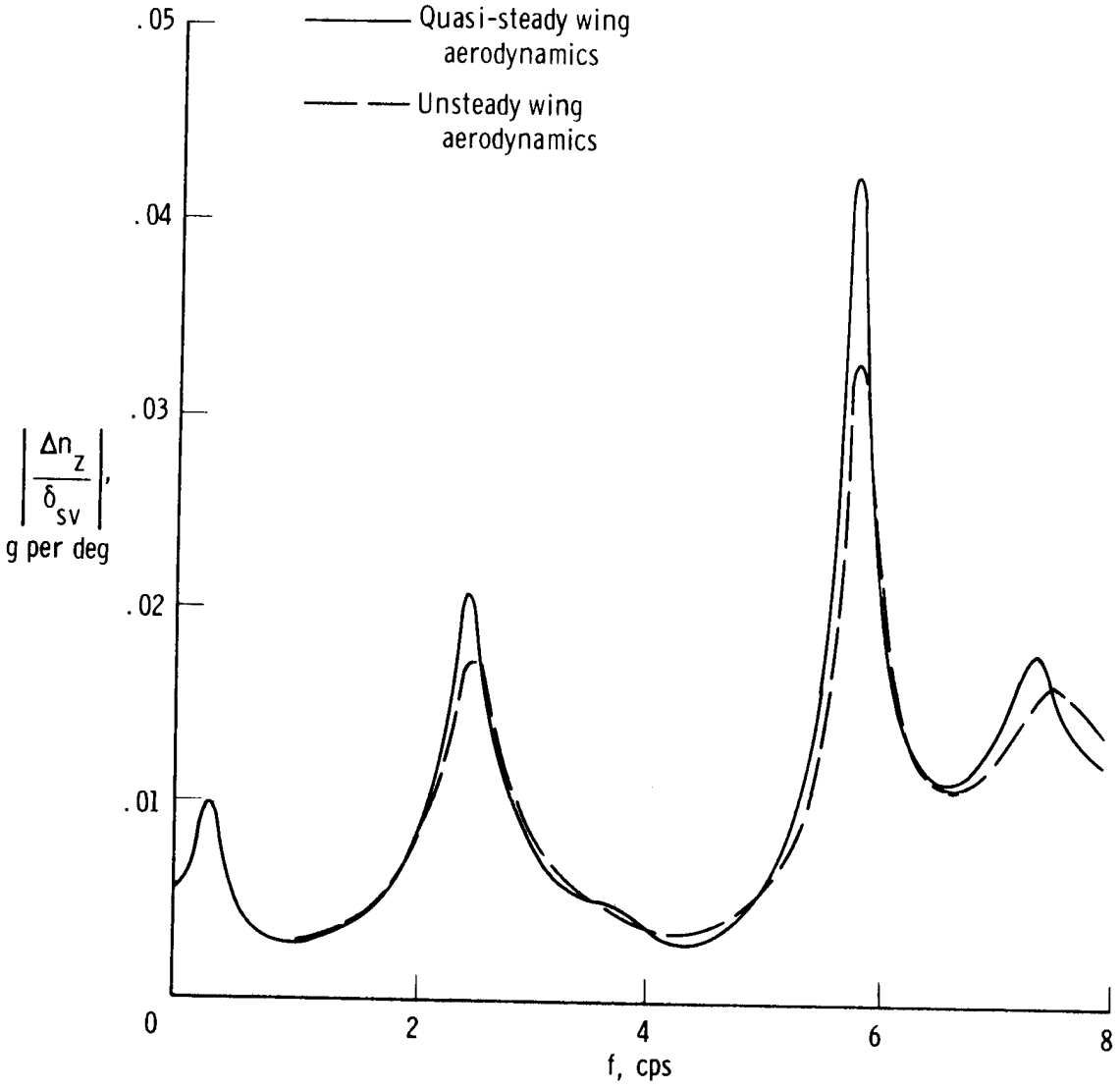

(e) Wing accelerometer; FS 56.18 m (2212 in.); BP 7.11 m (280 in.).

Figure 20. Concluded.

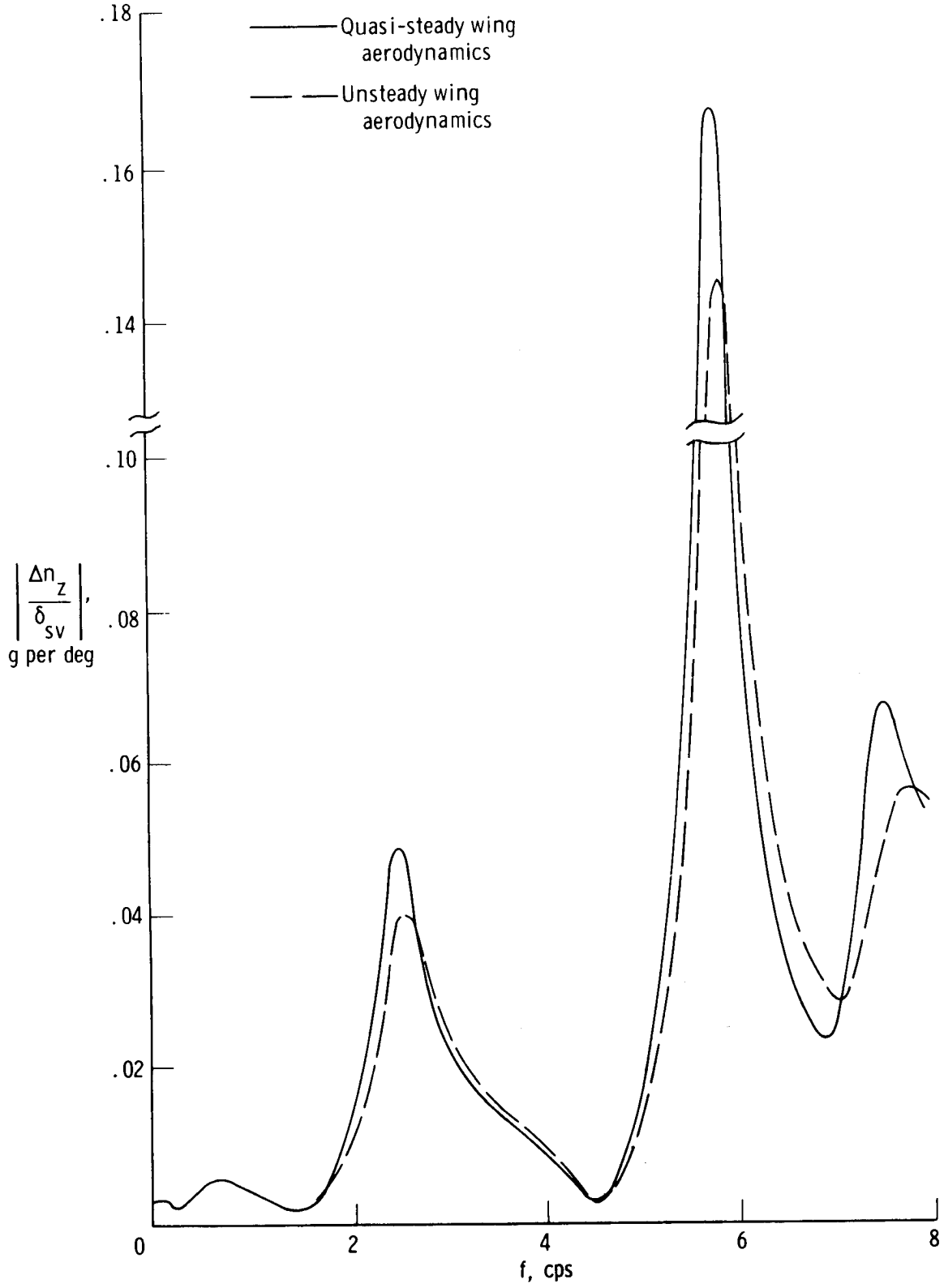

(a) Fuselage nose; FS 4.95 m (194.75 in.).

Figure 21. Comparison of the vertical acceleration response to shaker vane excitation calculated by using quasi-steady and unsteady wing aerodynamics. Updated analysis with FACS. Lightweight; M = 0.86; h_p = 7620 m (25,000 ft); $\delta_t = 25^\circ$.

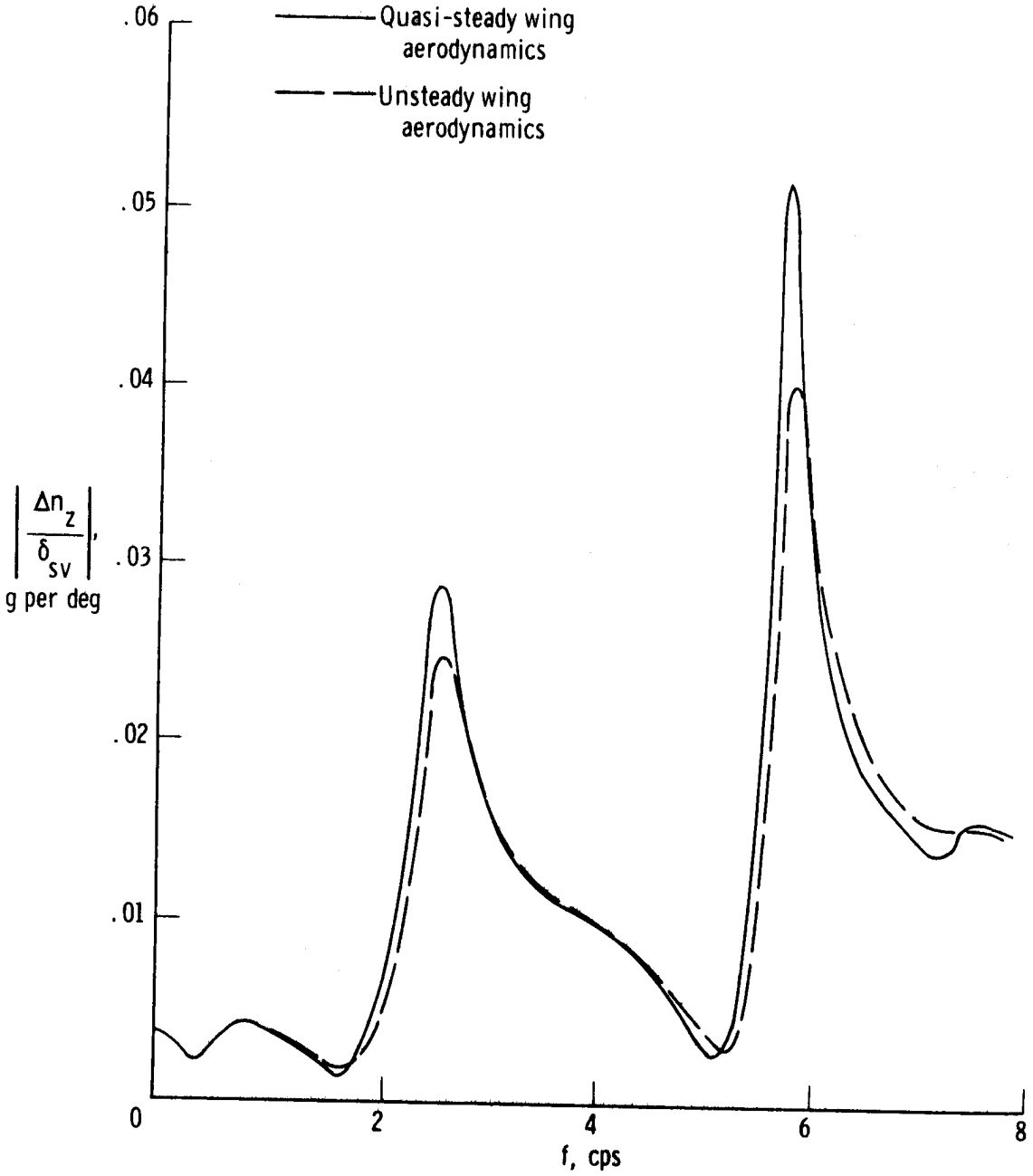

(b) Pilot's station; FS 11.12 m (438 in.).

Figure 21. Continued.

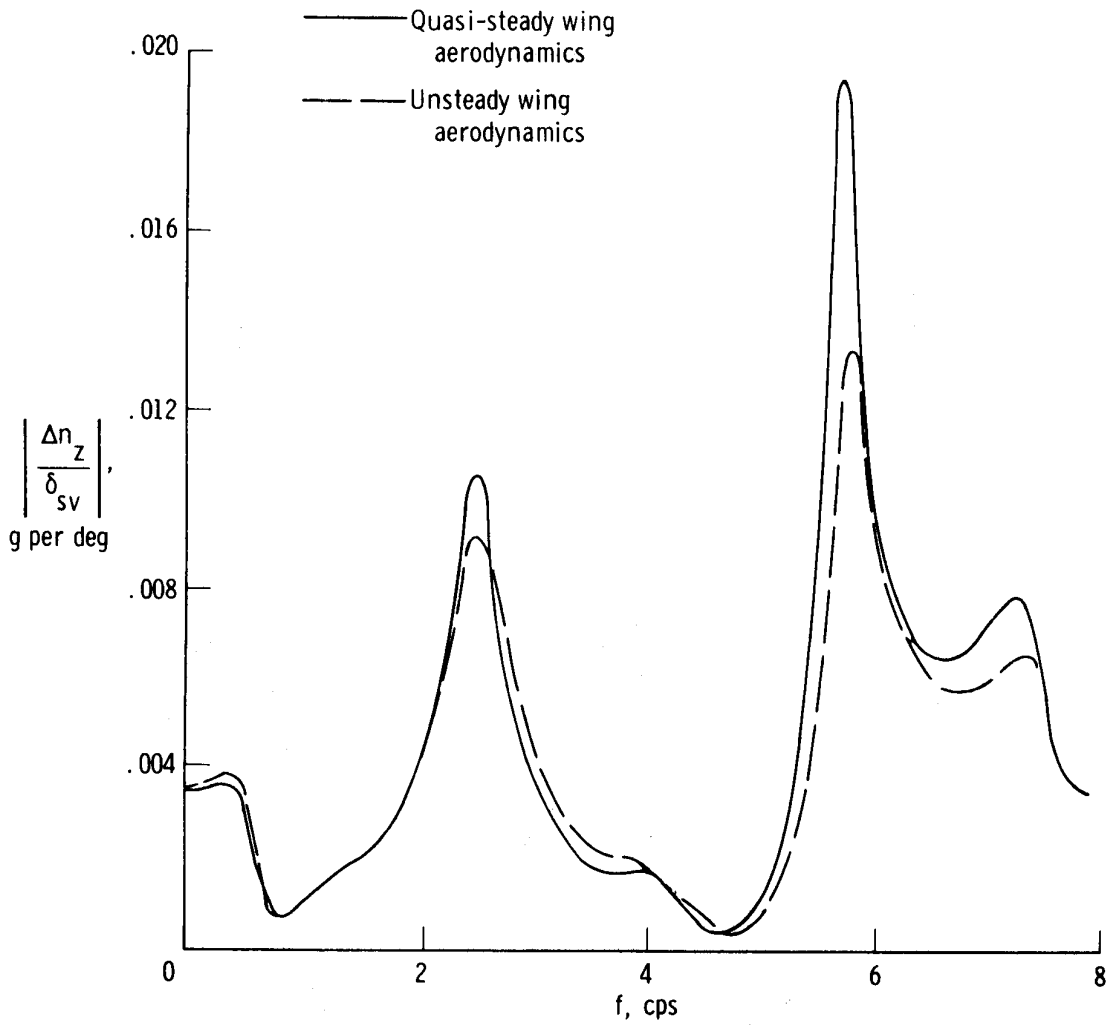

(c) Nosewheel well; FS 32.61 m (1284 in.).

Figure 21. Continued.

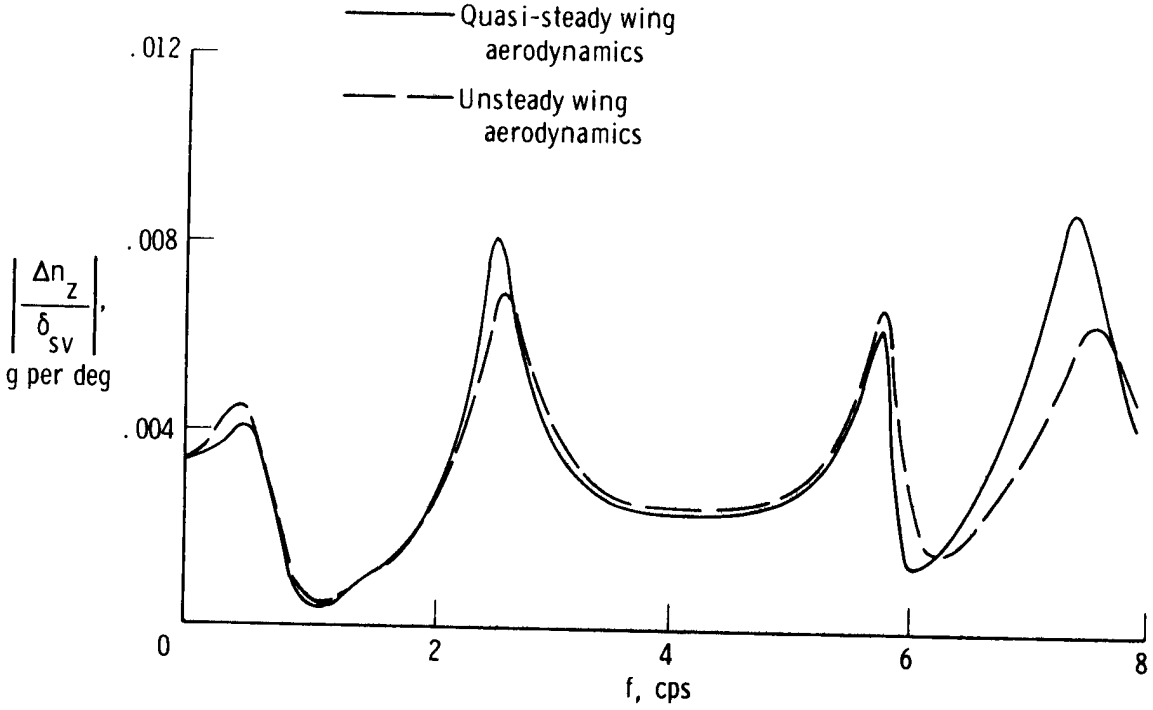

(d) Near center of gravity; FS 37.72 m (1485 in.).

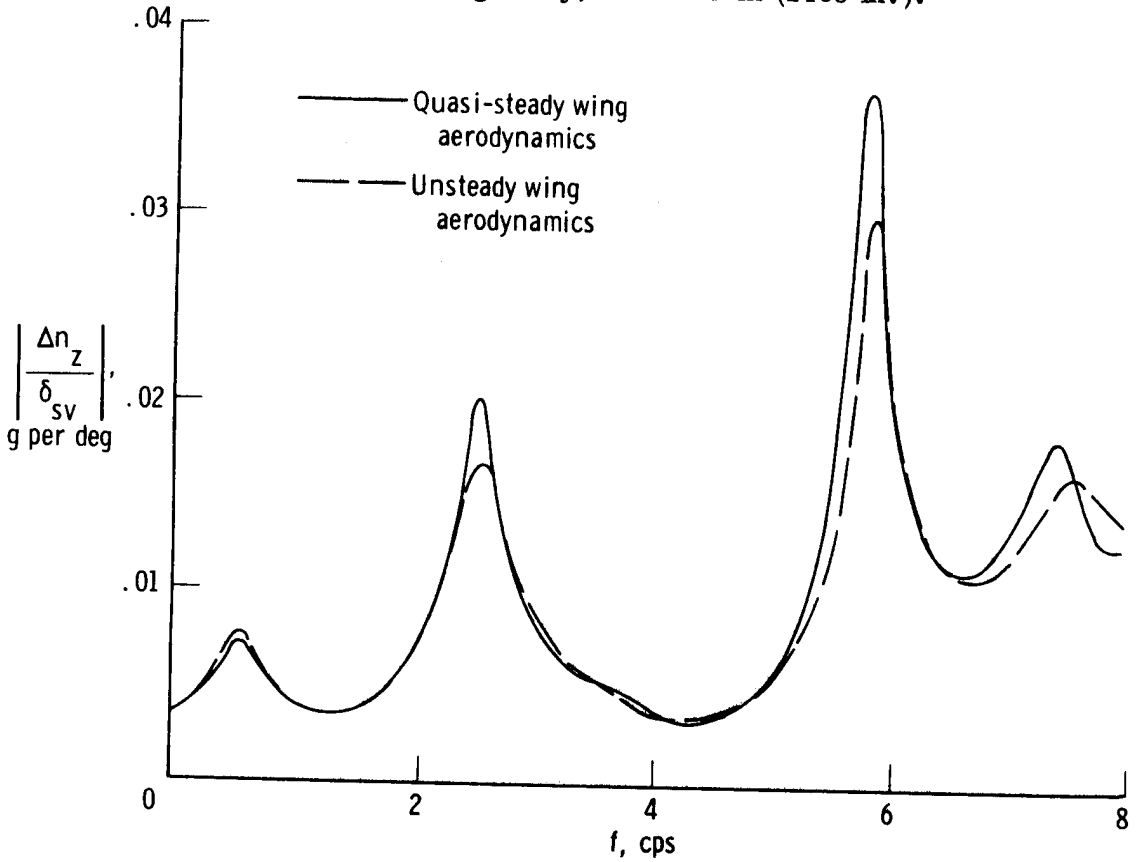

(e) Wing accelerometer; FS 56.18 m (2212 in.); BP 7.11 m (280 in.).

Figure 21. Concluded.

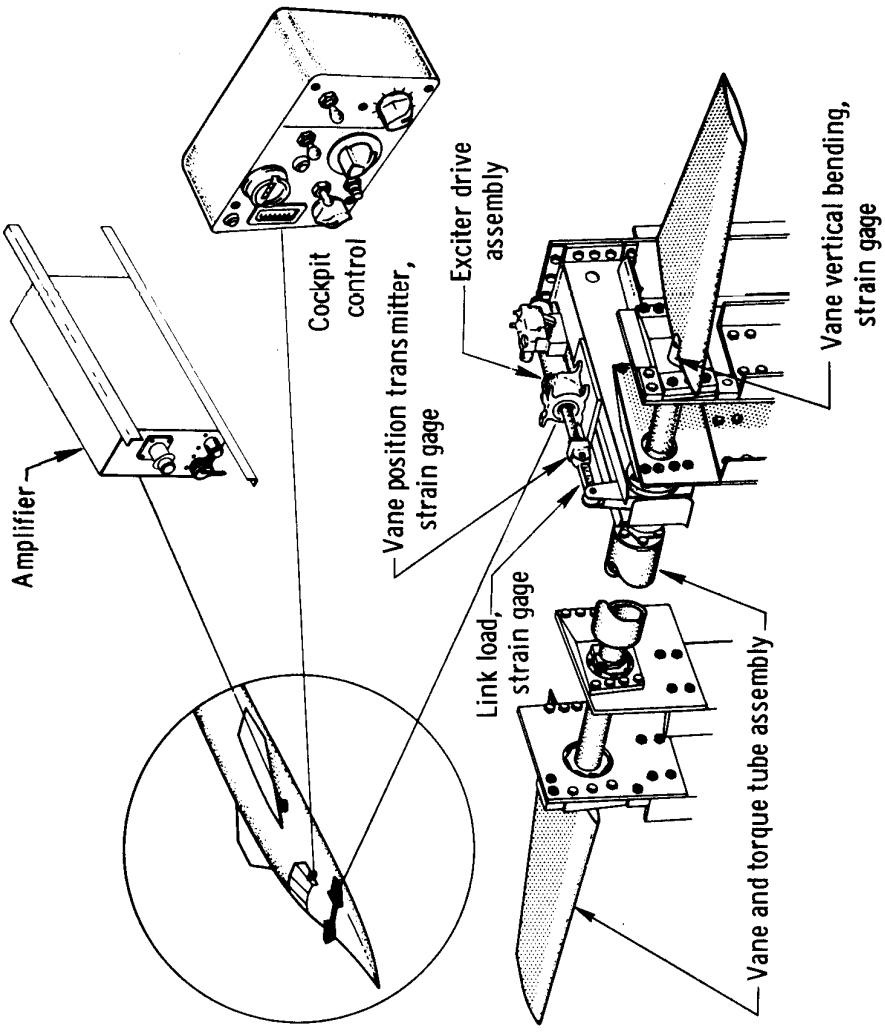

Figure 22. Shaker vane system.

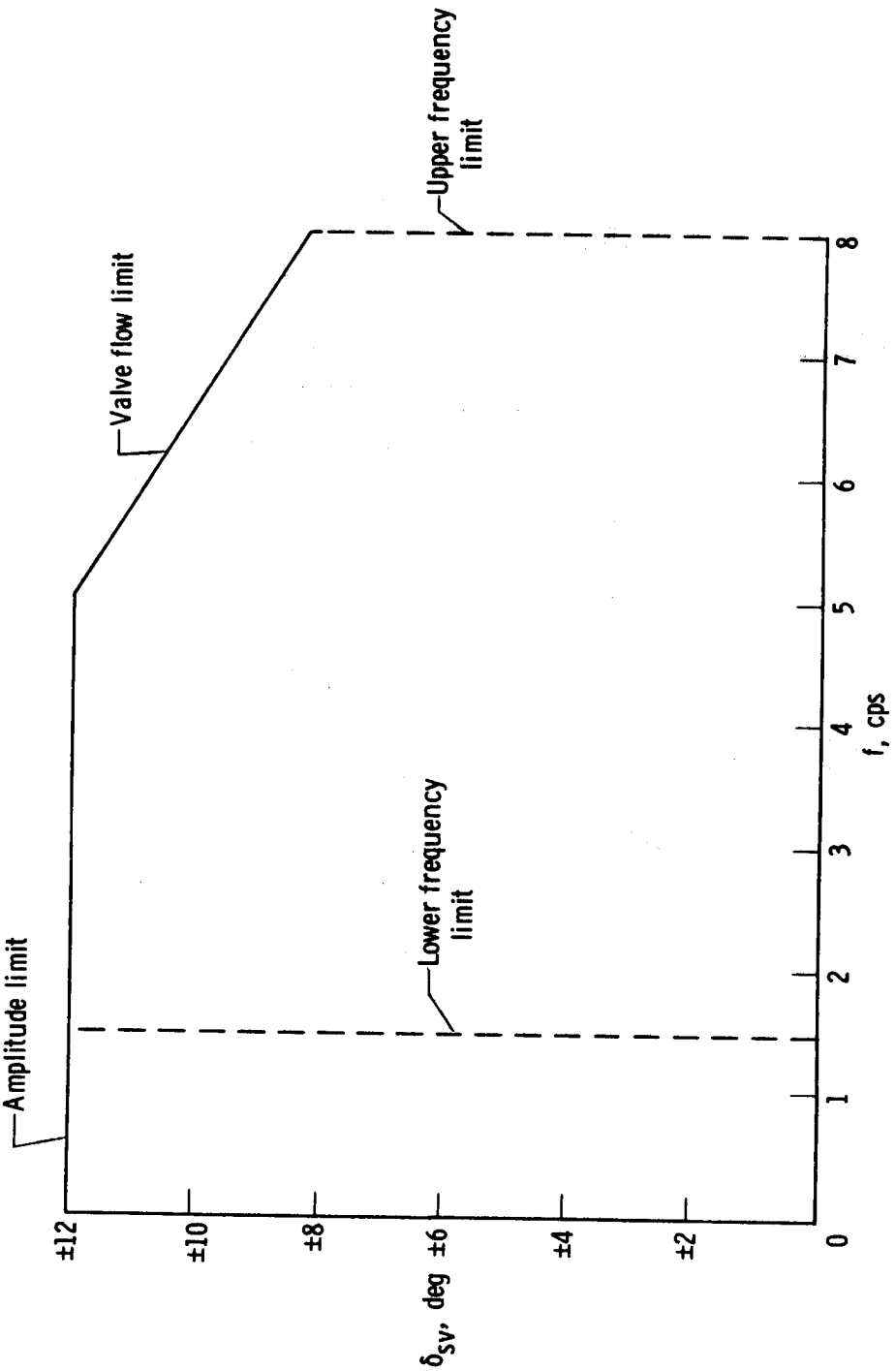

Figure 23. Variation of maximum shaker vane amplitude with vane oscillating frequency.

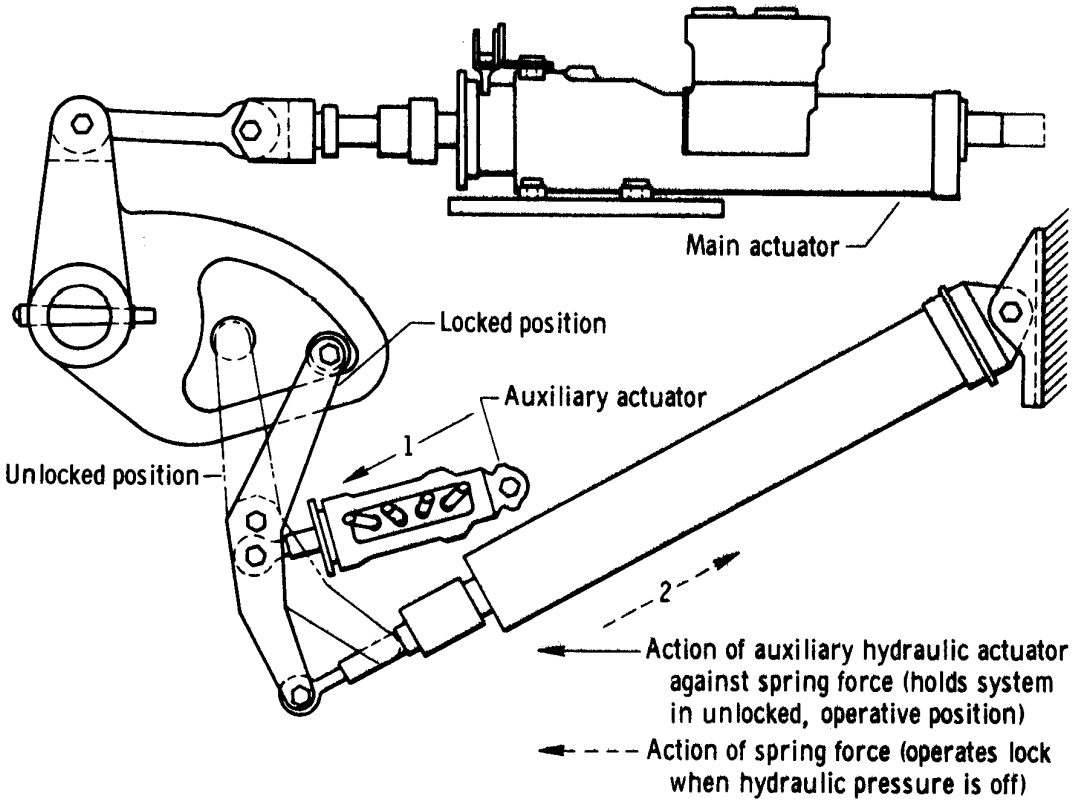

Figure 24. Schematic representation of shaker vane safety lock system.

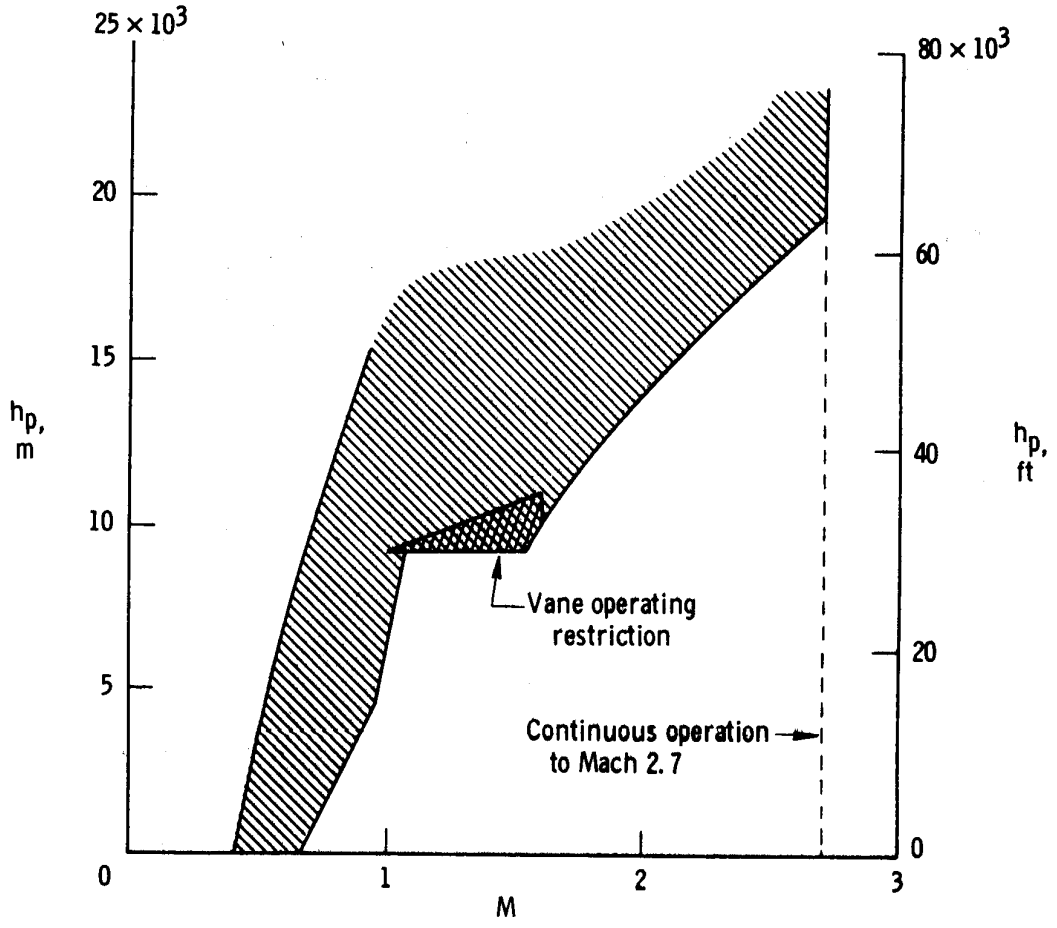

Figure 25. Operational range of the shaker vane.

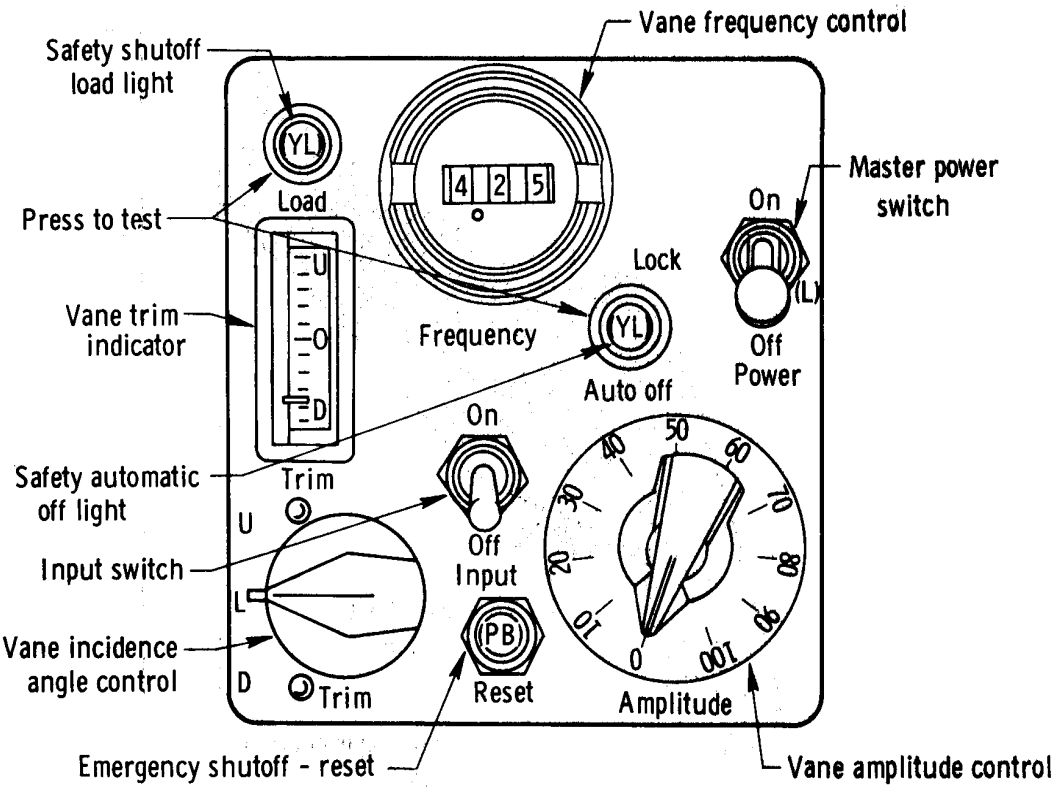

Figure 26. Shaker vane cockpit controls and display panel.

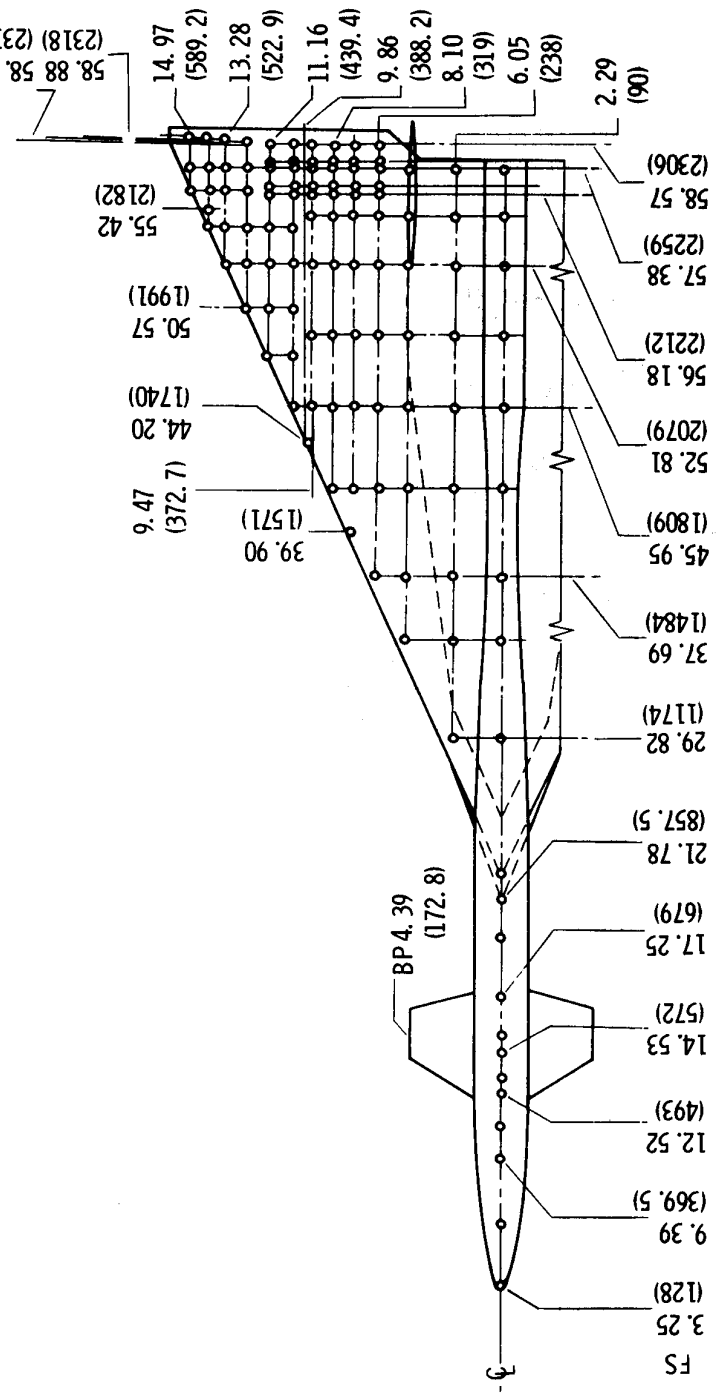

Figure 27. Control point geometry for XB-70 118-point grid system. Dimensions in meters (inches).

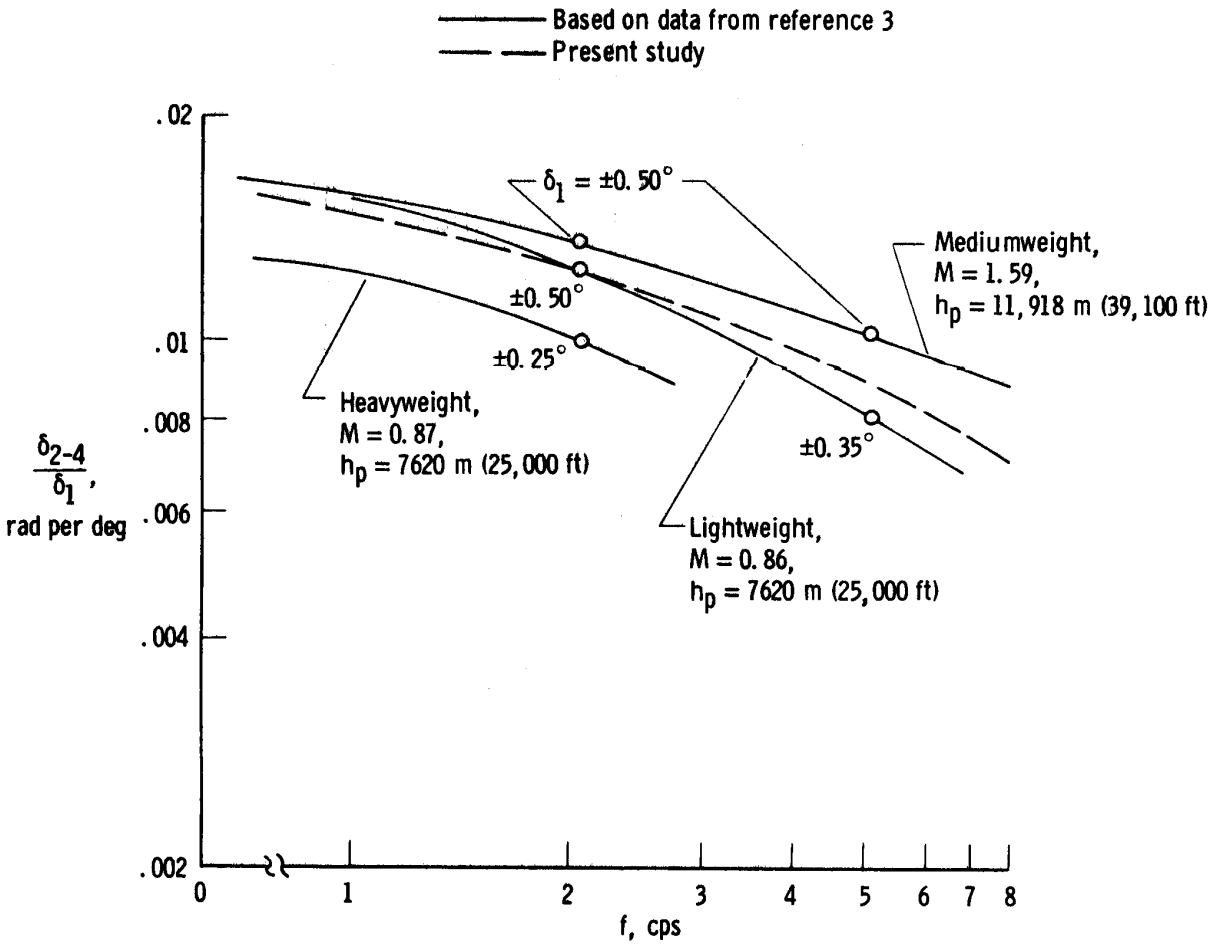

(a) Amplitude.

Figure 28. Frequency response from inboard elevon to outboard elevons.

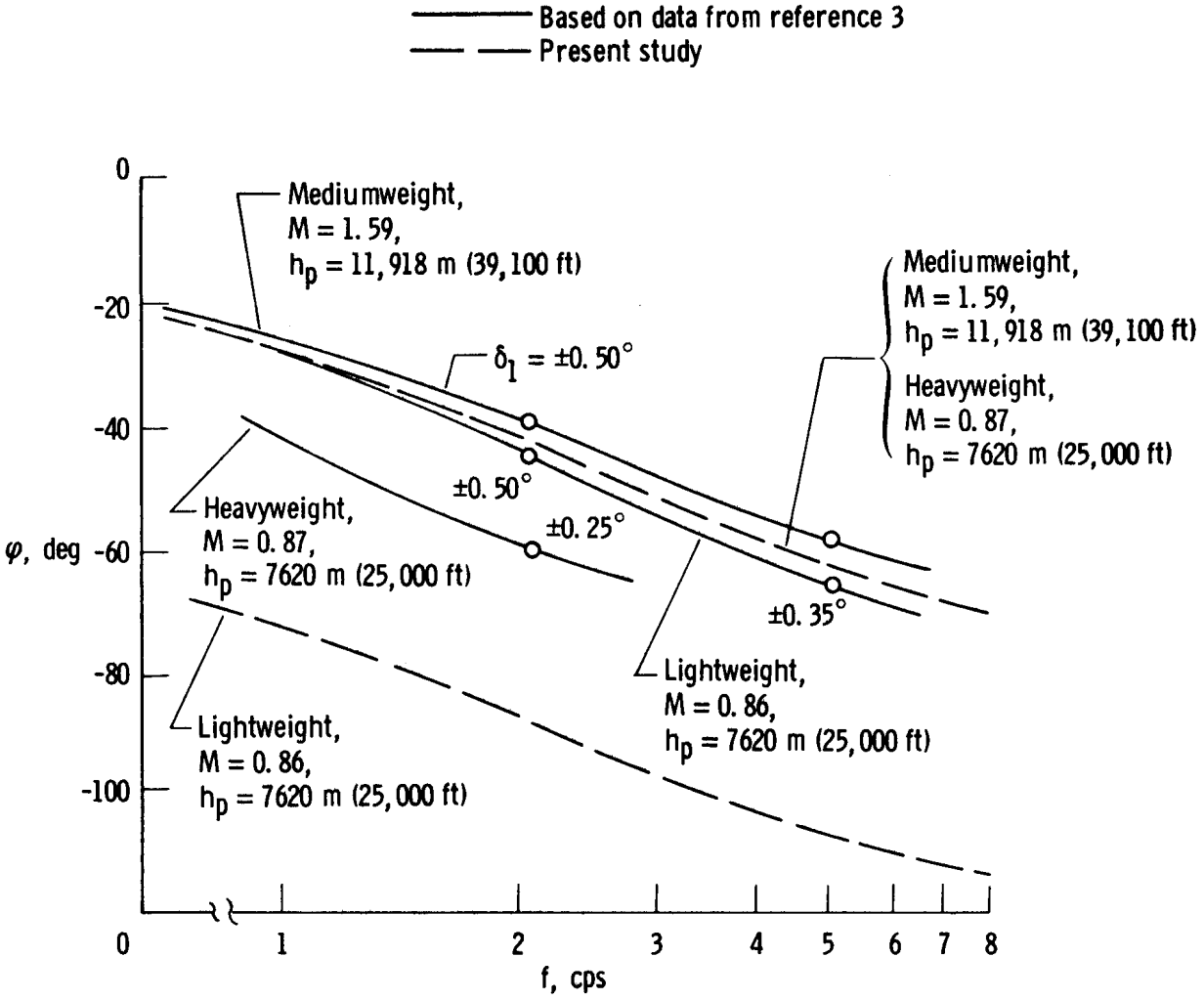

(b) Phase angle.

Figure 28. Concluded.

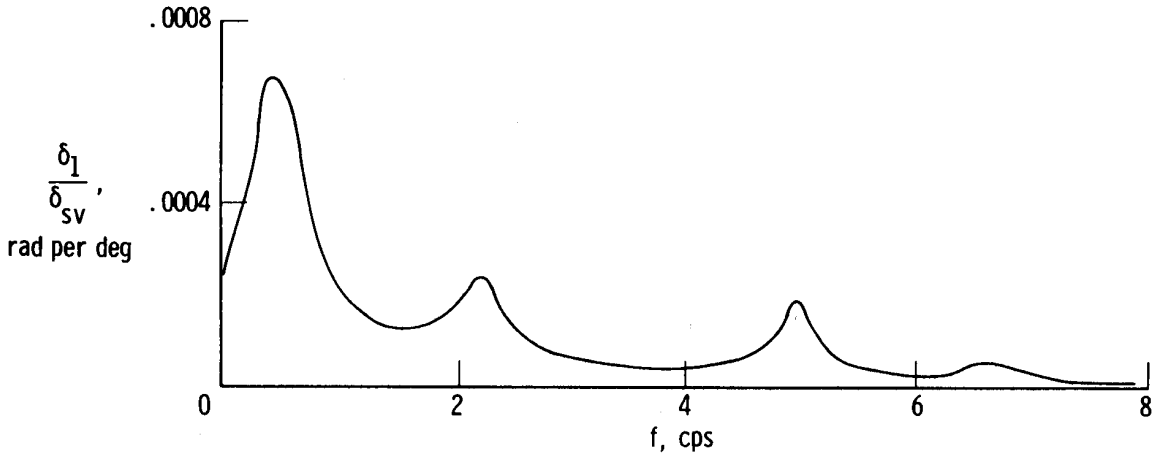

(a) Inboard elevon.

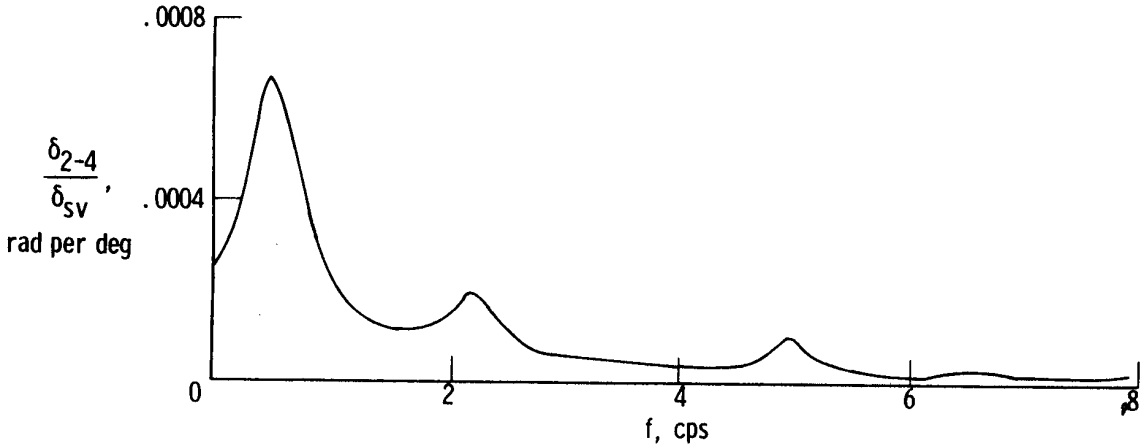

(b) Outboard elevons.

Figure 29. Elevon deflection due to shaker vane excitation. FACS operating; heavyweight; M = 0.87; h_p = 7620 m (25,000 ft); δ_t = 25°.

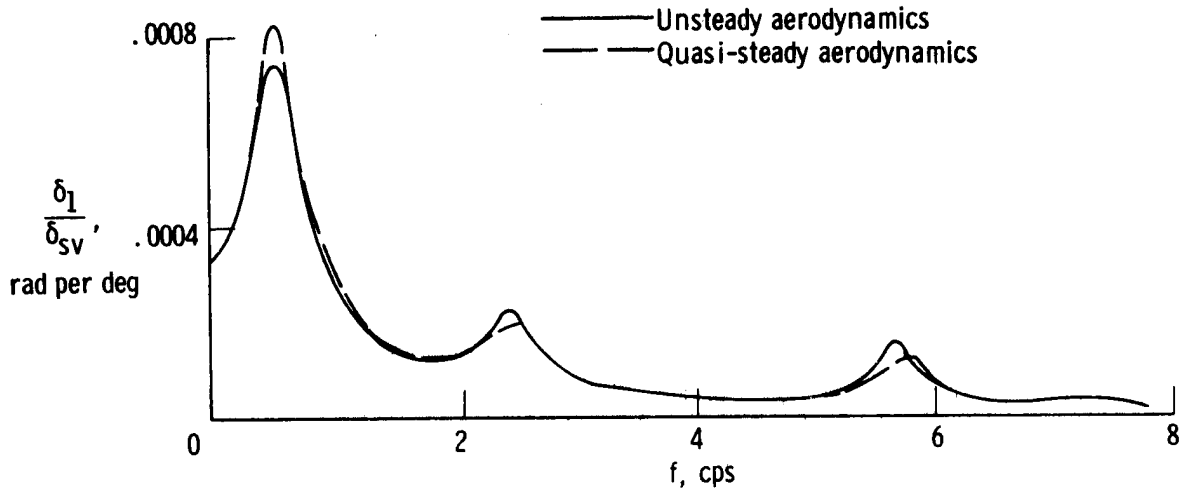

(a) Inboard elevon.

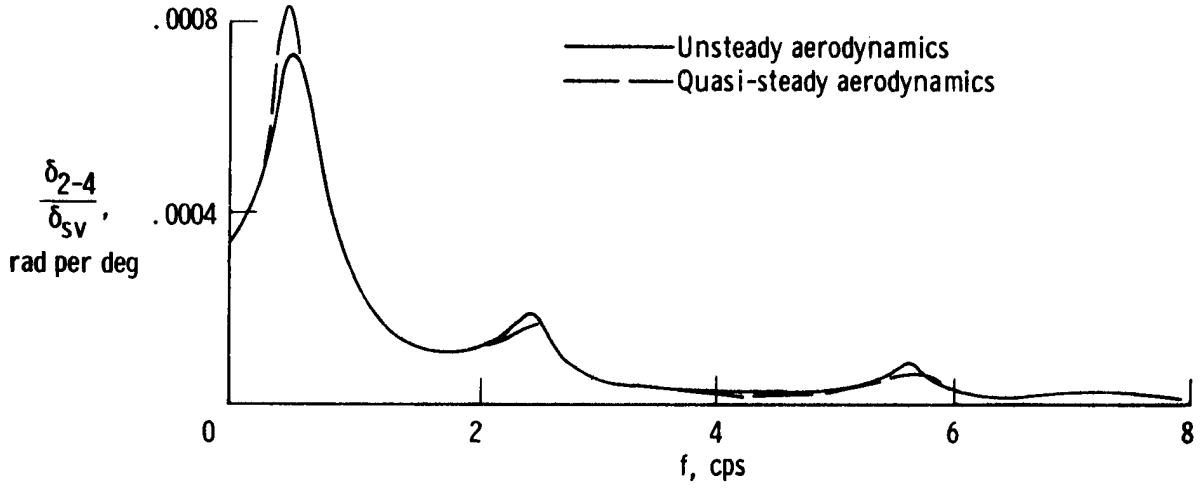

(b) Outboard elevons.

Figure 30. Elevon deflection due to shaker vane excitation. FACS operating; lightweight; M = 0.86; h_p = 7620 m (25,000 ft); δ_t = 25°.

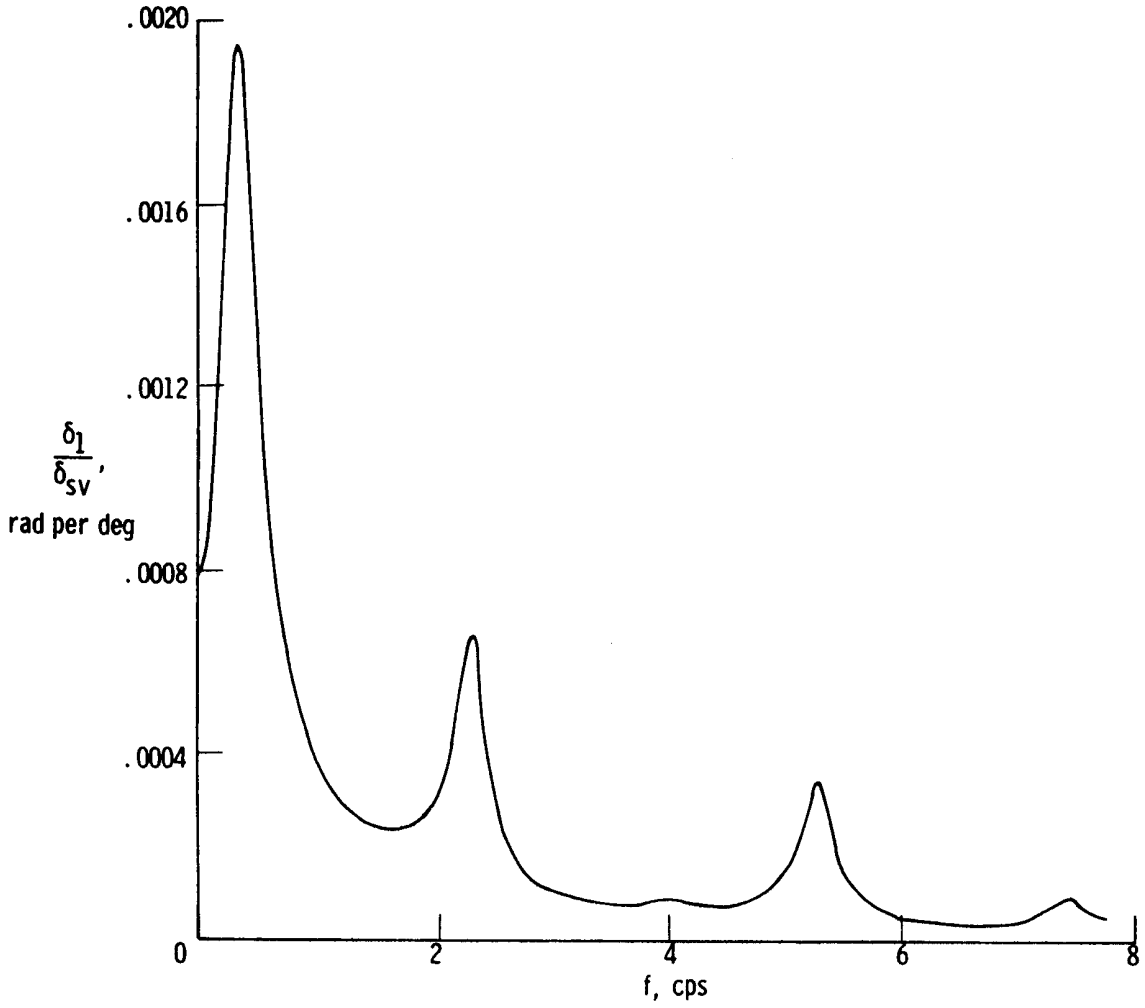

(a) Inboard elevon.

Figure 31. Elevon deflection due to shaker vane excitation. FACS operating; mediumweight; M = 1.59; h_p = 11,918 m (39,100 ft); δ_t = 65°.

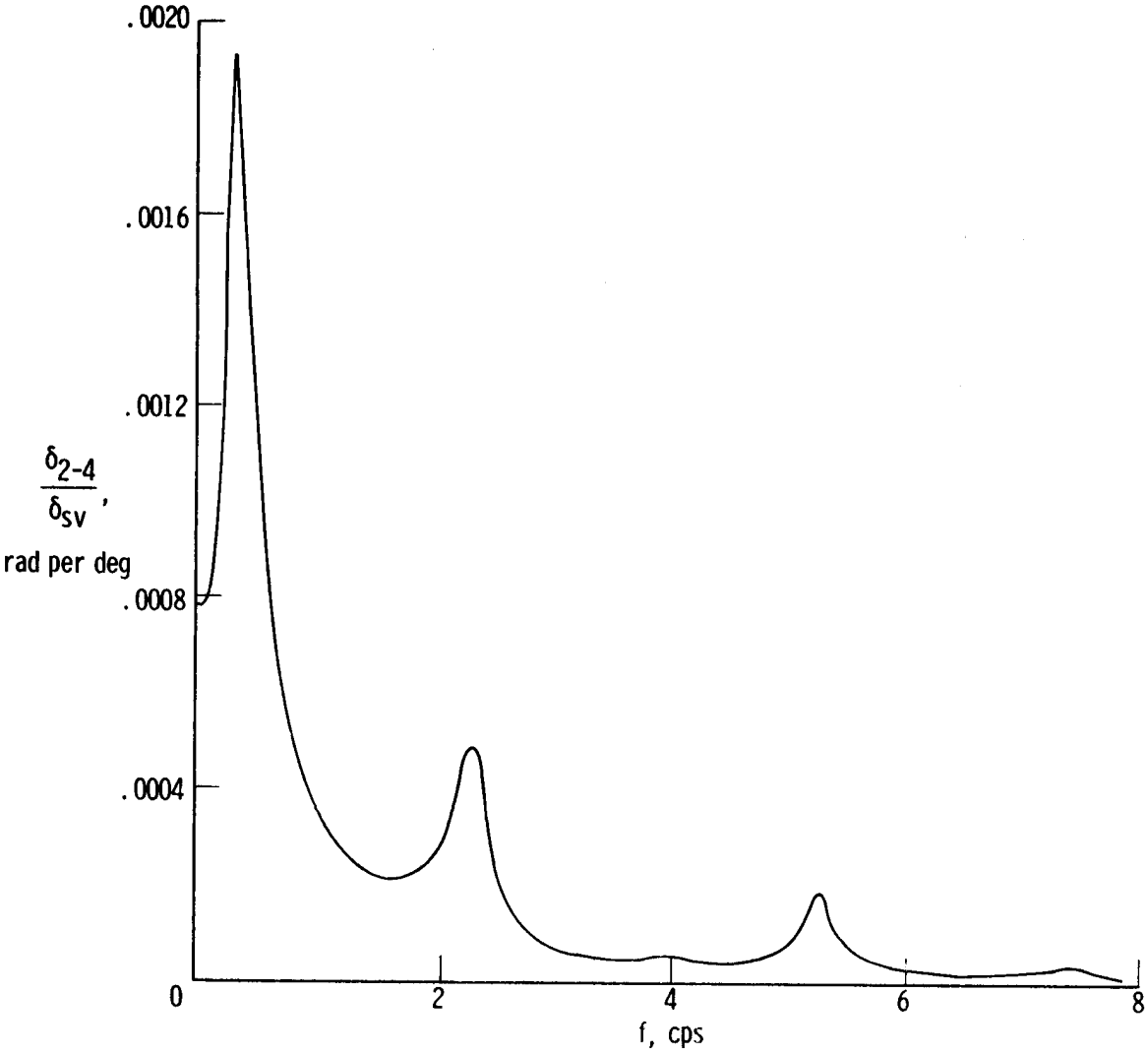

(b) Outboard elevons.

Figure 31. Concluded.

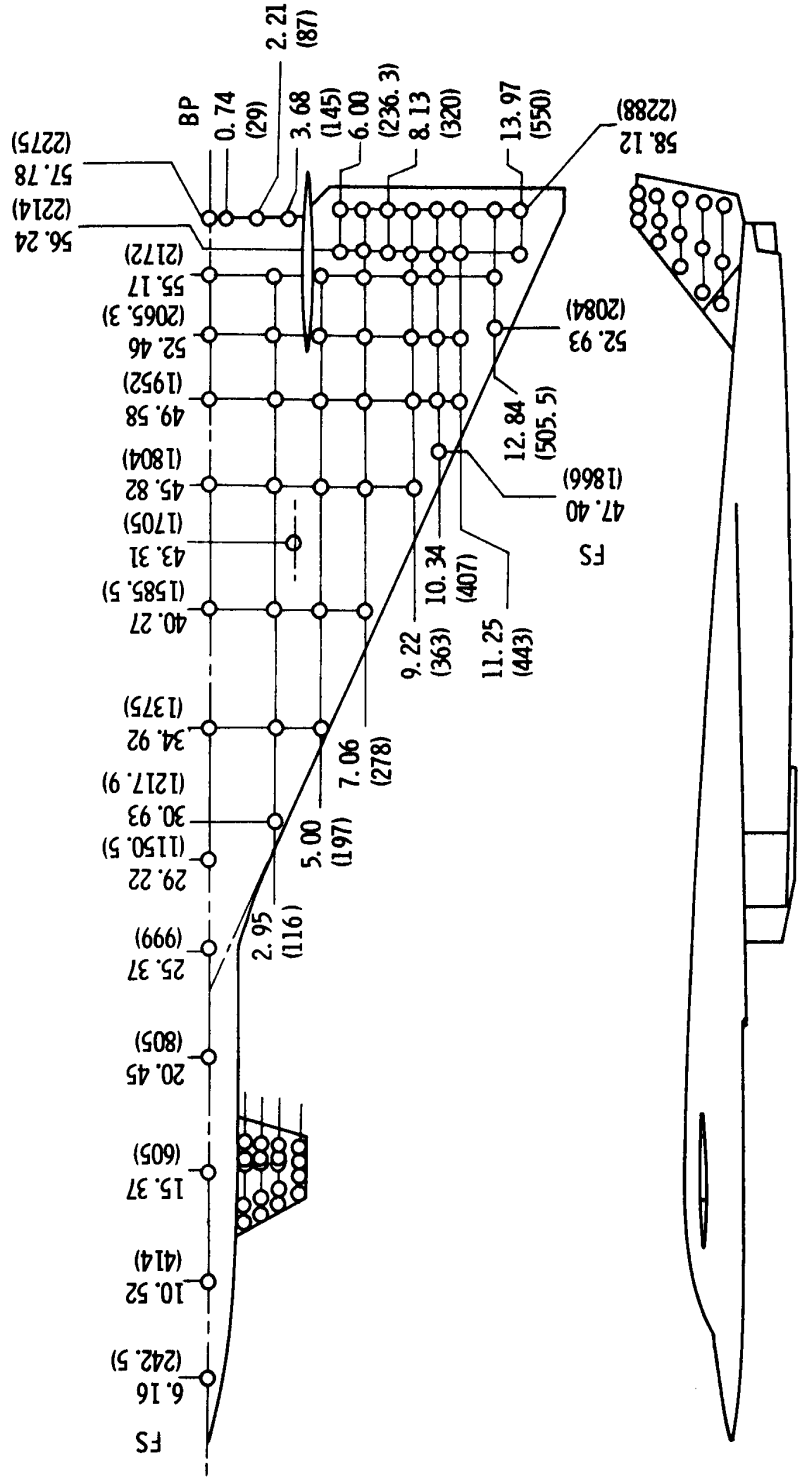

(a) Fuselage-wing. Dimensions in meters (inches).

Figure 32. Control point geometry for XB-70 97-point grid system.

Canard

Point	Fuselage station, m (in.)	Butt plane, m (in.)
1	13.00 (511.8)	1.65 (64.8)
2	13.96 (549.8)	
3	15.52 (611.1)	
4	15.76 (620.3)	
5	16.57 (652.5)	
6	13.42 (528.3)	2.38 (93.7)
7	14.18 (558.2)	
8	15.60 (614)	
9	15.81 (622.5)	
10	16.52 (650.4)	
11	13.90 (547.3)	3.22 (126.8)
12	14.43 (568)	
13	15.68 (617.3)	
14	15.87 (624.9)	
15	16.30 (641.9)	
16	14.44 (568.5)	4.16 (163.8)
17	15.01 (590.8)	
18	15.78 (621.1)	
19	15.94 (627.7)	
20	16.39 (645.2)	

Vertical tail

Point	Fuselage station, m (in.)	Waterplane, m (in.)
21	54.33 (2139.1)	0.96 (38)
22	56.13 (2209.8)	
23	58.61 (2307.5)	
24	54.85 (2159.3)	1.89 (74.5)
25	56.78 (2235.6)	
26	58.79 (2314.6)	
27	55.99 (2204.5)	2.86 (112.8)
28	57.48 (2262.8)	
29	58.98 (2322)	
30	57.09 (2247.7)	3.80 (149.6)
31	58.14 (2288.8)	
32	59.16 (2329)	
33	58.27 (2294)	4.80 (188.9)
34	58.83 (2316)	
35	59.33 (2336)	

(b) Canard and vertical tail.

Figure 32. Concluded.